REMARKS

Claim Rejections

Claims 1, 2, 6, 8 and 9 are rejected under 35 U.S.C. 103(a) as being unpatentable over Tao (2002/0015877) in view of any one of Eylem et al. (7160647) or Coetzer et al. (4366215).

Arguments

Applicant respectfully traverses the Examiner's rejections based on the following arguments.

On p. 2 of the outstanding Office Action the Examiners states:

However, applicant admits that Tao teaches a material for solid state cathode wherein said materials have general form of $La_xMn_yA_aB_bC_cO_d$ wherein A is an alkaline earth metal, B is selected from the group consisting of scandium, yttrium and a lanthanide metal, C is selected from the group consisting of iron, cobalt, nickel, copper, and zinc, x is from 0 to about 1.5, y is from 0 to about 1, a is from 0 to about 0.5, b is from 0 to about 0.5, c is from 0 to about 0.5, and d is between about 1 and about 5. This appears to teach a cathode material including copper and manganese.

Applicant argues that it is clear that LnCuO3 definitely has different chemical and structural meaning from C_cO_d in $La_xMn_yA_aB_bC_cO_d$ where is 0-0.5

In the Raveau reference [1], it clearly stated that the family of the manganites are expressed with the generic formulation of $Ln_{1-x}A_xMnO_3$ where Ln^{3+} is a lanthanide cation and A^{2+} is an alkaline earth metal ion. These oxides are known to exhibit an interesting electrical property due to the spectacular variation of their resistance, when exposed to a magnetic field. In Tao's claims, the formula used, such as $LaMnO_3$, $La_{0.84}Sr_{0.16}MnO_3$, $La_{0.84}Ca_{0.16}MnO_3$, and $La_{0.84}$ $Ba_{0.16}MnO_3$, are exactly the same as $Ln_{1-x}A_xMnO_3$ where Ln and A are specified. ***Therefore, based on this common scientific expression, what Tao***

teaches is limited to a manganite which cannot be broadly assumed as a cathode material including copper and manganese. In contrast, Applicant specifically recites in claims 1, 8, and 9 that the "***cathode...has copper*** partly converted to a trivalence copper ion...." (Emphasis added).

Based on Moskvin[2] and the foregoing, it is clear that Applicant recites cuprates in claims 1, 8, and 9. Specifically, according to the published work of Moskvin[2], the oxides based on copper ions such as $YBa_2Cu_3O_{6+x}$, $La_{2-x}Sr_xCuO_4$, $La_2CuO_{4-\delta}$, etc. should be named as cuprates. Other oxides based on Ni ions, Bi ions are named nickellates ($La_2NiO_{4-\delta}$) and bismuthates ((K, Ba)BiO_3) accordingly.

More importantly, when these major cations occupy certain lattice sites more than 50%, they will exhibit different physical properties. On the other hand, manganite, cuprate, nickellate, and bismuthates will behave differently. For instance, for manganite and cuprate systems, they exhibit distinct colossal magnetoresistance (CMR) phenomena (for manganite) versus high-temperature superconducting behavior (for cuprate), respectively. Such interesting variations have been recognized and discussed in many publications. *See, e.g.,* the enclosed references [3]-[6]. Based on claim 27 (shown below) in Tao, it is clear that the reference teaches ***manganite*** (with Mn>0.5 or 50% on the designated lattice site) which is clearly different from the ***cuprates recited in the present invention***. This assertion is fully supported by Park [3]. In this paper, it is clearly pointed out that Cu-doped manganite ($La_{0.825}Sr_{0.175}Mn_{1-y}Cu_yO_3$) and Mn-doped cuprate ($La_{1.85-2x}Sr_{0.15+2x}Cu_{1-x}Mn_xO_4$) showed different electrical properties. Therefore, when $La_xMn_yA_aB_bC_cO_d$ contains some Cu in C, Cu-doped manganite definitely is the correct term to use. Consequently, Cu-doped manganite cannot be said to teach or suggest the cuprates recited in Applicant's described in Applicant's claims 1, 8, and 9. In other words, ***based on the foregoing, it is clear that the skilled artisan would recognize that Tao teaches maganites and that all of Applicant's claims (regardless of the metal B selected from the recited group) are directed to cuprates***.

27. The fuel cell as in claim 26, wherein said solid state cathode is selected from the group consisting of $LaMnO_3$, $La_{0.84}Sr_{0.16}MnO_3$, $La_{0.84}Ca_{0.16}MnO_3$, $La_{0.84}Ba_{0.16}MnO_3$,

$La_{0.65}Sr_{0.35}M_{0.08}Co_{0.02}O_3$, $La_{0.79}Sr_{0.16}Mn_{0.85}Co_{0.15}O_3$,
$La_{0.84}Sr_{0.16}Mn_{0.8}Ni_{0.2}O_3$, $La_{0.84}Sr_{0.16}Mn_{0.8}Fe_{0.2}O_3$,
$La_{0.84}Sr_{0.16}Mn_{0.8}Ce_{0.2}O_3$, $La_{0.84}Sr_{0.16}Mn_{0.8}Mg_{0.2}O_3$,
$La_{0.84}Sr_{0.16}Mn_{0.8}Cr_{0.2}O_3$, $La_{0.6}Sr_{0.35}Mn_{0.8}Al_{0.2}O_3$,
$La_{0.84}Sc_{0.16}MnO_3$, and $La_{0.84}Y_{0.16}MnO_3$.

Coetzer et al. is cited as teaching a solid oxide cathode and an alkaline earth anode. Applicant does not acquiesce to this characterization and further notes that the reference fails to provide the above-noted deficiencies of Tao et al. Supererogatorily, Applicant notes that the Coetzer reference (excerpt below) teaches a AB_2O_4 spinel structure and that A or B may be choosen from Ti, V, Cr, Mn, Fe, Co, Ni, Cu, Zn, Mg, and Al. It is thus apparent that no Ln (lanthanide cation) is involved in the invention of Coetzer et al.

In addition, in Takanishi and Matsuda's invention (excerpt shown below), $Li_{1-x-a}A_{1-x}$ $Ni_{1-y-b}B_yO_2$, where A=Mg, Ca, Sr, Ba and B=transition metal, is basically using $LiNiO_2$ as the main host. $LiNiO_2$ ihas a layer-type structure with a+ Li-intercalating property. Both of these spinel or layer-type structures are completely irrelevant to the cuprates recited in Applicant's claims.

Cahit Eylem, Bellingham, MA (US);
Nikolay Iltchev, Norfolk, MA (US);
Stuart M. Davis, Norfolk, MA (US);
Ou Mao, Walpole, MA (US)

The Gillette Company, Boston, MA (US)

Keijiro Takanishi; Yoshio Matsuda; Jun Tsukamoto, all of Shiga, Japan

Toray Industries, Inc., Tokyo, Japan

Batteries are disclosed. In some embodiments, a battery has a cathode that includes $Cu_xM_yO_zX_t$, where M is a metal, X includes one or more halides and/or nitrate, x+y is from about 6.8 to about 7.2, and z and t are selected so that the copper in $Cu_xM_yO_zX_t$ has a formal oxidation state of +2 or greater.

A cathode material for a lithium ion secondary battery comprises a compound of the formula

$$Li_{1-x-a}A_xNi_{1-y-b}B_yO_2.$$

wherein:

A is an alkaline earth metal component selected from the group consisting of (1) at least two of magnesium, calcium, strontium and barium, (2) strontium alone and (3) barium alone;

B is at least one transition metal element other than Ni;

[54] [illegible]

[75] Inventors: **Johan Coetzer; Michael M. Thackeray**, both of Pretoria, South Africa

[73] Assignee: **South African Inventions Development Corp.**, Pretoria, South Africa

[57]

A method of making a cathode for a secondary electrochemical cell is disclosed. The method involves activating or preconditioning an oxide which has a spinel-type or oxo-spinel type structure of the formula AB_2O_4 with at least one of A or B being a transition metal, and A and B being di-, tri-, or tetravalent cations selected from Ti, V, Cr, Mn, Fe, Co, Ni, Cu, Zn, Mg and Al. The method provides a cathode, which is in the form of a stable three-dimensional framework structure. In a secondary electrochemical cell the structure of the cathode is capable of reversible charge/discharge reactions while being stable with regard to other physical or chemical changes in structure.

Eylem et al. is cited as teaching a solid oxide cathode and an alkaline earth anode. Applicant does not acquiesce to this characterization and further notes that the reference fails to provide the above-noted deficiencies of Tao et al. Supererogatorily, Applicant notes that Eylem et al. teach that the cathode material is expressed as $Cu_xM_yOx_zX_t$. This material is simply a copper oxide doped with higher valent metal ion, M, and a halide ion. The property of this material $Cu_xM_yOx_zX_t$ will be similar to CuO. That is why the oxidation state of copper is +2 or higher, as mentioned by inventor. Thus, the material is completely different from Applicant's recited claims from the view of crystal structure or from the view of physical property.

It follows that even if the teachings of Tao et al. were combined with Elyem or Coetzer et al., as suggested by the Examiner, the resultant combination does not teach or suggest: the cathode recited in Applicant's claims 1, 8, and 9.

In considering the above, the Examiner is respectfully reminded that, it is a basic principle of U.S. patent law that it is improper to arbitrarily pick and choose prior art patents and combine selected portions of the selected patents on the basis of Applicant's disclosure to create a hypothetical combination which allegedly renders a claim obvious. Instead, the Supreme Court, in *KSR International Co. v. Teleflex*, 550 U.S. ___, 127 S. Ct. 1727 (2007), the Court stated on p. 14 of the published opinion that:

> Often, it will be necessary for a court to look to interrelated teachings of multiple patents; the effects of demands known to the design community or present in the marketplace; and the background knowledge possessed by a person having ordinary skill in the art, all in order to determine whether there was an apparent reason to combine the known elements in the fashion claimed by the patent at issue. To facilitate review, this analysis should be made explicit. See In re Kahn, 441 F. 3d 977, 988 (CA Fed. 2006) ("[R]ejections on obviousness grounds cannot be sustained by mere conclusory statements; instead, there must be some articulated reasoning with some rational underpinning to support the legal conclusion of obviousness").

Applicant submits that the above-presented arguments clearly indicate that the Examiner has failed to provide an "articulated reasoning with some rational underpinning to support the legal conclusion of obviousness" for combining selected elements of Tao et al. with selected elements of Elyem, and Coetzer et al. *KSR*, 550 U.S. ___, 127 S. Ct. 1727 (2007)(p. 14 of published opinion). It is believed to be abundantly clear that the Examiner has taken selected portions of the 3 references, in a classic case of hind-sight reconstruction having the benefit of Applicant's disclosure. Clearly, such a combination is not an acceptable combination under 35 U.S.C. §103. The rejections of Applicant's claims as being rendered by the aforementioned combinations of references under 35 U.S.C. §103 is respectfully traversed.

Enclosed References in support of the above arguments

1. B. Raveau, "Transition metal oxides: Promising functional materials," Journal of the European Ceramic Society 25 (2005) 1965–1969.

2. A.S. Moskvin, "Pseudo-Jahn-Teller-centers and phase separation in the strongly correlated oxides with the nonisovalent substitution. Cuprates and manganites," Physica B 252 (1998) 186-197.

3. C.J. Zhang *, B.H. Kim, Y.W. Park, "Possible mutual percolation conductivity in perovskite oxides," Current Applied Physics 6 (2006) 964–968.

4. T. Venkatesan , R.P. Sharma, Y.G. Zhao, Z.Y. Chen, C.H. Lee, W.L. Cao, J.J. Li, H.D. Drew, S.B. Ogale, R. Ramesh, M. Rajeswari, T. Wu, I. Jin S. Choopun, M. Johnson, W.K. Chu, G. Baskaran, "Superconducting cuprates and magnetoresistive manganites: similarities and contrasts," Materials Science and Engineering B63 (1999) 36–43.

5. Guo-meng Zhao, M. B. Hunt, K. Conder, H. Keller and K. A. Miiller, "Oxygen isotope effects in the manganites and cuprates: polaronic charge carriers," Physica C 282-287 (1997) 202-205.

6. T. Egami1 and Despina Louca, "Electron-Lattice Coupling in Manganites and Cuprates," Journal of Superconductivity, Vol. 12, No. 1, 1999 23-26.

7. T. Venkatesan, R.P. Sharma, "Evolution of oxide electronics: examples from HTS and CMR," Materials Science and Engineering B41 (1996) 30–34.

Summary

In view of the foregoing remarks, Applicant submits that this application is now in condition for allowance and such action is respectfully requested. Should any points remain in issue, which the Examiner feels could best be resolved by either a personal or a telephone interview, it is urged that Applicant's local attorney be contacted at the exchange listed below.

Respectfully submitted,

Date: October 16, 2008 By: 

Demian K. Jackson
Reg. No. 57,551

TROXELL LAW OFFICE PLLC
5205 Leesburg Pike, Suite 1404
Falls Church, Virginia 22041
Telephone: 703 575-2711
Telefax: 703 575-2707

CUSTOMER NUMBER: 40144

Journal of Superconductivity, Vol. 12, No. 1, 1999

Electron-Lattice Coupling in Manganites and Cuprates

T. Egami[1] and Despina Louca[2]

The lattice effects of charge localization in manganites and cuprates are discussed from the local structural point of view. Pulsed neutron atomic pair-density function (PDF) analysis indicates that in $La_{1-x}Sr_xMnO_3$ the real structure deviates from the average crystal structure, and the local Jahn–Teller (JT) distortion of $Mn^{3+}O_6$ octahedra remains even in the metallic phase. This leads to a concept of the critical ionic size factor for the formation of JT polarons. The colossal magnetoresistance (CMR) phenomena are observed in the crossover region from localized to delocalized charge states. This concept also explains the asymmetry of the phase diagram which is difficult to understand in the current band picture. Similar consideration may help understand the lattice effects in superconducting cuprates.

1. INTRODUCTION

In the perovskite-type manganites $R_{1-x}A_xMnO_3$ (R = La, Pr, or Nd, A = Sr, Ba, Ca or Pb) the CMR behavior is observed as the system undergoes transition from an antiferromagnetic or ferromagnetic insulator (AFI or FI) to a ferromagnetic metal (FM) as hole doping (x) is increased [1], or as the average atomic radius of the A-site ions (rare earth and alkali ions), $\langle r_A \rangle$, is changed [2]. The two phase diagrams, where transition temperatures are plotted against x or $\langle r_A \rangle$, look alike. Currently the standard explanation of the latter is that as the atomic size $\langle r_A \rangle$ is reduced the electron band width is decreased because of the increased bending of the Mn–O–Mn bond, leading to formation of polarons and localization of holes that is equivalent to reducing x. However, the reduction in the band width estimated from the bond angle is very small [1]. Furthermore recent data indicate that even as the value of $\langle r_A \rangle$ is reduced the spin-wave stiffness is unchanged [3,4]. Since the spin-wave stiffness is related to the exchange constant and the band width, this explanation of the relation between $\langle r_A \rangle$ and x through the band width is strongly in doubt. In this paper, we propose an alternative explanation involving the structure dependence of the elastic energy to form polarons that controls the stability of lattice polarons. This concept is based upon the knowledge of the local atomic structure of the solids determined by the atomic pair-density function (PDF) analysis of the pulsed neutron powder diffraction data.

2. LOCAL STRUCTURE OF $La_{1-\xi}Sr_\xi MnO_3$

While the crystallographic analysis uses only the Bragg peaks and determines the average crystal structure, the PDF analysis utilizes the diffuse scattering as well as Bragg intensities, and describes the local atomic structure [5]. In a mixed-ion system such as the CMR manganites the local structure varies from site to site, and the actual bond lengths often deviates from those deduced from the average crystal structure.

The pulsed neutron PDF of $La_{1-x}Sr_xMnO_3$ shows a double peak in the range of 1.8–2.3 A representing the Mn–O bonds. As shown in Fig. 1 the Mn–O distances determined from the peak position of the PDF are different from those estimated from the crystal structure [6]. The crystal structure suggests that the Jahn–Teller distortion is quickly reduced by

[1]Department of Materials Science and Engineering, Laboratory for Research on the Structure of Matter, University of Pennsylvania, Philadelphia, Pennsylvania 19104.
[2]Los Alamos National Laboratory, Los Alamos, New Mexico 87545.

0896-1107/99/0200-0023$16.00/0

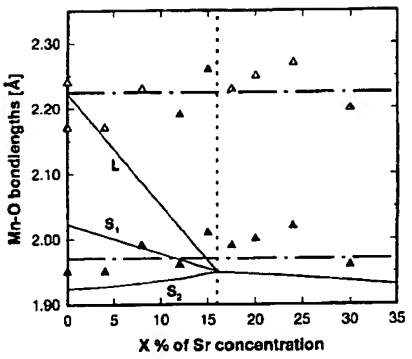

Fig. 1. The positions of the Mn–O peaks, short (1.97 A) and long (2.25 A), as a function of the Sr concentration, compared with the Mn–O distances calculated from the crystallographic structure (thin solid lines, L for long and S_1 and S_2 for short bonds) that coalesce at $x = 16\%$ [6].

hole doping, disappearing at 16% Sr as the structure becomes rhombohedral. However, the local structure shows two Mn–O distances at 1.97 and 2.23 A well into the rhombohedral phase [6]. This means that the magnitude of the JT distortion of the distorted MnO_6 octahedra remains unchanged by doping. In the rhombohedral structure apparently the local JT distortions are random in orientation, and are averaged out in the long range structure.

The effect of doping is to remove the local JT distortion from some of the Mn sites. The density of the Mn sites where the JT distortion is removed can be determined by the number of short Mn–O bonds that changes from 4 when the JT distortion is present to 6 when it is absent. In the insulating phase the Mn sites where the JT distortion is removed represent the anti-JT lattice polarons. In the paramagnetic phase the polaron is centered on a single Mn site (small polaron) while at low temperatures it is spread over three sites (extended polaron) [6]. The density of the anti-JT Mn sites at 10 K was found to change smoothly through the metal-insulator (MI) transition at $x_c = 0.16$ where it is only around 5, well below 6. Just above x_c local JT distortion survives even in the metallic phase. This behavior is indicative of the percolative nature of the MI transition [6].

3. CRITICAL IONIC SIZE FOR POLARON FORMATION

We now argue that the variation in the polaron stability with composition is determined mainly by the elastic energy to form a polaron, rather than the band width. If the elastic energy cost is high, polarons will not be formed, carriers remain free and the doped system is a normal metal. If the elastic energy cost is low, polarons are stable, resulting in an antiferromagnetic insulator. The CMR behavior is observed in the crossover regime.

Starting from $A^{3+}Mn^{3+}O_3$, when the JT distortion is locally removed by a doped hole, the lattice becomes locally distorted. The nature of distortion, however, depends upon the structure. When the Mn–O–Mn is straight (Mn–O–Mn bond angle 180°) in order to reduce one bond length to remove the JT distortion other Mn–O bonds need to be stretched to accommodate this local strain (longitudinal accommodation, Fig. 2a). On the other hand if the Mn–O–Mn bond is bent, the local strain can be accommodated by the change in the bending angle (transverse accommodation, Fig. 2b). Longitudinal accommodation is energetically far more costly than transverse accommodation, since stretching the Mn–O bond requires much more energy than bending it. Thus it is conjectured that polarons that require longitudinal accommodation will not be formed, and polarons are stable only when transverse accommodation is possible.

The critical condition when the transverse accommodation changes over to longitudinal accommodation can readily be located. In $LaMnO_3$ the a–b plane consists of long Mn–O bonds ($L = 2.23$ A) and short Mn–O bonds ($S = 1.97$ A). When a polaron is created, a pair of Mn–O–Mn bonds that are made

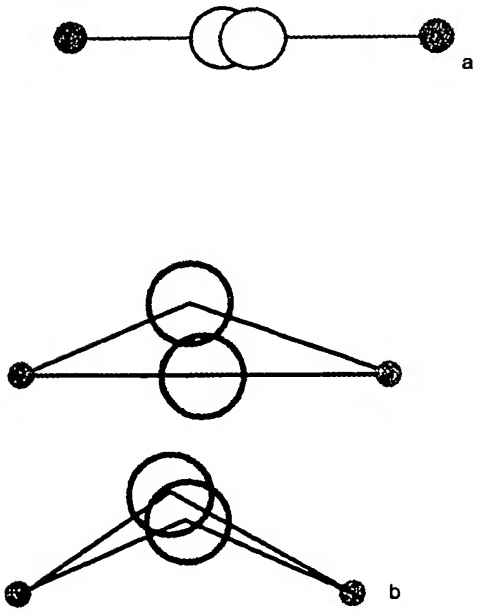

Fig. 2. (a) longitudinal (bond stretching) accommodation of bond shrinkage, and (b) transverse (bond bending) accommodation.

of $L+S$ will change to $S+S$. The condition that the Mn–O bond within the polaronic Mn site is not under tension (longitudinal accommodation) is that the Mn–Mn distance is less than $S+S$. Thus, the distance between the A-site and oxygen, R_{A-O}, has to be smaller than $\sqrt{2}S = 2.786$ A. This means that the critical ionic size of an A-site ion is 1.386 A in XII coordination. This value is slightly larger than the XII coordinated ionic radius of La (1.36 A) [7]. If the A-site ion size is greater than 1.386 the Mn–O–Mn bond in the polaron is straight and under tension, so that polarons will not form. If the A-site ion size is smaller than 1.386 A, stability of anti-JT polaron would increase with decreasing A-site ionic radius.

On the other hand, if we start from the other side, $A^{2+}Mn^{4+}O_3$ that has no JT distortion, a polaron is represented by the Mn site that is locally JT distorted. Thus we start from the system of $S+S$ Mn–O–Mn bonds, and doping will locally create pairs of $S+L$ bonds within a polaron. In this case transverse accommodation is always possible, since even when the Mn–O–Mn bond is straight it can become bent within the polaron. Thus for n-type doping JT polarons are always stable, frequently forming a charge-ordered phase (polaron lattice) and resulting in an antiferromagnetic insulating phase. In this way the p-type doping of a JT distorted phase creating anti-JT polarons is very different from the n-type doping of a non-JT phase creating JT polarons. This naturally explains the asymmetry between the JT side and the non-JT side of the phase diagram which is difficult to understand in the current band picture.

It is instructive to consider a phase diagram for x vs. $\langle r_A \rangle$ (Fig. 3). For $x > 0.5$ polarons are always stable. For $x < 0.5$, on the other hand, in the range $\langle r_A \rangle > \langle r_A \rangle_{UC} = 1.386$ A polarons are unstable, and the system is a ferromagnetic metal, except when the value of x is small. When $\langle r_A \rangle$ is smaller than $\langle r_A \rangle_{LC}$ polarons are stable and the system is an antiferromagnetic or ferromagnetic insulator. The value of $\langle r_A \rangle_{LC}$ can be estimated from the fact that the La–Y–Ca system becomes a ferromagnetic insulator when the average A-site radius is less than 1.33 A [2]. In the crossover regime $1.386\text{ A} > \langle r_A \rangle > 1.33$ A polarons are marginally stable, and are influenced by many factors. They are highly susceptible to a magnetic field, thus producing the CMR effect. At small values of x polarons are spatially separated, resulting in a semiconducting behavior, but with the increased polaron concentration the orbital ordering will melt away first [8], and then the system will become a bad metal with local lattice distortions [6]. The metal-insulator (M-I) transition is most likely governed by the polaron

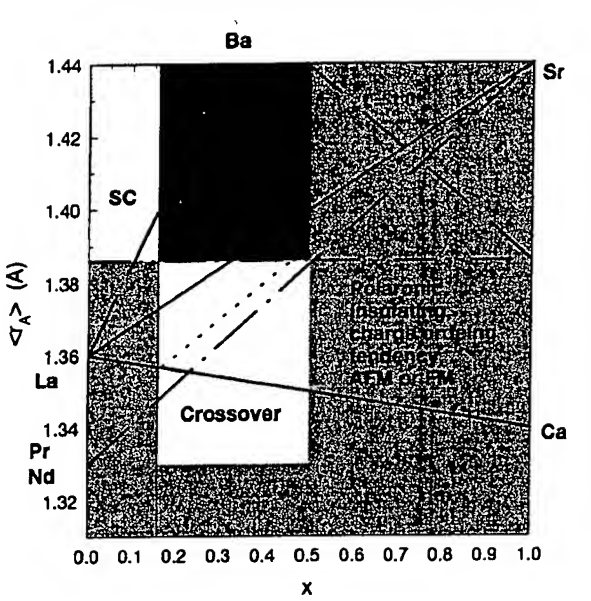

Fig. 3. The phase diagram of $R_{1-x}A_xMnO_3$ as a function of x and the average XII coordinated radius of the A-site ion, $\langle r_A \rangle$. For $0.16 < x < 0.5$, above $\langle r_A \rangle = 1.386$ A polarons are unstable resulting in a ferromagnetic metal, while below 1.33 A they are stable resulting in a ferromagnetic or antiferromagnetic insulator. In between in the crossover regime where polarons are marginally stable, they are easily influenced by various external forces, giving rise to the CMR phenomena. For $x > 0.5$ polarons are always stable. The solid lines indicate the average A-site radius for each alloy system. The chained line shows the condition for the tolerance factor being unity above which the compound is difficult to form without high pressure.

percolation, at around $x = 1/6$ [6]. The increase in the stability of polarons as the value of $\langle r_A \rangle$ is reduced also explains the increase in the isotope effect on the transition temperature [9].

By plotting the x dependence of $\langle r_A \rangle$ for each mixed-ion system it is possible to explain their properties very naturally. The La–Sr system starts as a semiconductor at low doping, becomes metallic at $x = 0.16$, but stays in the crossover region up to $x = 0.325$ (Fig. 3). Indeed up to $x = 0.35$ local lattice distortion is observed even though the system is metallic; resistivity is high, and the CMR effects are observed. Beyond $x = 0.35$ no local distortion nor the CMR effect is observed. According to Fig. 3, the La–Ca system remains in the crossover region up to $x = 0.5$. Indeed in the La–Ca system the Curie temperature remains low and the CMR effect is more pronounced than in the La–Sr system. Also charge ordering (polaron lattice formation) is observed at many compositions with a rational fraction. The Ca-rich phase is insulating because charges are localized as polarons.

On the other hand the La–Ba system leaves the cross-over region with small doping ($x = 0.1$). Indeed this system is difficult to form, and does not show much of the CMR effect. In systems based upon Pr or Nd polarons are more stable than in the La based system, so that T_c is low as observed [4].

In this calculation we used the XII coordinated ionic radii, because we are more concerned about the structure *within* the polaron. Within the polaron the Mn–O–Mn bond is straight at the critical condition. On the other hand Hwang *et al.* [2] and Zhao *et al.* [9] focused on the average structure and used the IX-coordinated ionic radius. If we follow their convention we can translate the argument above to obtain the critical ionic size for polaron stability of $\langle r_A \rangle = 1.245$ A, the critical tolerance factor $t_c = 0.93$, and the lower critical tolerance factor 0.905. The crossover region is defined by $0.905 < t < 0.93$.

4. IMPLICATIONS TO CUPRATES

The discussions on the CMR manganites above demonstrate the ionic size effect on the stability of JT polarons, and that the CMR effect is observed in the cross-over regime where polarons are marginally stable. There are several observations that suggest that analogy may hold true to some extent for the superconducting cuprates as well:

1. The in-plane Cu–O distances in YBCO and BSCO type compounds are narrowly distributed around $R_{Cu-O} = 1.94$ A.
2. Cu–O–Cu bond is always slightly bent, at least locally, except for the *n*-type superconductors. Note that it is bent even in the so-called infinite layer compound as shown by experiment [10] and by the LDA calculation [11].
3. In the LSCO family when the tilt angle exceeds a critical angle (3.6°) superconductivity disappears [12].
4. The LSCO family that are prone to tilting of the CuO_6 octahedra tend to have a lower superconducting transition temperature than the YBCO family.

Implications are that polaron stability competes against superconductivity, while the *inclination* for polaron formation may be required for high temperature superconductivity. It appears that superconductivity is observed in the regime where polarons are marginally stable. It is interesting to note that dynamic charge stripes with the periodicity $2a$ (a is the Cu–Cu distance) was suggested by the phonon dispersion for $La_{1.85}Sr_{0.15}CuO_4$ [13], which must be related to the static stripes (polaron lattice) with the periodicity of $4a$ observed at the charge density of 1/8 [14]. While this argument does not lead to the identification of the actual mechanism of superconductivity, it suggests that the lattice must be intimately involved in the mechanism of superconductivity. Specifically, it is suggested that carriers being in the form of marginally stable polarons may be crucial for superconductivity to take place.

ACKNOWLEDGMENTS

The authors thank their research collaborators on the present subject, W. Dmowski, E. Brosha, H. Roder, and A. R. Bishop. They are also grateful to J. B. Goodenough, D. Khomskii, L. P. Gor'kov, V. Z. Kresin, A. Bianconi, C. Di Castro, K. A. Muller, S.-W. Cheong, J. W. Lynn, J. A. Fernandez-Baca, P. Dai, M. Tachiki, Y. Endoh, A. J. Millis, M. Arai, and S. J. L. Billinge for useful discussions. The work at the University of Pennsylvania was supported by the National Science Foundation through DMR-9628134.

REFERENCES

1. S.-W. Cheong and H. Y. Hwang, in *Colossal Magnetoresistance Oxides*, Y. Tokura, ed. (Gordon & Breach), in press.
2. H. Y. Hwang *et al.*, *Phys. Rev. Lett.* **75**, 914 (1995).
3. J. W. Lynn *et al.*, *Phys. Rev. Lett.* **76**, 4046 (1996).
4. J. A. Fernandez-Baca *et al.*, *Phys. Rev. Lett.* **80** (1998).
5. B. H. Toby and T. Egami, *Acta Crystallogr. A* **48**, 336 (1992).
6. Despina Louca *et al.*, *Phys. Rev. B* **56**, R8475 (1997).
7. R. D. Shannon, *Acta Cryst.* **A32**, 751 (1976).
8. H. Yoshizawa *et al.*, *Phys. Rev. B* **52**, R13145 (1995).
9. G. M. Zhao *et al.*, *Nature* **381**, 676 (1996).
10. S. J. L. Billinge *et al.*, *Phys. Rev. B* **43**, 10340 (1991).
11. S. Y. Savrasov and O. K. Andersen, *Phys. Rev. Lett.* **77**, 4430 (1996).
12. B. Buchner *et al.*, *Phys. Rev. Lett.* **73**, 1841 (1994).
13. T. Egami, R. J. McQueeney, Y. Petrov, G. Shirane, and Y. Endoh, *J. Superconductivity*, to be published.
14. J. N. Tranquada *et al.*, *Nature* **375**, 561 (1995).

ELSEVIER

Materials Science and Engineering B41 (1996) 30–34

MATERIALS SCIENCE & ENGINEERING B

Evolution of oxide electronics: examples from HTS and CMR

T. Venkatesan*, R.P. Sharma

Center for Superconductivity Research, University of Maryland, College Park, MD 20742, USA

Abstract

The last decade has seen the emergence of epitaxial metal-oxide films as one of the leading electronic material systems of the future. This emergence was primarily stimulated by the advent of high temperature superconductors but more recently the resurgence of interest in magnetoresistance phenomena has led to considerable excitement regarding the epitaxial manganite films in which significant field induced nonlinearities have been seen. In this article we will make a brief comparison between some of the important areas of similarity and differences between the cuprates and the manganites and draw some general inferences regarding the field of oxides and their importance to materials science and technology.

Keywords: Manganite films; Oxide electronics; Structural distortions

1. Introduction

We are caught today in the dizzying ascent of the information technology with information processing and transmission occurring at ever increasing speeds. Other fast growing areas of information technology are information storage and generation. In these areas innovations are taking place in the fabrication of non-volatile memory devices and novel sensor devices respectively where, metal-oxide based materials could play a very prominent role [1]. In Table 1 is shown the increasingly large number of functionalities associated with metal oxide films in general and the list of achievable material properties are very exciting indeed. The

Table 1
The diverse functionalities of metal oxides

Property	Example of metal oxide	Application
High optical transparency	MgO, ZrO	Optical coatings
Low loss electro-optic effect	$LiNbO_3$, $LiTaO_3$	Optical waveguides and integrated optics SAW devices
Piezoelectricity	$BaTiO_3$, $PbZr_xTi_{1-x}O_3$	Transducers micro-electro-mechanical systems
Ferroelectricity	$PbTiO_3$, $BiTiO_3$	Non-volatile memories
Pyroelectricity	$PbTiO_3$	Room temperature IR detectors
Ferro magnetism	γ-Fe_2O_3	Magnetic memories
Optical non-linearity	Nb_2O_5 $SiO_2 \cdot Na_2O \cdot Ba_2O_3$ TiO_2	All-optical switches
High optical gain	Nd^{3+} doped $Y_3Al_5O_{12}$	Lasers
Transparent conductors	$InSnO_x$	Novel device coatings
Epitaxial metals	LaNiO3, LaCoO3	Device electrodes with low grain boundary metal diffusion
Scintillators	$Bi_{12}GeO_{20}$	Radiation detectors
Electroluminescence	Ho doped $Gd_3Ga_5O_{12}$	Flat panel display screens
Ionic conductors	$LaSrCoO_3$, $LaCaCoO_3$	Solid electrolyte fuel cells
High temperature superconductivity	$YBa_2Cu_3O_7$, $HgBa_2CaCuO_3$	SQUID, superconducting electronics
Colossal magneto-resistance	$Nd_{0.7}Sr_{0.3}MnO_3$	Magnetic sensors, bolometers

* Corresponding author.

PII S0921-5107(96)01618-2

materials clearly suggest extensive applications in the fabrication of a variety of sensors and transducers which form the basis for a technological future evolving towards increased automation.

Ultimately, development of a heterostructure materials technology involving semiconductors such as silicon and gallium arsenide in conjunction with metal–oxides such as superconducting cuprates, ferroelectric titanates (for non-volatile ferroelectric memories), piezoelectric niobates (for surface acoustic wave devices), magnetoresistive manganites (for magnetic field sensors), etc. would lead to increased functionalities in future integrated circuits. Not to mention possible enhancements of todays integrated circuits. For example, reproducible technologies for the fabrication of high dielectric constant oxides for capacitors is already a problem recognized industry wide. Significant research effort has begun and will be necessary for us to exploit the properties of these oxide materials. The study of the properties of these materials and their mechanisms are in fact becoming fashionable problems in condensed matter physics.

Over the last decade, impressive progress has occurred in the fabrication of epitaxial films of virtually all the oxide materials of technological importance [2,3]. While most techniques have been successful in eventually developing a process for the fabrication of any of the family of materials listed in Table 1, one technique stands out among the many. This is pulsed laser deposition (PLD) whose emergence coincided with the ascent of the high temperature superconducting thin film technology [4,5]. This technique has enabled the rapid prototyping of most coatings for attaining the desired properties so that the time between the recognition of a need and the final identification of the material system to do the job could be significantly minimized.

2. Transport

Very briefly we will introduce two of the most exciting metal–oxides of this decade: the high temperature superconducting (HTS) cuprates and the colossal magnetoresistive (CMR) manganites. In Fig. 1 is shown the R versus T characteristics of $YBa_2Cu_3O_7$ (YBCO) for an in-plane aligned film on $LaSrGaO_3$ (LSGO) substrate [6]. Besides the evidence for the existence of a superconducting transition T_c in both the b and c directions one clearly can see the anisotropy of the resistivity in the normal state with an anisotropy of the c axis–b axis resistivity of the order of 18 at 100 K. This arises from the planar nature of the molecules with the charge transport along the Cu–O planes which end up defining a two dimensional conducting path. The conduction along the c-axis direction is much more complicated compared with the transport of holes along the Cu–O planes. This anisotropy factor is seen in virtually all the cuprate superconductors with differing magnitudes. However, the transport properties of the manganites are pretty much isotropic in nature with the transport occuring along the Mn–O–Mn bond whose angle is affected by a variety of factors such as the radius of the rare earth ion, oxygen vacancies, external pressure, and the divalent dopant ion. Since the transfer integral of the charge along this pathway is affected by the overlap of the highly directional electronic bonds of the Cu 3d and the O 2p electronic orbitals, the transport properties are dramatically affected by the changes in the bond angles. A typical R versus T curve for the manganites is shown in Fig. 2; that for $Nd_{0.7}Sr_{0.3}MnO_3$ (NSMO) [7].

The CMR materials exhibit a paramagnetic semiconducting phase above the peak temperature T_p, with a well defined activation energy of 0.12 eV and below T_p exhibit a ferromagnetic metallic phase but the transport is isotropic unlike the cuprates [8]. The peak resistivity temperature is fairly close to the ferromagnetic Curie temperature T_c. The excitement of the CMR stem from the fact that when a magnetic field is applied the

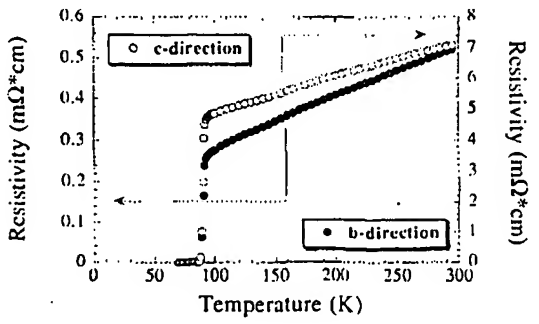

Fig. 1. Resistance vs. temperature for an in-plane oriented YBCO film on LSGO substrate [6].

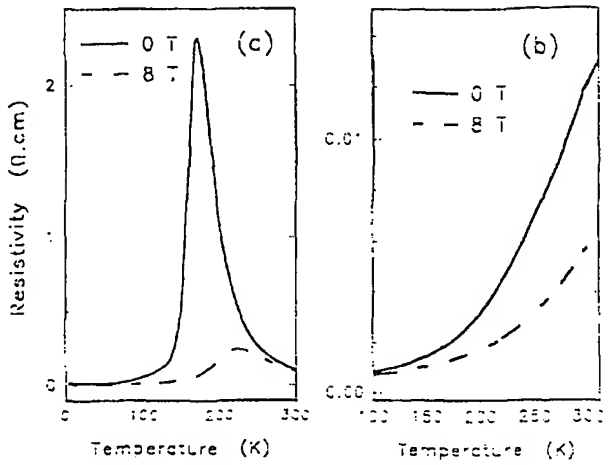

Fig. 2. Resistance vs. temperature on a linear scale for an as deposited (a) $Nd_{0.7}Sr_{0.3}MnO_3$ film and (b) $La_{0.7}Ba_{0.3}MnO_3$ film at zero and 8T field.

resistance can be changed by several orders of magnitude as is shown in Fig. 3.

In the case of the superconductor the origin of the high temperature superconductivity and a microscopic mechanism for the superconductivity is still being pursued vigorously with no clear solution in sight [9]. The normal state properties of the cuprates is itself an area of intense study without the emergence of a complete picture [10]. The manganites share a similar situation with respect to our understanding of their transport properties. However, in the case of the manganites a better understanding of the transport properties may be more likely to emerge in the near future, with significant drive from the magnetoelectronics community [11]. It is fairly clear in the case of the manganites that spin–spin scattering plays an important role in the form of double exchange though the further role of lattice distortions via Jahn-Teller distortions, both dynamic and static, have been proposed to get a better agreement between theory and experimental transport data [12].

3. Role of structural distortions

Both Cu^{2+} and Mn^{3+} are strong Jahn-Teller ions [13]. A consequence of this is that there are strong electron phonon coupling in these crystals and as a result distortions are likely to play a major role in the transport properties of these materials. One of the techniques to measure the lattice displacement of atoms arising from Jahn-Teller effects is MeV ion channeling [14]. In this technique the linear alignment of atoms in a crystalline lattice are probed by the backscattering of MeV He ions from the atoms of the crystal. When the ion is incident along a major axis of the crystal the ions are channeled (i.e., steered by the nuclei of the crystal atoms in between the rows and planes of the crystal) and the scattering cross section of the incident ion is reduced since the impact parameter for the ion become large.

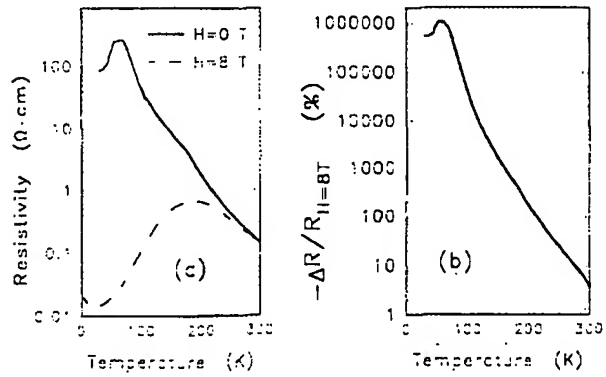

Fig. 3. Resistance vs. temperature for NSMO on a logarithmic scale with and without magnetic field [7]. A very large magnetoresistance effect is seen.

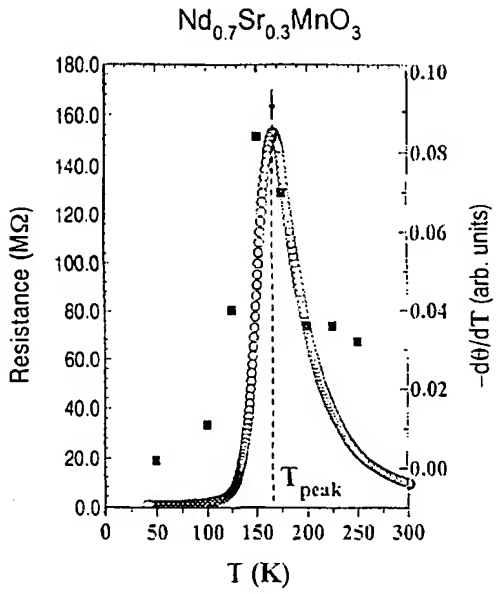

Fig. 4. The temperature derivative of the channeling FWHM vs. temperature and the correspondence with resistance for NSMO [15].

This channeling effect is preserved even when the crystal angle is changed to within a critical angle and regular backscattering is restored at larger angles. The critical angle for channeling is estimated by measuring the full width at half maximum (FWHM) of the backscattering yield as a function of the ion incident angle. The FWHM is dependent on the linear arrangement of the atoms in the solid. Any deviation of the atoms from their regular ordered position will affect this FWHM and the measurement is capable of estimating atomic distortions of the order of a picometer (0.01 Å). In Fig. 4 is shown the ion channeling measurements in a typical manganite plotted as a function of temperature and its correlation with the resistance behavior with temperature [15]. A temperature derivative of the channeling angle almost overlaps the resistance plot indicating the strong correlation between lattice distortions and the resistance of the manganites. The measured lattice distortions are of the order of a few picometers, significantly larger by an order of magnitude compared with volumetric measurements indicating a strong dynamic distortion which is most likely to have its origin in the Jahn-Teller effect. The data unambiguously points out the importance of lattice distortions in understanding the transport properties in the manganite system.

A similar measurement of the structural distortions in the high temperature superconductor also yields many surprising features. In Fig. 5 is shown the channeling FWHM reduced to displacement of lattice atoms (both static and dynamic effects being lumped together) for the Cu atoms and many interesting features are seen here also. The thermal vibrational amplitude estimated

from simple Debye theory does not fit the data well and seems to over estimate the vibrations seen. However, such estimates agree well with the experiment for the case of Cu, Y (or Er) and Ba for the case of non-superconducting samples, and in the case of superconducting samples the thermal vibrations of the Y (or Er) and Ba atoms simply follow the Debye theory as well. Thus, one has to conclude that either Debye theory does not apply to the Cu atoms only in the superconducting phase or that the Cu atoms do exhibit vibration anomalies that are associated with various transitions as a function of temperature in the superconducting solid. While a detailed analysis of this data is inappropriate for this review we would only like to point out that lattice distortions (both dynamic and static) are closely interrelated with observation of superconductivity in the high T_c cuprates [16].

4. Summary

While the Jahn-Teller debate for the manganite case may eventually shed some light for the high T_c cuprates one can speculate on the importance of these materials in general for technological applications, particularly in the area of sensors. If one ponders the role of sensors in technology and automation one can say that eventually one would like to replicate all the human sensory perceptions by devices employing an appropriate materials technology. This would imply the material to have reasonable sensitivity to the environment via different stimulations. While covalently bonded compounds such III–V materials or silicon tend to be less environmentally sensitive owing to the bond strength, the oxides tend to have significant ionicity of the bonds which makes them interesting for many of the sensor type applications. The system is more responsive to external perturbation such as pressure, fields, radiation, etc. making them ideal sensor materials. Thus, the field of sensors is where the largest impact of the metal–oxides is likely to be and here this system has more to offer than most other systems. Recent results of enhanced properties in harmonically integrated oxide structures [17] where the dielectric, ferroelectric and other properties are enhanced in layered superlattices of these oxides is another manifestation of the nature of the bonds in these oxides. Thus, the future for these materials looks very bright indeed both from a basic research and a technological view point.

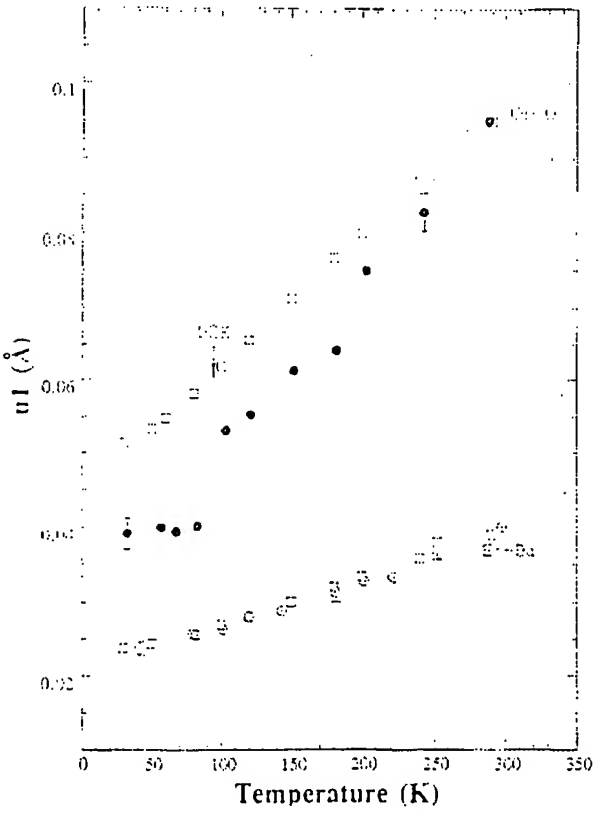

Fig. 5. The vibration amplitude as a function of temperature for Cu (●), Er and Ba (○) atoms in $ErBa_2Cu_3O_7$ as a function of temperature and comparison with simple Debye theory prediction (□) [16].

Acknowledgements

Much of the work was performed in collaboration with a large number of people at the University of Maryland and elsewhere and a partial list includes, R. Ramesh, R.L. Greene, S.M. Bhagat, D. Drew, S. Tyagi, S.B. Ogale, A. Raychaudhuri, J. Gopalakrishnan, C.M. Williams, S. Lakeou, J.M. Byers, M. Rubinstein, Q. Li, D. Dominguez, C. Kwon, M. Rajeswari, A.M. Dhote, J.L. Peng, X.X. Xi, H.L. Ju, S.E. Lofland, V. Talyansky, C.S. Chen, M.C. Robson, S.G. Kaplan, M. Quijada, G.C. Xiong, L. Senapathi, S.N. Mao, J.S. Ramachandran, R. Shreekala, S.I. Patil.

References

[1] T. Venkatesan, *Thin Solid Films*, *216* (1992) 52.
[2] O. Auciello and J. Engeman (eds.), *Multi-component and Multilayered Thin Films and Devices, NATO Advanced Study Institute Proceedings*, Kluwer, Dordrecht, 1993.
[3] D.K. Fork, J.M. Phillips, R. Ramesh and R. Wolf (eds.), *Epitaxial Oxide Thin Films and Hetrostructures, MRS Proceedings*, Vol. 341, MRS, Pittsburgh PA 15237, 1994.
[4] T. Venkatesan, in J.C. Miller (ed.), *Springer Series in Materials Science, Laser Ablation*, Vol. 28, Springer-Verlag, Heidelberg, 1994.
[5] G.K. Hubler and D.B. Chrisey (eds.), *Pulsed Laser Deposition of Thin Films*, Wiley, New York, 1993.
[6] S.E. Lofland, S.M. Bhagat, I. Takeuchi, Z. Trajanovic, P. Warburton, P. Ratnam and T. Venkatesan, *Solid State Commun.*, *94* (1995) 471.

[7] G.C. Xiaong, Q. Li, H. Ju, R.L. Greene and T. Venkatesan, *Appl. Phys. Lett.*, 66 (1995) 1427; G.C. Xiong, Qi Li, H.L. Ju, R.L. Greene and T. Venkatesan, *Appl. Phys. Lett.*, 67 (1995) 3031; T. Venkatesan, *Review on Colossal Magnetoresistive Films Prepared by Pulsed Laser Deposition, Proc. 12th Yokohama Twentieth Century Forum on Fullerenes and Laser Processing.*

[8] G.C. Xiong, S.M. Bhagat, Q. Li, M. Dominguez, H.L. Ju, R.L. Green, T. Venkatesan, J.M. Byers and M. Rubinstein, *Solid State Commun.*, 97 (1996) 599.

[9] D.L. Cox and M.B. Maple, *Phys. Today*, February (1995) 32.

[10] Various References in *Physical Properties of High Temperature Superconductors*, Vol. I–III, World Scientific, Singapore, 1989–1992.

[11] K. Derbyshire and E. Korczynski, *Solid State Technol.*, Sept. (1995) 57; G. Prinz and K. Hathaway (eds.), *Phys. Today*, Special Issue on Magnetoelectronics, April (1995).

[12] A.J. Millis, P.B. Littlewood and B.I. Shraiman, *Phys. Rev. Lett.*, 74 (1995) 5144; A.J. Millis, B.I. Shraiman and R. Mueller, Unpublished.

[13] C. Kittel, *Solid State Physics*, 6th edn., Wiley, New York, 1986, p. 409.

[14] W.K. Chu, J.W. Mayer and M. Nicolet, *Rutherford Backscattering Spectrometry*, Academic Press, New York, 1978; L.C. Feldman, J.W. Mayer and S.T. Picraux, *Materials Analysis by Ion Channeling*, Academic Press, New York, 1992.

[15] R.P. Sharma, G.C. Xiong, C.W. Kwon, R. Ramesh, R.L. Greene and T. Venkatesan, Unpublished.

[16] R.P. Sharma, L. Rehn, P.M. Baldo and J.Z. Liu, *Phys. Rev.*, B40 (1989) 4396.

[17] H. Tabata, H. Tanada and T. Kawai, *Appl. Phys. Lett.*, 65 (1994) 1970.

ELSEVIER

Physica C 282–287 (1997) 202–205

PHYSICA C

Oxygen isotope effects in the manganites and cuprates: Evidence for polaronic charge carriers

Guo-meng Zhao, M. B. Hunt, K. Conder*, H. Keller and K. A. Müller

Physik-Institut der Universität Zürich, CH-8057 Zürich, Switzerland

*Laboratorium für Festkörperphysik ETH Zürich, CH-8093, Switzerland

We present various oxygen-isotope effects in the manganites from magnetization and thermal-expansion measurements. We found that the ferromagnetic transition temperature T_C, the magnitude of the jump in the thermal-expansion coefficient $\Delta\beta(T_C)$ at T_C all depend strongly on the oxygen mass. Upon replacing ^{16}O with ^{18}O, T_C can be lowered by as much as 20 K, and $\Delta\beta(T_C)$ can be raised by about 20%. The observed novel isotope effects clearly demonstrate that charge carriers in these materials are strongly coupled to the local Jahn-Teller distortions, so that polarons are formed.

We also report the experimental evidence for polaronic supercarriers in the cuprate superconductors $La_{2-x}Sr_xCuO_4$. From magnetization and thermal-expansion measurements, we can quantitatively determine the oxygen-isotope effects on the in-plane penetration depth $\lambda_{ab}(0)$ and on the carrier density n. We find a negligible isotope effect on n, but a large effect on $\lambda_{ab}(0)$. Our results show that polaronic charge carriers exist and condense into Cooper pairs in the cuprate superconductors.

1. Oxygen isotope effects in the manganites

Recently, very large (colossal) magnetoresistance has been observed in the manganese-based perovskites $Ln_{1-x}A_xMnO_3$ (where Ln is a trivalent rare earth ion and A is a divalent alkali earth ion) [1,2]. Because of their unusual magnetic properties and potential applications, these materials have recently attracted intensive research interest. The physics in manganites has primarily been described by the double-exchange model [4,3]. However, Millis, Littlewood and Shraiman [5] have pointed out that double-exchange alone cannot fully explain the data of $La_{1-x}Sr_xMnO_3$. They proposed that lattice-polaronic effects due to strong electron-phonon coupling (arising from a strong Jahn-Teller effect) should be involved.

In most materials, magnetic phenomena at room temperature and below are essentially unaffected by lattice-vibrations because the electronic and lattice subsystems are decoupled according to the Born-Oppenheimer adiabatic approximation. The atoms can usually be considered as infinitely heavy and static in theoretical descriptions of the magnetic phenomena. However, this approximation would break down in compounds where there is a strong Jahn-Teller (JT) effect. Höck *et al.* [6] studied JT ions in a conductor within a linear chain model. They showed that small JT polarons can be formed when the JT stabilization energy is comparable with the bare conduction bandwidth. Polarons are not 'bare' charge carriers, but are carriers dressed by local-lattice distortions. In other words, the electronic and lattice subsystems are no longer decoupled, so one would expect that lattice vibrations should affect the electronic quantities, and thus there should be effects of varying isotope mass on some magnetic properties such as the ferromagnetic transition temperature T_C.

To be more specific, the polaronic nature of the conduction carriers can be demonstrated by the isotope effect on the effective bandwidth W_{eff} of polarons, which in turn depends on the isotope mass M [7]:

$$W_{eff} \propto W \exp(-\gamma E_b/\hbar\omega), \qquad (1)$$

where E_b is the binding energy of polarons, and is independent of the isotope mass M, γ is a

PII S0921-4534(97)00198-6

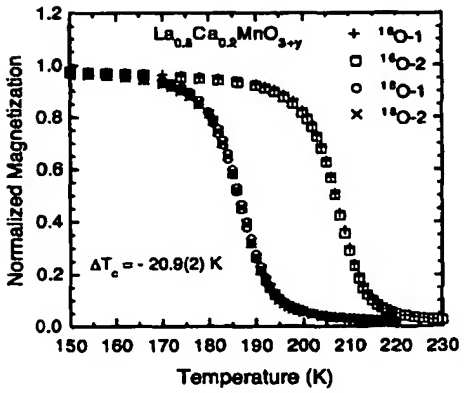

Figure 1. Oxygen isotope effect on the Curie temperature of $La_{0.8}Ca_{0.2}MnO_{3+y}$.

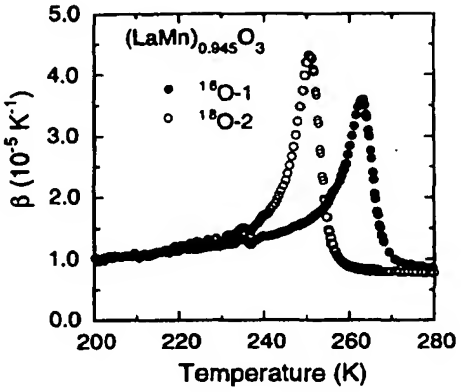

Figure 2. The linear thermal-expansion coefficient β(T) for the ^{16}O and ^{18}O samples of $(LaMn)_{0.945}O_3$.

dimensionless constant ($0 \leq \gamma \leq 1$) depending on E_b/W, ω is the characteristic frequency of the optical phonons ($\omega \propto 1/\sqrt{M}$). In the ferromagnetic manganites, it is easy to study the isotope effect on W_{eff}. This is due to the fact that in the strong-coupling limit, where the Hund's rule coupling J_H is very large compared to W_{eff} ($J_H \gg W_{eff}$), the Curie temperature $T_C \propto W_{eff}$ (Ref. [3,5]).

1.1. Giant oxygen-isotope shift of T_C in $La_{1-x}Ca_xMnO_{3+y}$

In Fig. 1 we show the magnetization (normalized to the magnetization well below T_C) for pairs of ^{16}O and ^{18}O samples of $La_{0.8}Ca_{0.2}MnO_{3+y}$ (i.e., 2 for each isotope). The detailed procedures for sample preparation and isotope exchange were described in Ref. [8]. For the ferromagnet $La_{0.8}Ca_{0.2}MnO_{3+y}$ with a strong JT effect, the ^{18}O samples have lower T_C's than the ^{16}O samples by ~21 K. On the other hand, no oxygen isotope effect on T_C could be detected in the ferromagnet $SrRuO_3$ with a negligible JT effect [8].

Since there is no oxygen-isotope effect on T_C in the ferromagnet $SrRuO_3$ with a negligible JT effect, the giant isotope effect observed in the Ca-doped ferromagnets is very likely related to the strong JT effect in this system. For a compound with a strong JT effect, the electron-phonon interaction is usually large, leading to the formation of JT polarons [6].

1.2. Oxygen-isotope effect on thermal expansion in the manganites

In Fig. 2 we show the linear thermal-expansion coefficient β(T) for the ^{16}O and ^{18}O samples of $(LaMn)_{0.945}O_3$. The thermal-expansion was measured using a capacitance dilatometer with a length resolution of ~0.1Å (Ref. [9]). The thermal-expansion coefficient has a sharp asymmetric peak at T_C, corresponding to a large thermal-expansion jump $\Delta\beta(T_C)$. It is surprising that the jump $\Delta\beta(T_C)$ depends strongly on the oxygen-mass; $\Delta\beta(T_C)$ for the ^{18}O sample is larger than that for the ^{16}O sample by 24(3)%. A similar isotope effect was also observed in $La_{0.67}Ca_{0.33}MnO_3$ (Ref.[9]). We also showed [9] that the T_C can be changed by varying either the Mn^{4+} concentration or the oxygen mass, while $\Delta\beta(T_C)$ can be varied only by changing the oxygen mass. This implies that the observed large oxygen-isotope effects on both T_C and the thermal-expansion jump are intrinsic.

The conventional theory of ferromagnetism cannot explain the oxygen-isotope effects observed here. In order to find an explanation,

we may relate $\Delta\beta(T_C)$ to the pressure effect ($d\ln T_C/dP$). If the ferromagnetic transition is of second order, then

$$d\ln T_C/dP = 3\Delta\beta(T_C)/\Delta C_P(T_C), \quad (2)$$

where $\Delta C_P(T_C)$ is the jump of the specific heat. From equation 2 we see that there must be a corresponding dependence of $d\ln T_C/dP$ on the oxygen mass M provided that $\Delta C_P(T_C)$ is independent of M. Indeed we showed that [9] $\Delta C_P(T_C)$ depends strongly on M.

2. Evidence for polaronic supercarriers in $La_{2-x}Sr_xCuO_4$

Now it is known that high-T_c superconductivity involves the pairing of charge carriers, forming spin-singlet Cooper pairs, but the precise nature of these carriers remains unclear. The cuprates are known to exhibit a strong Jahn-Teller effect which would lead to the formation of Jahn-Teller polarons [6]. Still, direct evidence that Jahn-Teller polarons exist in the superconducting state of the cuprates has been lacking, although some indirect evidence comes from their recent discovery [8] in the structurally similar but nonsuperconducting manganite $La_{1-x}Ca_xMnO_3$. Moreover, there has recently been increasing evidence that polaronic charge carriers are present in the normal-state of the layered cuprates [10,11]. However, it is not clear whether these normal-state polaronic carriers should condense into Cooper pairs. To show that this occurs, one has to demonstrate that the effective supercarrier mass along the CuO_2 planes (m^*_{ab}) depends strongly on ionic mass M in these layered cuprate superconductors.

Since the magnetic penetration depth $\lambda(0)$ is proportional to $\sqrt{m^*/n_s}$, then

$$\Delta m^*/m^* = 2\Delta\lambda(0)/\lambda(0) + \Delta n_s/n_s, \quad (3)$$

where Δ means any small change of a quantity upon isotope substitution. Thus the isotope dependence of m^* can be determined if one can independently measure the isotope dependences of $\lambda(0)$ and of n_s.

The isotope dependence of $\lambda(0)$ can be determined from that of the Meissner fraction $f(0)$ which, for decoupled and fine-grained samples, depends on the penetration depth $\lambda(0)$ and on the average grain radius R, as seen from the Shoenberg formula for spherical grains [12]:

$$f(T) = \frac{3}{2}[1-3(\frac{\lambda(T)}{R})\coth(\frac{R}{\lambda(T)})+3(\frac{\lambda(T)}{R})^2], \quad (4)$$

where $\lambda(T) = \sqrt[3]{[(\lambda_{ab}(T)]^2\lambda_c(T)}$ for layered compounds. From equation 4, one can see that a change in $\lambda(0)$ will lead to a change in $f(0)$, so the isotope dependence of $\lambda(0)$ can be determined from the isotope dependence of $f(0)$.

The isotope dependence of n_s should be equal to the isotope dependence of the normal carrier density n in clean superconductors. Since the structural phase transition temperature T_s (from the tetragonal to orthorhombic phase) in the $La_{2-x}Sr_xCuO_4$ system is very sensitive to n, a very small difference in n will lead to a huge difference in T_s. Thus the isotope dependence of n can be measured precisely if one can accurately determine the isotope shift of T_s. It has also been found that there is an anomaly at T_s in the thermal-expansion coefficient of this system [13]. Therefore the isotope shift of T_s can be precisely determined by a thermal-expansion measurement.

Fig. 3 shows the temperature dependence of the Meissner effect for the ^{16}O and ^{18}O samples of $La_{1-x}Sr_xCuO_4$ with $x = 0.105$. The results for other compositions were shown in Ref. [14,15]. The T_c of the ^{18}O sample is lower than that of the ^{16}O sample by ~1.5 K, and the low-temperature Meissner fraction of the ^{18}O sample is reduced by 6(1)% relative to the ^{16}O sample. This is in agreement with the result reported in Ref. [15], indicating the excellent reproducibility of these isotope experiments.

In Fig. 4 we show the linear thermal-expansion coefficient $\beta(T)$ for the another set of ^{16}O and ^{18}O samples of $La_{1.895}Sr_{0.105}CuO_4$, which shows the same oxygen isotope effects as the one shown in Fig. 3. One can see that there is an anomaly in $\beta(T)$ at a temperature of ~265 K (see arrow), which corresponds to the tetragonal-orthorhombic transition temperature T_s [13]. It is clear that the two curves nearly overlap, implying that the two isotope samples have the same T_s

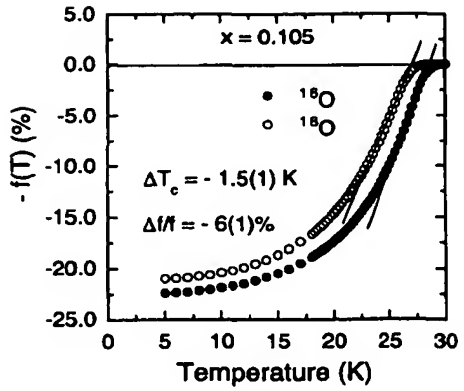

Figure 3. Temperature dependence of the Meissner effect for ^{16}O and ^{18}O samples of $La_{2-x}Sr_xCuO_4$ with $x = 0.105$.

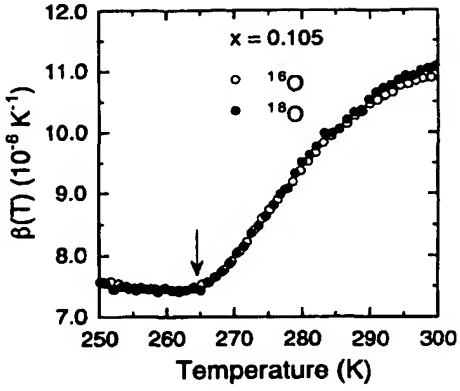

Figure 4. The linear thermal-expansion coefficient β(T) for the ^{16}O and ^{18}O samples of $La_{1.895}Sr_{0.105}CuO_4$.

within the uncertainty of our measurements ($\leq$0.3 K). In addition, we also showed [14] that $dT_s/dn \approx dT_s/dx = B = 2900$ K. Using $\Delta T_s \leq 0.3$ K and $n = 0.105$, we obtain $|\Delta n/n| = |(1/nB)\Delta T_s| \leq 0.1\%$. Thus, there is a negligible oxygen-isotope effect on n. Moreover, we have shown that the ratio of the normal-state susceptibilities (including a small Curie term contributed from some localized carriers) for the two isotope samples is temperature-independent down to a temperature near T_c. This implies that the two isotope samples must have the same mobile carrier concentration near T_c even if charge localization occurs. Since $n_s = n$ for clean superconductors, this result also implies that there is a negligible oxygen-isotope effect on the supercarrier density n_s.

The observed large oxygen-isotope effect on $f(0)$ and negligible effect on n_s imply that the effective supercarrier mass m^*_{ab} depends strongly on the oxygen mass. This suggests that polaronic charge carriers exist and condense into Cooper pairs in the cuprate superconductors. The quantitative data analysis can be seen in Ref. [14].

REFERENCES

1. S. Jin *et al.*, Science **264**, 413 (1994)
2. R. von Helmolt*et al.*, Phys. Rev. Lett. **71**, 2331 (1993)
3. P. W. Anderson, and H. Hasegawa, Phys. Rev. **100**, 675 (1955)
4. C. Zener, Phys. Rev. **82**, 403 (1951)
5. A. J. Millis *et al.*, Phys. Rev. Lett. **74**, 5144 (1995)
6. K.-H, Höck, H. Nickisch, and H. Thomas, Helv. Phys. Acta. **56**, 237 (1983)
7. A. S. Alexandrov, and N. F. Mott, Int. J. Mod. Phys. **8**, 2075-2109 (1994)
8. Guo-meng Zhao, K. Conder, H. Keller, and K. A. Müller, Nature **381**, 676 (1996)
9. Guo-meng Zhao, M. B. Hunt, and H. Keller, Phys. Rev. Lett. **78**, 955 (1997).
10. Proc. Int. Workshop on "Anharmonic Properties of High-T_c Cuprates", edited by D. Mihailowic, G. Ruani, E. Kaldis, and K. A. Müller (World Scientific, Singapore, 1994)
11. X. X. Bi, P. C. Eklund, Phys. Rev. Lett. **70**, 2625 (1993)
12. D. Shoenberg, Proc. R. Soc. London, Ser. A**175**, 49 (1940)
13. Y. Okajima, S. Hashimoto, and K. Yamaya, Physica C **235-240**, 1317 (1994)
14. Guo-meng Zhao, M. B. Hunt, H. Keller, and K. A. Müller, Nature **385**, 236 (1997)
15. Guo-meng Zhao *et al.*, Phys. Rev. B**52**, 6840 (1995)

Available online at www.sciencedirect.com
SCIENCE DIRECT®
Current Applied Physics 6 (2006) 964–968
Current Applied Physics
An official journal of the KPS
www.elsevier.com/locate/cap
www.kps.or.kr

Possible mutual percolation conductivity in perovskite oxides ☆

C.J. Zhang *, B.H. Kim, Y.W. Park

School of Physics and Nano Systems, Institute-National Core Research Center, Seoul National University, Seoul 151-747, Republic of Korea

Received 20 November 2004; accepted 30 January 2005
Available online 19 July 2005

Abstract

The transport properties of Mn doped cuprate oxide $La_{1.85-2x}Sr_{0.15+2x}Cu_{1-x}Mn_xO_4$ and Cu doped manganite oxide $La_{0.825}Sr_{0.175}Mn_{1-y}Cu_yO_3$ are investigated. In both series, the resistivity for the intermediate doping samples exhibits an anomalous decrease. We argue that in both systems, the Cu–O–Cu $pd\sigma$ path and the Mn–O–Mn double exchange path form mutual percolation paths and contribute to the conductivity. The resistivity data for both systems are fitted by using the mutual percolation model.

PACS: 75.30.–m; 74.25.Fy; 74.72.Dn

Keywords: Percolation conductivity; Transport properties; Perovskite oxide

The discoveries of high temperature superconductivity and the colossal magnetoresistance effect in perovskite oxides have stimulated considerable scientific and technological interest because of their exotic electronic and magnetic properties [1,2]. The parent materials, i.e., La_2CuO_4 and $LaMnO_3$, are both antiferromagnetic (AFM) insulator. Doping with bivalent cation Sr^{2+} for La^{3+} gives rise to rich magnetic and electronic phenomena. For instance, in $La_{2-x}Sr_xCuO_4$ the long-range AFM correlation is depressed with a small amount of Sr^{2+} doping, and it generates the superconductivity within doping level $0.06 \leqslant x \leqslant 0.26$. $La_{1-y}Sr_yMnO_3$ exhibits a metal-insulating (MI) transition associated with a ferromagnetic–paramagnetic (FM–PM) transition and CMR effect near the Curie temperature at doping level $0.17 \leqslant y \leqslant 0.5$. In both compounds, there is a similar $Cu(Mn)O_2$ conductive plane. It is suggested that the occurrence of the Cu–O–Cu superexchange interaction or the Mn–O–Mn double exchange interaction in the $Cu(Mn)O_2$ plane is closely related to the various electronic and magnetic properties in both compounds [3,4]. For typical superconductor $La_{2-x}Sr_xCuO_4$, the charge carriers are holes induced by the Sr doping, and the transport property is dominated by the $pd\sigma$ hybridization interaction between Cu–O–Cu in the CuO_2 plane. For the typical CMR oxide $La_{1-y}Sr_yMnO_3$, they are e_g electrons of Mn^{3+} ions, and the transport property is dominated by the double-exchange (DE) interaction between Mn^{3+}–O–Mn^{4+} in the MnO_2 plane. The similarity in composition and crystal structure of cuprate superconductor to the CMR materials led us to investigate how the magnetic properties would be changed if Cu (Mn) is partially replaced by Mn(Cu) in $La_{2-x}Sr_xCuO_4$ ($La_{1-y}Sr_yMnO_3$) system. In this paper we report the mutual percolation phenomenon in the intermediate doping samples in $La_{1.85-2x}Sr_{0.15+2x}Cu_{1-x}Mn_xO_4$ and $La_{0.825}Sr_{0.175}Mn_{1-y}Cu_yO_3$. This mutual percolation phenomenon may reveal some interplay of high temperature superconductors and CMR materials.

☆ Original version presented at QTSM&QFS 2004 (International Conference on Quantum Transport in Synthetic Metals and Quantum Functional Semiconductors), Gangwon-do, Korea, 20–23 November 2004.

* Corresponding author.
E-mail address: cjzhang@phya.snu.ac.kr (C.J. Zhang).

1567-1739/$ - see front matter © 2005 Elsevier B.V. All rights reserved.
doi:10.1016/j.cap.2005.01.048

Polycrystalline samples were synthesized by means of a conventional solid state reaction method using high-purity powders of La_2O_3, $SrCO_3$, MnO_2, and CuO. The mixed powders, pressed into pellets, were then reacted at 1150–1350 °C for 48 h under oxygen atmosphere. X-ray diffraction (XRD) analysis was carried out by a Rigaku-D/max-γA diffractometer using high-intensity CuKα radiation to screen for the presence of an impurity phase and the changes in structure. The lattice parameters were determined from the *d*-value of XRD peaks by a standard least-squares refinement method. Resistivity was measured using a standard four-probe method in a closed-cycle helium cryostat between 16 K and room temperature. For the $La_{0.825}Sr_{0.175}Mn_{1-y}Cu_yO_3$ series, we fixed the Sr concentration at 0.175 because at this Sr concentration the $La_{1-y}Sr_yMnO_3$ system exhibits a metal-insulator transition at room temperature [5,6].

Fig. 1 gives the temperature dependence of resistivity for $La_{1.85-2x}Sr_{0.15+2x}Cu_{1-x}Mn_xO_4$ samples. The temperature dependence of resistivity of $0.1 \leqslant x \leqslant 0.3$ samples exhibits typical semiconductor-like behavior. At low temperature, the resistivity increases rapidly with decreasing temperature. While in $x > 0.32$ samples, the resistivity exhibits different behavior. In detail, the resistivity only shows very little increase with decreasing temperature. At 20 K, the resistivity of $x \geqslant 0.32$ samples is three orders of magnitude smaller than that of $x = 0.3$ sample. The results of resistivity indicate that the transport mechanisms in $x < 0.3$ samples and $x > 0.32$ samples are absolutely different.

The temperature dependence of resistivity for $La_{0.825}Sr_{0.175}Mn_{1-y}Cu_yO_3$ shown in Fig. 2. In the doping range $0 \leqslant y \leqslant 0.32$, the resistivity increases rapidly with increasing x and decreasing temperature. But in the range $1/3 \leqslant y \leqslant 0.4$, the transport behavior is abnormal. The resistivity at room temperature decreases with increasing Cu doping when $y \geqslant 1/3$. These results also indicate that the transport mechanisms in $y < 0.32$ samples and $y > 1/3$ samples are absolutely different.

In both systems, the resistivity for the heavily doping samples exhibit an anomalous decrease. For the $La_{1.85-2x}Sr_{0.15+2x}Cu_{1-x}Mn_xO_4$ system, our previous study has suggested the coexistence of Cu–O–Cu $pd\sigma$ conductivity and Mn–O–Mn DE conductivity in the heavily doped samples [7]. The abnormal $\rho \sim T$ relations in the $La_{1.85-2x}Sr_{0.15+2x}Cu_{1-x}Mn_xO_4$ samples are due to the formation of Mn–O–Mn DE channels in the background of Cu–O–Cu $pd\sigma$ paths. On the other hand, the anomalous transport properties in the $La_{0.825}Sr_{0.175}Mn_{1-y}Cu_yO_3$ system can be explained by the formation of Cu–O–Cu $pd\sigma$ paths in the Mn–O–Mn DE background. The anomalous decrease of resistivity in both systems beyond a certain critical doping concentration can be treated as a percolation phenomenon. The

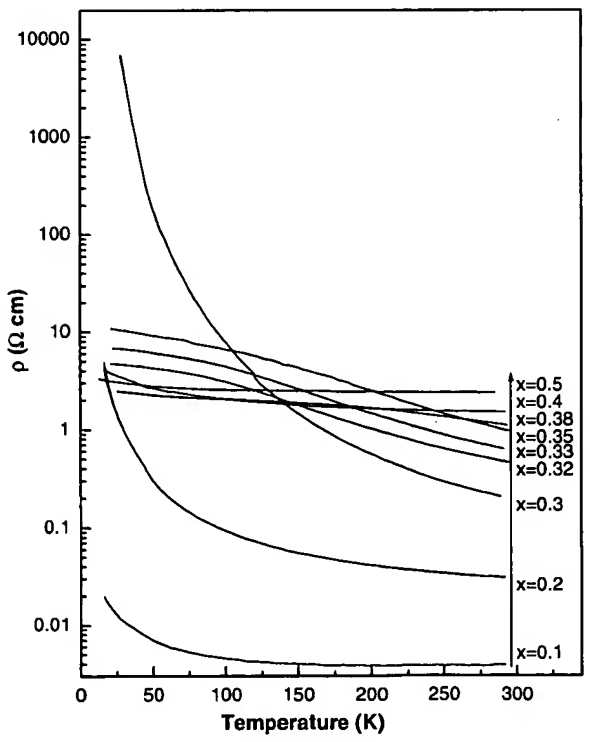

Fig. 1. The temperature dependence of resistivity for $La_{1.85-2x}Sr_{0.15+2x}Cu_{1-x}Mn_xO_4$.

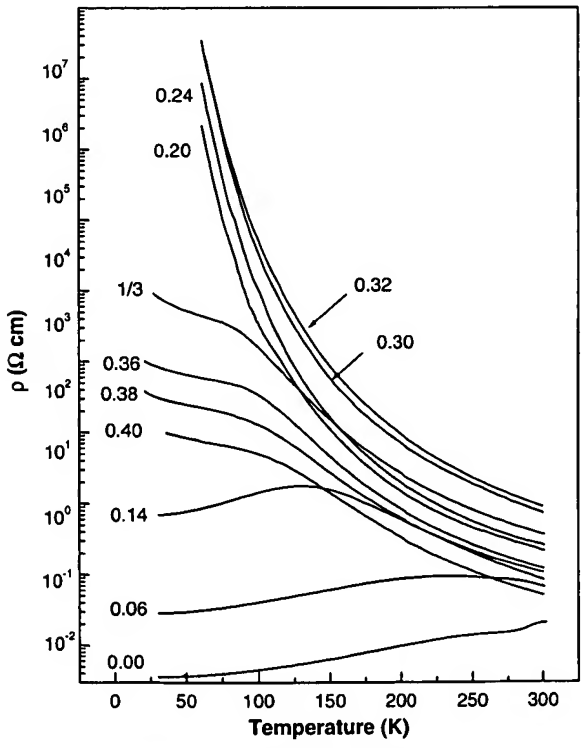

Fig. 2. The temperature dependence of resistivity for $La_{0.825}Sr_{0.175}Mn_{1-x}Cu_xO_3$.

critical doping concentrations $x_c = 0.3$ and $y_c = 0.32$ are the percolation threshold values of $La_{1.85-2x}Sr_{0.15+2x}Cu_{1-x}Mn_xO_4$ and $La_{0.825}Sr_{0.175}Mn_{1-y}Cu_yO_3$, respectively [8].

When the doping concentrations are lower than the threshold, the $\rho \sim T$ relations follow certain conduction rules. For the $La_{1.85-2x}Sr_{0.15+2x}Cu_{1-x}Mn_xO_4$ system, the introduction of magnetic ions Mn would not only induce the magnetic coupling between Mn and hole spins and form the so-called small polarons, but also introduce random magnetic potential and coulomb potential. We investigate the possibility of small polaron model and Mott's law of variable-range hopping (VRH) model for $0.10 \leqslant x \leqslant 0.3$ samples. It seems that the small polaron model does not fit the resistivity data well. According to the VRH model, the $\rho \sim T$ relation obeys the following rule:

$$\rho^{Cu} = \rho_0^{Cu} e^{(T_0^{Cu}/T)^{\alpha}} \tag{1}$$

We fit the $\rho \sim T$ curves according to this model using the exponent as $\alpha = 1/4$. The results are plotted as solid lines in Fig. 3(a). We find formula (1) nearly fit the $\rho \sim T$ curves of $0.10 \leqslant x \leqslant 0.3$ samples.

For $La_{0.825}Sr_{0.175}Mn_{1-y}Cu_yO_3$, the doping of Cu introduces random potential into the Mn–O–Mn background. In the range of $0.20 \leqslant y \leqslant 0.32$, we find that the resistivity can be fitted by VRH model (shown in Fig. 4(a))

$$\rho^{Mn} = \rho_0^{Mn} e^{(T_0^{Mn}/T)^{1/4}} \tag{2}$$

When the doping content is low, the carriers may be localized in the form of polarons. A lot of recent experimental results have given evidence of the existence of small polarons in the $La_{1-y}Sr_yMnO_3$ system [9,10]. We fit the resistivity of samples $y \leqslant 0.20$ using the small polaron model:

$$\rho^{Mn} = \rho_0^{Mn} T e^{E_c/kT} \tag{3}$$

For $x > x_c$ and $y > y_c$, the $\rho \sim T$ curves fit none of the above mentioned formulas. In these samples, the Cu–O–Cu conductive paths and the Mn–O–Mn conductive paths form mutual percolation paths and contribute to the total conductivity respectively. We analysis the $\rho \sim T$ curves for these samples based on the double percolation model. In $La_{1.85-2x}Sr_{0.15+2x}Cu_{1-x}Mn_xO_4$ system, the conductivity is dominated by the Cu–O–Cu paths when the Mn doping content is less than x_c, i.e., $x \leqslant x_c = 0.3$. With increasing Mn doping, the Cu–O–Cu paths are affected by the Mn impurity and the resistivity increases monotonously. When the Mn doping content is higher than x_c, the Mn–O–Mn paths form and conduct as percolation paths in the intermediate doping samples. On the other hand, one can convert the chemical composition of $La_{1.85-2x}Sr_{0.15+2x}Cu_{1-x}Mn_xO_4$ to $La_{-0.15+2x'}Sr_{2.15-2x'}Mn_{1-x'}Cu_{x'}O_4$ ($x' = 1-x$). When the Cu doping content x' in $La_{-0.15+2x'}Sr_{2.15-2x'}Mn_{1-x'}Cu_{x'}O_4$ is low, the resistivity in $La_{-0.15+2x'}Sr_{2.15-2x'}Mn_{1-x'}Cu_{x'}O_4$ would be dominated by the Mn–O–Mn paths and the Cu ion conducts as impurity. One can imagine that when the Cu doping content x' reach another critical percolation threshold x'_c, the Cu–O–Cu paths would form and conduct as percolation paths.

In order to fit the resistivity data using the mutual percolation model, we get $\rho(300\,K) \sim x$ relation for the $La_{1.85-2x}Sr_{0.15+2x}Cu_{1-x}Mn_xO_4$ from Fig. 1, as shown in Fig. 3(b), where solid circles represent the

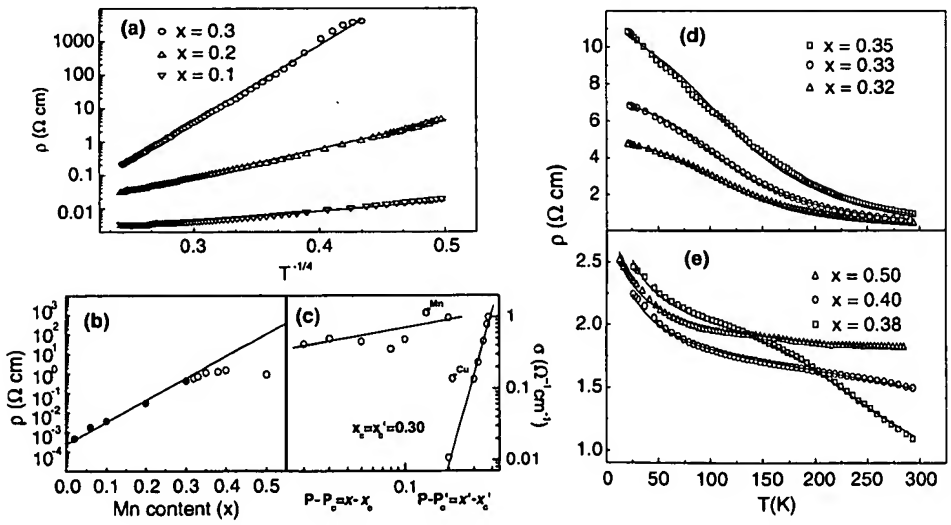

Fig. 3. (a) The fitting results of $\rho \sim T$ curves for $La_{1.85-2x}Sr_{0.15+2x}Cu_{1-x}Mn_xO_4$. (b) The $\rho(300\,K) \sim x$ relation for $La_{1.85-2x}Sr_{0.15+2x}Cu_{1-x}Mn_xO_4$ ($0.10 \leqslant x \leqslant 0.50$), where solid circles represent resistivity of $x \leqslant x_c$ and hollow circles larger than threshold. (c) $\sigma^{Mn} \sim (x-x_c)$ and $\sigma^{Cu} \sim (x'-x'_c)$ relations. (d) and (e) The fitting results of $\rho \sim T$ curves for $La_{1.85-2x}Sr_{0.15+2x}Cu_{1-x}Mn_xO_4$ ($0.32 \leqslant x \leqslant 0.50$).

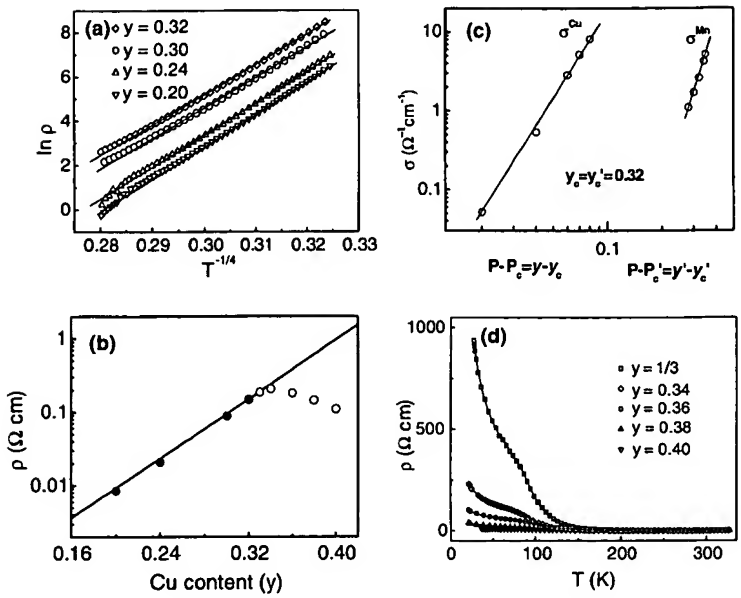

Fig. 4. (a) The fitting results of $\rho \sim T$ curves for $La_{0.825}Sr_{0.175}Mn_{1-y}Cu_yO_3$. The solid lines are fitting curves and the hollow symbols are experimental data. (b) $\rho(300\ K) \sim y$ relation for $La_{0.825}Sr_{0.175}Mn_{1-y}Cu_yO_3(0.20 \leqslant y \leqslant 0.40)$. (c) $\sigma^{Cu} \sim (y-y_c)$ and $\sigma^{Mn} \sim (y'-y_c')$ relations. (d) The fitting results of $\rho \sim T$ curves for $La_{0.825}Sr_{0.175}Mn_{1-y}Cu_yO_3$ $(1/3 \leqslant y \leqslant 0.40)$.

resistivity for $x \leqslant x_c$ and hollow circles represent the resistivity for $x > x_c$. With the increasing x, solid circles follow the exponent rule. According to this rule, we can get ρ^{Cu} and σ^{Cu} for the intermediate samples as an extrapolation of the experimental data. Supposing background resistivity and percolation resistivity are in parallel, the resistivity of the samples can be described as

$$\rho = \frac{\rho^{Cu}\rho^{Mn}}{\rho^{Cu} + \rho^{Mn}} \tag{4}$$

where ρ is the total resistivity for the intermediate doping samples, and $\rho^{Cu}(\rho^{Mn})$ is the resistivity contributed by the Cu–O–Cu (Mn–O–Mn) percolation paths. We use the experimental resistivity data of the intermediate samples as ρ in formula (4) and the extrapolation value in Fig. 3(b) as the ρ^{Cu}. Using formula (4) we can get the $\rho^{Mn}(\sigma^{Mn})$ value as the percolation resistivity of Mn–O–Mn paths in the intermediate doping samples. The $\sigma^{Mn} \sim (x-x_c)$ relation for the intermediate doping samples is shown in Fig. 3(c) (here $x_c = 0.3$ and $\sigma^{Mn} = 1/\rho^{Mn}$). On the other hand, we treat the ρ^{Cu} value in the intermediate samples as the percolation resistivity of Cu–O–Cu in $La_{-0.15+2x'}Sr_{2.15-2x'}Mn_{1-x'}Cu_{x'}O_4$. As $La_{1.85-2x}Sr_{0.15+2x}Cu_{1-x}Mn_xO_4$ and $La_{-0.15+2x'}Sr_{2.15-2x'}Mn_{1-x'}Cu_{x'}O_4$ have the same lattice, we think the percolation threshold value x_c' for the latter compound has the same value with the former one, i.e., $x_c' = x_c = 0.3$. We also plot the $\sigma^{Cu} \sim (x' - x_c')$ relation in Fig. 3(c). For the $La_{0.825}Sr_{0.175}Mn_{1-y}Cu_yO_3$ system, the results are shown in Fig. 4.

According to the percolation conduction rule [11], the conductivity contributed by the percolation paths would be:

$$\sigma = \sigma_0(p - p_c)^t \tag{5}$$

where p is the percolation probability and p_c is the percolation threshold. We convert the p and p_c in formula (5) into the doping concentration x and x_c, and modify formula (5) to

$$\lg(\sigma) = \lg(\sigma_0) + t\lg(x - x_c) \tag{6}$$

According to formula (6), the $\lg(\sigma) \sim \lg(x-x_c)$ relation for the percolation paths should exhibit linear behavior. That is the case in Figs. 3(c) and 4(c).

In the intermediate doping samples, each percolation paths follow their own conductive rules and contribute to the strange $\rho \sim T$ behaviors. For $La_{1.85-2x}Sr_{0.15+2x}Cu_{1-x}Mn_xO_4$ system, the $\rho \sim T$ for $0.38 \leqslant x \leqslant 0.50$ samples show different behavior comparing to that of $0.32 \leqslant x \leqslant 0.35$ samples. For the group of $0.32 \leqslant x \leqslant 0.35$, ρ^{Cu} and ρ^{Mn} in formula (4) are according to formula (1) and (2), respectively. When $0.38 \leqslant x \leqslant 0.50$, the σ increases quickly, which indicates that the small polaron conductive formula (3) is reasonable. Using formula (1), (2) and (4) to fit the $\rho \sim T$ data of $0.32 \leqslant x \leqslant 0.35$, the results are plotted in Fig. 3(d). Using formula (1), (3) and (4) to fit the $\rho \sim T$ data of $0.38 \leqslant x \leqslant 0.5$, the results are plotted in Fig. 3(e). The fitting results are in good accordance with the experimental data. For $La_{0.825}Sr_{0.175}Mn_{1-x}Cu_xO_3$ system, formula (1), (3) and (4) fit the experimental $\rho \sim T$ data, the

results are plotted in Fig. 4(d). The theory is in good accordance with the experiments.

In summary, it exhibits anomalous $\rho \sim T$ behaviors in the intermediate doping range of $La_{1.85-2x}Sr_{0.15+2x}Cu_{1-x}Mn_xO_4$ and $La_{0.825}Sr_{0.175}Mn_{1-x}Cu_xO_3$ as well. For the resistivity results, theoretical analysis and experimental fit point out that the Cu–O–Cu $pd\sigma$ paths and the Mn–O–Mn double exchange paths are interdiffused percolation paths in both systems. We suggest that there is a mutual percolation process in doped perovskite oxides.

Acknowledgement

This work was supported by the National Research Laboratory program under contract no. M1-0104-00-0023 and partially supported by the BK21 for C. J. Zhang.

References

[1] J.G. Bednorz, K.A. Muller, Z. Phys. B 64 (1986) 198.
[2] R. Von Helmolt, J. Wecker, B. Holzapfel, L. Schultz, K. Samwer, Phys. Rev. Lett. 71 (1993) 2331.
[3] P.W. Anderson, Science 235 (1987) 1196.
[4] A.J. Millis, P.B. Littlewood, B.J. Shraiman, Phys. Rev. Lett. 74 (1995) 5144.
[5] A. Urushibara, Y. Moritomo, T. Arima, A. Asamitsu, G. Kido, Y. Tokura, Phys. Rev. B 51 (1995) 14103.
[6] A. Asamitsu, Y. Moritomo, Y. Tomioka, T. Arima, Y. Tokura, Nature (London) 373 (1995) 407.
[7] Yi Yin, Changjin Zhang, Li Pi, Yuheng Zhang, Phys. Rev. B 65 (2004) 024407.
[8] J.C. Dyre, T.B. Schrøder, Rev. Mod. Phys. 72 (2000) 873.
[9] G. Jeffrey Snyder, C.H. Booth, F. Bridges, Ron Hiskes, Steve Dicarolis, M.R. Beasley, T.H. Geballe, Phys. Rev. B 55 (1997) 6453.
[10] D.C. Worledge, L. Mieville, T.H. Geballe, Phys. Rev. B 57 (1998) 15267.
[11] D. Stauffer, A. Aharony, Introduction to Percolation Theory, second ed., Taylor and Francis, London, 1992.

ELSEVIER

Physica B 252 (1998) 186–197

PHYSICA B

Pseudo-Jahn-Teller-centers and phase separation in the strongly correlated oxides with the nonisovalent substitution. Cuprates and manganites

A.S. Moskvin*

Department of Theoretical Physics, Ural State University, 620083, Ekaterinburg, Russian Federation

Received 28 November 1997

Abstract

We introduce briefly the principal ideas of a new model approach to the strongly correlated oxides like cuprates ($YBa_2Cu_3O_{6+x}$, $La_{2-x}Sr_xCuO_4$, $La_2CuO_{4+\delta}$, ...), manganites ($La_{1-x}Sr_xMnO_3$, ...), nickellates ($La_2NiO_{4+\delta}$), bismuthates ((K, Ba)BiO_3) as systems where the nonisovalent substitution promotes the local disproportionation reaction with the formation of the polar (electron and hole) pseudo-Jahn-Teller (PJT) centers phase being a system of the local singlet or triplet bosons moving in a lattice of the hole PJT centers.

The unconventional properties of the substituted strongly correlated oxides are connected with an active interplay of the charge, spin, orbital and local structural (or PJT) modes taking account of the strong charge inhomogeneity, multi-granularity, static and dynamic phase separation and percolation phenomena.

PACS: 71.27. + a

Keywords: Strongly correlated systems; Cuprates; Manganites

1. Introduction

Unconventional properties of the oxides like $YBa_2Cu_3O_{6+x}$, $La_{2-x}Sr_xCuO_4$, (K,Ba)BiO_3, $La_{1-x}Sr_xMnO_3$, $La_2CuO_{4+\delta}$, $La_2NiO_{4+\delta}$, including systems with high-T_c superconductivity and colossal magnetoresistance reflect a result of the response of the system to the nonisovalent substitution that stabilizes the intermediate valence phases providing the most effective screening of the charge inhomogeneity. These phases in oxides can involve novel molecular cluster configurations like the Jahn-Teller sp-center [1] (see Table 1) with anomalously high local polarizability. In Table 1 we present some examples of such centers for the oxides unstable with respect to the disproportionation reaction like

$$M + M \rightarrow M^+ + M^-,$$

where M is a basic metal–oxygen center (CuO_4^{6-}, NiO_4^{6-}, MnO_6^{9-}, BiO_6^{8-}, respectively), the

* Corresponding author. Fax: + 7 3432 615 978; e-mail: alexandr.moskvin@usu.ru.

0921-4526/98/$ – see front matter
PII: S0921-4526(98)00155-0

Table 1

	s	p	s^2	sp
Cuprates (D_{4h})	$\underline{b}_{1g}(Cu^{2+})$	$\underline{e}_u$	$\underline{b}_{1g}^{*2}: {}^1A_{1g}(Cu^{3+})$	$\underline{b}_{1g}^{*}\underline{e}_u^{*}: {}^{1,3}E_u$
Nickellates (D_{4h})	$\underline{b}_{1g}\underline{a}_{1g}: {}^3B_{1g}(Ni^{2+})$	$\underline{a}_{1g}\underline{e}_u: {}^{1,3}E_u$	$\underline{b}_{1g}^{*2}\underline{a}_{1g}^{*}: {}^2A_{1g}(Ni^{3+})$	$\underline{b}_{1g}^{*}\underline{a}_{1g}^{*}\underline{e}_u^{*}: {}^{2,4}E_u$
Manganites (O_h)	$t_{2g}^3e_g: {}^5E_g(Mn^{3+})$	$t_{2g}^4e_g\underline{t}_{2u}: {}^{3,5}\Gamma_u$	$t_{2g}^{*3}: {}^4A_{2g}(Mn^{4+})$	$t_{2g}^{*}\underline{t}_{2u}^{*}: {}^{2,4}T_{2u}$
Bismuthates (O_h)[a]	$\Xi_0 6s^2: A_{1g}(Bi^{4+})$	$\Xi_0 6s^2\underline{t}_{1u}: {}^2T_{1u}$	$\Xi_0: {}^1A_{1g}(Bi^{5+})$	$\Xi_0: 6s^{*}\underline{t}_{1u}^{*}: {}^{1,3}T_{1u}$

[a] Ξ_0 is a molecular core with completely filled shells.

$M^{\pm}$ centers are the corresponding polar (hole and electron) centers. All these oxides are the so-called charge transfer semiconductors, where a fundamental absorption band is determined by the charge transfer $s \rightarrow p$ transition from the nondegenerate and predominantly metallic even s-state to the low lying degenerate and predominantly oxygen odd p-state. An ionization or a hole doping for the sp-like M center can be accompanied by the quasi-degeneracy effect: a hole can be localized either at the predominantly metallic (s) or at the predominantly oxygen (p) molecular orbital with competition of the two configurations, s^2 and sp, respectively. As a result, we have for the hole center M^- a ground manifold of the terms with different parity, spin multiplicity and orbital degeneracy providing a multi-mode behavior of such centers. First of all these are unstable with respect to the pseudo-Jahn-Teller (PJT) effect [2] with active even and odd local displacement modes of different symmetry and to a formation of the appropriate vibronic states [3,4]. A common feature of the hole PJT centers listed in Table 1 is the appearance of a nonzero electric dipole moment and nonquenched orbital moment with an appropriate magnetic moment.

The hole PJT center with its high polarizability can be a center of an effective local pairing with a formation of the local singlet (e.g. cuprates) or triplet (e.g. manganites) boson as two electrons paired in molecular shell. Thus we come to the electron PJT center: $M^- = M^+ +$ (local boson). A local boson can correspond to the completely filled molecular shell with the ${}^1A_{1g}$ symmetry (e.g. b_{1g}^2 for the cuprates and nickellites, $6s^2$ for the bismuthates) or to the half-filled molecular shell, e.g. e_g^2 with the ${}^3A_{2g}$ symmetry in the manganites. Two polar centers can have a similar structure of the ground manifold. It is worth to notice that the PJT nature of the polar centers results in a strong (vibronic) reduction of the disproportionation reaction probability.

As a whole, the oxides under consideration can be called *the strongly correlated PJT oxides.*

For the CuO_4 center based strongly correlated copper PJT oxides the nonisovalent substitution can promote a disproportionation reaction

$$2CuO_4^{6-} \rightarrow [CuO_4^{5-}]_{JT} + [CuO_4^{7-}]_{JT}$$

with the creation of the system of the polar (the hole CuO_4^{5-} or the electron CuO_4^{7-}) PJT centers [3,4]. These centers are distinguished by the local spinless boson or by two electrons paired in the completely filled molecular orbital of the CuO_4 cluster. New phase can be considered as a system of the local bosons moving in the lattice of the hole PJT centers or as the generalized quantum lattice bose-gas. An origin and anomalous properties of the PJT centers are driven by a near degeneracy of the molecular terms ${}^1A_{1g}$ (Zhang–Rice singlet), ${}^1E_u$, ${}^3E_u$ (Fig. 1) for the configurations b_{1g}^2 and $b_{1g}e_u$, respectively, that can create conditions for the PJT effect with the active local displacement modes of the Q_{e_u}, $Q_{b_{1g}}$ ($Q_{b_{2g}}$) types [2–4]. In other words, a formation of the PJT center in copper oxides is initiated by the sharp correlational decrease in the energy of the $b_{1g} - e_u$ transition that determines the fundamental absorption band for the parent cuprates.

As an important indication to the disproportionation reaction with the occurrence of the local bosons one can consider a reveal of the high

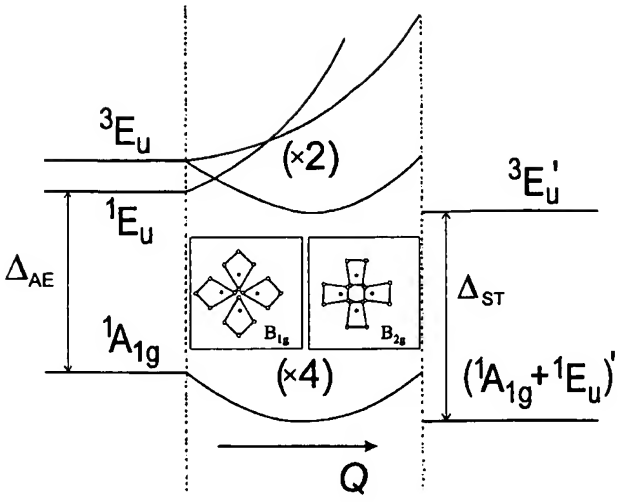

Fig. 1. A ground state manifold for the polar PJT center in the CuO_2-plane with an illustration of the PJT effect and the possible ground state JT modes. The four types of distortion isomers of the CuO_4 clusters corresponding to the four minima of the ground state adiabatic potential are schematically depicted in the insets for the B_{1g} and B_{2g} symmetry types, respectively.

temperature ($T \leqslant 1000$ K) carriers with the charge $q = 2e$ for a number of the CuO_4 clusters based oxides [5].

2. Correlations and the near degeneracy effects for the CuO_4 clusters in high T_c copper oxides

At first sight an analysis of the electronic structure and of the energy spectrum of the parent compounds such as $La_{2-x}M_xCuO_4$, $YBa_2Cu_3O_{6+x}$ at $x = 0$ does not display any exotic peculiarities except quasi two-dimensional antiferromagnetism determined by the strong exchange interaction for the $b_{1g}(d_{x2-y2})$ holes in the "basic" CuO_4^{6-} clusters. At the same time it is worth to pay attention to one important feature, namely to the "exciton-band" form of the fundamental absorption in the 1.5–3.0 eV region strongly pronounced in systems like R_2CuO_4 (R = La, Nd, Eu, Gd), $YBa_2Cu_3O_{6+x}$, CuO [6–8].

A peculiar character of the absorption connected with the allowed charge-transfer transition $b_{1g} \rightarrow e_u$ between the copper–oxygen b_{1g} hybrid and the purely oxygen e_u orbital (see Fig. 2) evidences the strongly correlated nature of the e_u-electrons with formal existence of two types of the e_u-states with and without strong correlation. This peculiarity is connected with the fact that maximal hole density occurred for oxygen ions just in the e_u-states of the

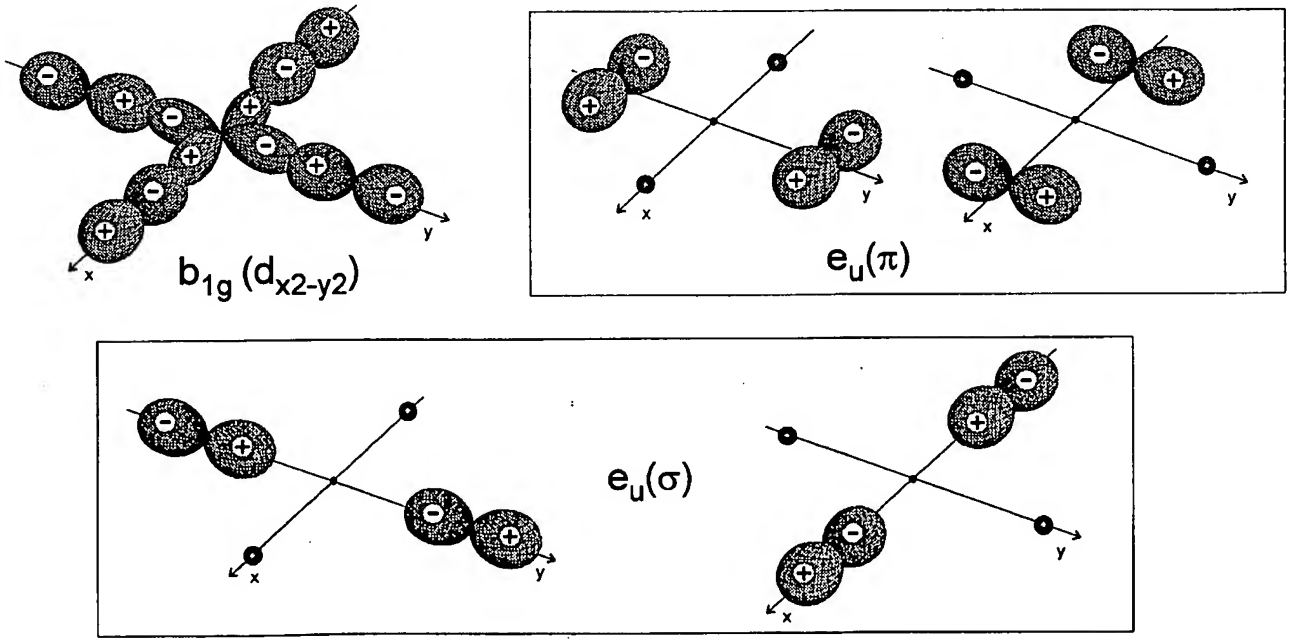

Fig. 2. Angular distribution of the electron (hole) density for the hybrid $Cu_{3d}O_{2p}$-$b_{1g}(d_{x2-y2})$ and for two types of the purely O_{2p}-e_u states.

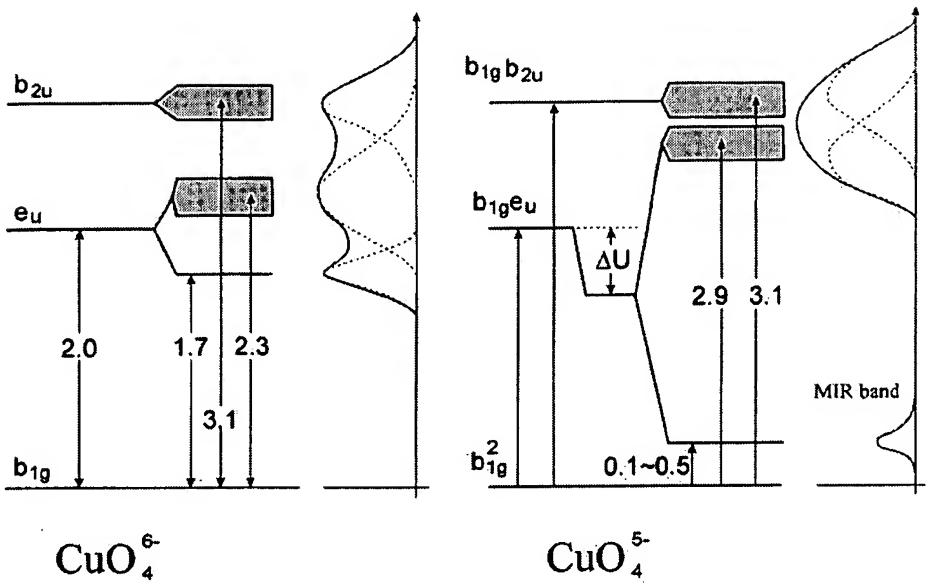

Fig. 3. Correlation effects in the energy spectrum of the basic CuO_4^{6-} cluster and the hole CuO_4^{5-} center with numerical values (in eV) typical for oxides like CuO. On the right hand side, we show a formation of the fundamental absorption spectra for the parent and hole doped oxides with peculiar MIR band in the latter case.

CuO_4 cluster and can be easily explained in the framework of the non-rigid anionic background model [9]. This model introduces a new "correlation" degree of freedom with two possible states of anionic background for the valent O_{2p}-holes corresponding to two possible projections of the correlation pseudospin $s = \frac{1}{2}$ and is described by the simplified Hamiltonian

$$H_{\text{corr}} = V_1\hat{\sigma}_x + V_3\hat{\sigma}_z, \tag{1}$$

where $V_{1,3}$ are the operators acting within the valence states. Simple approximation used in [9] conjectures the linear n_{2p}-dependence for $V_{1,3}$, where n_{2p} is the O_{2p}-hole number. According to the optical data [6–8] the correlation pseudospin splitting for the CuO_4^{6-} cluster can attain the value ~ 0.5 eV. It is worth to mention that the model by Hirsch [9] results in a formal doubling of the molecular orbitals, in particular, we have two types of the orthogonal (!) b_{1g} (upper correlational sublevel) and b_{1g}^* (lower correlational sublevel) states distinguishing by the correlational pseudospin projection.

An increase in the O_{2p}-hole concentration with the hole doping $CuO_4^{6-} \rightarrow CuO_4^{5-}$ results in a sharp increase of the e_u-correlational splitting in the hole CuO_4^{5-} centers.

Fig. 3 shows qualitatively the results of the taking account of the considered "e_u-correlation" for the energy spectrum of the basic CuO_4^{6-} cluster and the hole CuO_4^{5-} cluster with numerical estimates typical for the simplest cuprate CuO [3,8].

Thus we come to a conclusion about a near-degeneracy for two configurations b_{1g}^{*2} and $b_{1g}^*e_u^*$ with b_{1g}^* and e_u^* being a lowest correlational sublevels. This result does not drastically change upon taking into account an electrostatic interaction V_{ee} between two holes. Moreover, just the V_{ee} contribution was considered earlier [3] as the main reason for a near degeneracy of $^1A_{1g}$ (Zhang–Rice singlet) and $^{1,3}E_u$ terms formed by b_{1g}^{*2} and $b_{1g}^*e_u^*$ configurations. So, both the correlation effects lead to a near degeneracy in the ground state of the hole center CuO_4^{5-} with possible PJT resulting in a formation of the hole PJT center $[CuO_4^{5-}]_{JT}$.

Unusual properties of the $^1A_{1g}$,$^{1,3}E_u$ manifold involving terms distinguished by the spin multiplicity, parity and orbital degeneracy provide an unconventional behavior for the hole PJT center $[CuO_4^{5-}]_{JT}$ with an active interplay of various modes. This center can be considered as a center of

the effective electron pairing or the local boson condensation within a formally empty b_{1g}^2 configuration. The hole PJT center with the local singlet boson represents an unconventional electron PJT center $[CuO_4^{7-}]_{JT}$ which is essentially distinguished from the "primitive" CuO_4^{7-} center considered as a nondegenerate system with the completely filled Cu 3d and O 2p shells.

A transfer from the hole to the electron PJT center (charge fluctuation) as an addition of the completely filled shell in general cannot be accompanied by the crucial change of the electronic structure and could result only in the change of the local "bare" parameters such as A–E-separations $\Delta_{AE} = E(^1E_u - E(^1A_{1g}))$, or singlet–triplet separation $\Delta_{st} = E(^3E_u - E(^1E_u)$ (see Fig. 1) right up to the full reversal of the ground JT-mode ($E_uB_{1g} \leftrightarrow E_uB_{2g}$). In other words, the charge fluctuations in the PJT centers phase in general should be strongly coupled with the local spin and structural fluctuations that result in a remarkably complicated multimode behavior.

Main hopes to the direct demonstration of the validity of the above model are connected with a revealing of the isolated PJT center. In this connection we refer to the recent paper [10] whose authors have performed the NQR study of the hole centers CuO_4^{5-} in $La_2Cu_{0.5}Li_{0.5}O_4$. Their results can be interpreted as convincing evidence of the singlet–triplet PJT structure of the hole center. This conclusion is based on the following:

1. The authors have revealed the spin singlet ground state (S = 0) and the low lying spin triplet state (S = 1) with the singlet–triplet separation $\Delta_{ST} = 0.13$ eV.
2. They observed anomalous weak temperature dependence of the relaxation rate at low temperatures which proves the occurrence of the spinless multiplet structure in the CuO_4^{5-} cluster ground state.
3. They have revealed an appreciable spin contribution to the low temperature relaxation indicating the simultaneous occurrence of the ground state multiplet structure, the sufficiently low singlet–triplet separation and the intrinsic singlet–triplet spin–orbital mixing.
4. They observed the relaxation inequivalence of the various Cu sites quite natural for the PJT centers in the conditions of the static Jahn-Teller effect.

We think that further investigations of this system can provide valuable information about PJT centers.

In our opinion direct evidence for the Jahn–Teller nature of the PJT centers with active role of the copper–oxygen hybrid Q_{eu}-mode was displayed by the maximum entropy method (MEM) in $YBa_2Cu_3O_{6+x}$ at $x \approx 1$ [11]. The authors observed the characteristic squarish deformation of the nuclear density for the Cu atom in the CuO_2 plane due to the anomalous strong anharmonic low temperature ($T = 15$ K) thermal motion.

A situation similar to cuprates can be realized in other oxides. In Table 1 we list some examples of the sp-like basic M centers and the appropriate hole M^- centers for the PJT cuprates, nickellates, bismuthates and manganites.

A nonisovalent substitution $La^{3+} \rightarrow Ca^{2+}, Sr^{2+}, \ldots$ in the rare earth manganites like $LaMnO_3$ can result in a disproportionation reaction

$$2MnO_6^{9-} \rightarrow [MnO_6^{8-}]_{JT} + [MnO_6^{10-}]_{JT}$$

with the formation of the unconventional PJT analogues of the conventional Mn^{4+} and Mn^{2+} ions, respectively. It is worth to mention that these ions in most of the known weakly covalent and weakly correlated insulators are considered as usual S-type ions with an orbitally nondegenerate ground term. For the hole PJT center $[MnO_6^{8-}]_{JT}$ we have to deal with the quasi-degeneracy of the conventional even $t_{2g}^3 : {}^4A_{2g}$ configuration and the charge transfer odd configuration $t_{2g}{}^4\underline{t}_{2u} : {}^{2S+1}\Gamma_u$, where $\underline{t}_{2u}$ is a purely oxygen odd hole state.

Unusual properties of the $4A_{2g}, {}^{2S+1}\Gamma_u$ manifold with terms distinguished by the spin multiplicity, parity and orbital degeneracy provide an unconventional behavior for the hole PJT centers with an active interplay of various modes. This center with its high polarizability can be the center of an effective local pairing. An appropriate electron PJT center $[MnO_6^{10-}]_{JT}$ will be distinguished by the appearance of two electrons coupled within e_g-shell

with the formation of the triplet local boson (e_g^2-configuration with the $3A_{2g}$ symmetry).

So, the manganites $LaMnO_3$ can be considered as systems unstable with respect to the disproportionation with the formation of the PJT centers phase being a system of local triplet bosons moving in a lattice of the PJT centers $[MnO_6^{8-}]_{JT}$. Generally speaking, we deal with a complicated multi-component strongly correlated quantum bose-liquid with the hybrid charge–spin-local structure eigenmodes. As a result we conjecture the appearance of a wide spectrum of the low energy excitations.

It seems that an existence of two types of the PJT centers, of hole and electron, should be easily detected by various resonance methods especially by such local probes as NMR or NQR. However, for real situations, it is necessary to take account of the local boson movement and the life times of the polar centers. For instance, the shape of the metal or oxygen nuclear resonance spectrum for the PJT centers phase can be described by a "bi-lorentzian" like [12]

$$I(\omega, \Omega) = \frac{W_e W_h(\omega_e - \omega_h)^2(\tau_e + \tau_h)\tau_e\tau_h}{[\tau_e\tau_h(\omega-\omega_e)(\omega-\omega_h)]^2 + [\tau_e(\omega-\omega_e)+\tau_h(\omega-\omega_h)]^2}, \quad (2)$$

where W_i is the probability to find a nucleus within the electron or hole JT-center, τ_i and $\omega_i = \Omega + \Delta_i$ are the life time and the resonance frequency for the corresponding centers, respectively. As usual, the frequency Ω is randomly distributed near the mean value $\langle\Omega\rangle = \omega_0$, thus the spectrum shape is obtained by averaging $I(\omega,\Omega)$ with the Gaussian distribution of Ω:

$$S(\omega) \propto \int I(\omega,\Omega)\exp[-(\Omega-\omega_0)^2/2\sigma^2]\,d\Omega. \quad (3)$$

Depending on the life time values we can obtain both two well separated lines for the electron and hole centers, respectively, and one more or less asymmetric line. It seems that such a situation is exhibited both in cuprates [12] and manganites [13].

3. Classical and quantum phase separation in strongly correlated PJT oxides with the nonisovalent substitution

An optimal way to the formation of the PJT centers phase or the initiation of the disproportionation reaction in a parent system like La_2CuO_4, $YBa_2Cu_3O_6$, $LaMnO_3$, La_2NiO_4 is to create charge inhomogeneity by nonisovalent chemical substitution including interstitial atoms and vacancies. This process results in an increase of the energy of the parent phase and creates proper conditions for its competition with other phases capable of providing an effective screening of the charge inhomogeneity potential. The strongly degenerate PJT centers phase is one of the most favorable ones for this purpose. At the beginning (nucleation regime) a new phase appears in the form of the so-called CI (charge inhomogeneity) center as a kind of peculiar quasi-atom with a charge inhomogeneity source as a nucleus and with a certain number of the neighboring PJT centers forming the boson shells. In general, the CI center can be considered as a region of the pinning of the certain multi-mode ground or excited state with a different relationship between the potential and kinetic contributions to the total energy providing the localized or delocalized boson states, respectively.

As one of the recent remarkable experimental indications to the formation of the CI centers in the cuprates note the zero field copper NMR data in $Y_{1-x}Ca_xBa_2Cu_3O_6$ by Mendels et al. [14]. The nonisovalent substitution in the antiferromagnetic state was accompanied by the anomalous decrease in the concentration of the NMR resonating copper nuclei: every Ca^{2+}-ion excluded from the NMR about 50 copper ions (!), that could be connected with their disproportionation within the CI center.

A parent phase and a novel PJT centers phase can coexist in the phase separated or "underdoped" regime. At different stages of this "chemical" phase separation regime we have to deal with the isolated CI centers, with the percolation effect and finally with a complete removal of the parent phase (see Fig. 4). This situation results in many unconventional properties of the copper oxides with the CI centers including a possible coexistence of the

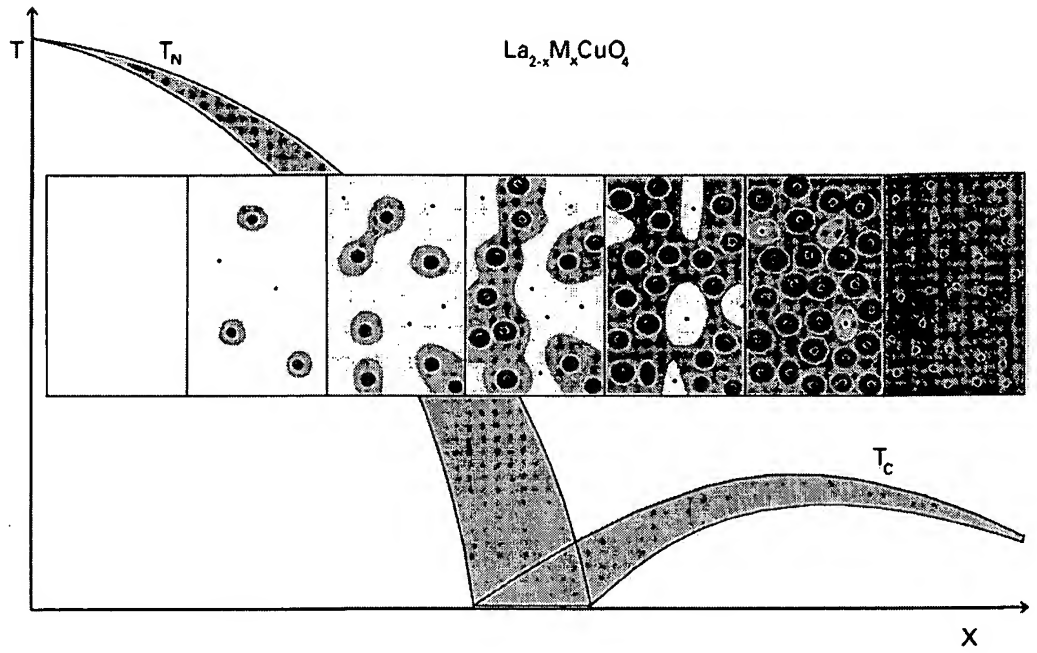

Fig. 4. An illustration to the phase separation and percolation phenomena within the CuO_2-planes for the cuprates like $La_{2-x}M_xCuO_4$. A part of the phase diagram T_N-x and T_C-x is schematically sketched. A novel metallic-superconducting phase is shown as an inhomogeneous one.

spatially separated antiferromagnetism and superconductivity [15], an appearance of the specific effects connected with the interphase boundaries displacement accompanied by a change in the relative phase volume [16], percolation phenomena, etc.

Above we considered a "classical" (static or dynamic) regime of the phase separation with a coexistence of the spatially separated thermodynamic phases which was really observed, for instance, in the cuprate $La_2CuO_{4+\delta}$ [15]. For the oxides under consideration it is possible to consider a "physical" phase separation including a "quantum" regime of the phase separation as a new version of the intermediate valence state with an appearance of the local regions with the quantum superposition of the parent and the polar PJT centers phase ("quantum disproportionation") like

$$\Psi(2CuO_4) = c_1\Psi(2CuO_4^{6-}) + c_2\Psi(CuO_4^{5-} + CuO_4^{7-}), \quad (4)$$

where $c_{1,2}$ are the appropriate quantum amplitudes. A most probable correlation length for the quantum phase separation state is of nanoscopic scale.

For the inhomogeneous systems with a set of multi-component order parameters the ground state can represent a strongly fluctuating quantum liquid as a result of a dynamic equilibrium of the fluctuations of the different phases (including the parent phase) characterized by the corresponding life time and correlation length. As a specific particular case this "dynamic phase separation" regime includes a "static phase separation" regime with coexistence of two phases in the region of the first order phase transition. For such systems we have to consider different multigranularity effects and percolation phenomena.

The above viewpoint on the phase separation phenomena is generally compatible with the pioneer ideas for the cuprates by Emery and Kivelson [17] and some other model approaches. So on the basis of the neutron scattering data Egami [18] conjectured the appearance of a nano-scale heterogeneous structure which is composed of a plenty mobile-carrier existing region of metallic conductivity and semi-localized scarce carrier region with

antiferromagnetic spin ordering. Recently, Zaanen [19] described the copper oxides as a quantum liquid of static and dynamic stripes.

The CI centers can in general have a complicated radial–tangential electronic structure with the anisotropic radial and angular density distribution of the partially localized and mobile bosons. The real structure of the CI centers will be determined by the resultant minimization of the boson transfer energy, the boson–boson interaction energy and the inhomogeneity potential energy V_{dis} taking into account the boundary conditions or the quantum size effects.

The disproportionation reaction in the rare earth manganites is stimulated by the nonisovalent chemical substitution as in $La_{1-x}Sr_xMnO_3$ and can also be accompanied by the static and/or dynamic phase separation of the classical or quantum origin. It is worth to mention that from the beginning of the intensive studies the substituted manganites are qualitatively described within the model approach similar to the phase separation [13,20].

Note that the most original and elaborated approach to this problem is developed by Nagaev [20].

4. Mid-infrared absorption in strongly correlated oxides

In any case a formation of the polar PJT center in oxides is initiated by the sharp correlational decrease in the energy of the s–p-transition that determines the fundamental absorption band for the parent oxides. Thus the "parent" absorption band shifts from the rather usual position around ~ 2–3 eV to the mid-infrared region (MIR) forming the so-called MIR band. The appearance of the MIR absorption is a common feature of the strongly correlated oxides under consideration. The MIR band structure reflects the phase state of the PJT centers system providing a kind of its portrait. For the localized polar centers within various charge ordering modes the MIR absorption consists of two more or less separated bands (low energy L band and high energy H band) linked to an absorption in the electron and hole centers, respectively. A boson delocalization results in an essential change of the MIR absorption up to an appearance in the limit of the large transfer integrals of the single M band peaked at an energy

$$\Delta_M = c_e\Delta_e + c_h\Delta_h, \quad (5)$$

where $c_{e,h}$, $\Delta_{e,h}$ are the concentration and the MIR band peak energy for the electron and hole centers, respectively. Boson delocalization is accompanied by an increase of the conductivity and formation of the Drude-like boson contribution to the optical properties.

An experimental observation of the MIR absorption bands in all the oxides under consideration convincingly prove the existence of the PJT centers. The MIR absorption in the cuprates [3] is determined by the allowed charge transfer transition $b_{1g}^2 : {}^1A_{1g} \rightarrow b_{1g}\, e_u : {}^1E_u$ and represents the correlation analogue of the corresponding single particle $b_{1g} \rightarrow e_u$ transition (see Fig. 3). The relation between the energies of these MIR bands for the electron (Δ_e) and hole (Δ_h) centers, respectively, enables us to make some conclusions about the vibronic reduction of the boson transfer integral and therefore about the potentially possible critical temperature T_c, isotope shift effect and baric coefficient [21]. So, the condition $\Delta_e = \Delta_h$ is necessary for the maximal T_c. A structure of the MIR absorption bands in general can be modeled by a "bilorentzian" like Eq. (2) and contains an important information on the phase state of the PJT centers, in particular, about the boson relaxation rate.

Fig. 5 shows schematically the MIR bands for the rare earth manganites in the localized (L, H bands) and delocalized (M band) states of the PJT centers system. The suggested model spectra are based on the experimental data for $LaMnO_3$ [13], $La_{0.9}Sr_{0.1}MnO_3$ [22] and for $Nd_{0.7}Sr_{0.3}MnO_3$ [23]. These experimental data enable us to distinctly identify the high energy (H) band centered at $\Delta_H \approx 1.2$ eV and the low energy (L) band centered at $\Delta_L \approx 0.1$ eV. The cooling from an ambient temperature is accompanied by the appearance of the M band centered at $\Delta_M \approx 0.5\ \text{eV} \approx \frac{1}{2}(\Delta_L + \Delta_H)$, whose intensity increases upon lowering the temperature especially with transition to the metallic ferromagnetic state. A coexistence of the (L + H) and M bands can be evidence to a favor of the phase separation with a coexistence of the localized paramagnetic or antiferromagnetic phases and delocalized metallic

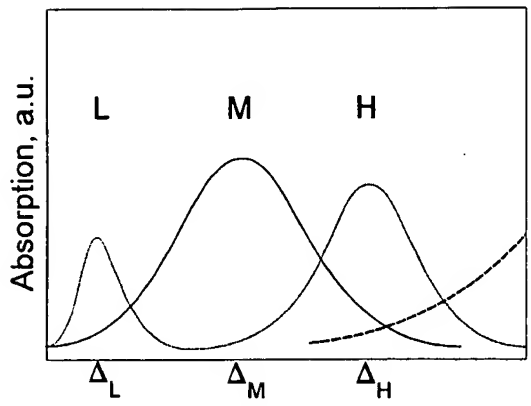

Fig. 5. Schematic picture of the MIR band for the substituted rare-earth manganites with the localized (L-, H-bands) or delocalized (M-band) states of the PJT centers system. A tail of the fundamental absorption band is also shown.

ferromagnetic phase with or without the appropriate percolation. Besides, the various phase regions of the polar PJT centers system can coexist with the regions of the parent oxide phase, thus determining the complicated multi-phase inhomogeneous structure of the substituted oxide.

5. Generalized quantum lattice bose-liquid

For inhomogeneous systems with a set of the multicomponent order parameters the ground state can represent a strongly fluctuating quantum liquid as a result of a dynamic equilibrium of the fluctuations of the different phases characterized by the corresponding lifetime and correlation length. A description of such systems is extremely complicated and needs simplified model approaches.

A simplest approximation for the cuprates corresponds to the full neglect the intermode coupling. A singlet boson system in this case is described by the well known Hamiltonian of the quantum lattice bose-gas (QLBG) [24,25]

$$H_B(\text{singlet}) = \sum_{m>n} t(mn)\hat{B}^+(m)\hat{B}(n) + \sum_{m>n} V(mn)\hat{N}(m)\hat{N}(n) + \mu\sum_m \hat{N}(m) + \text{h.c.}, \quad (6)$$

where $t(mn)$ is the boson transfer integral, $N(m)$ is the boson number on m site, $V(mn)$ is the boson–boson interaction energy, μ is the chemical potential determined by a constant concentration constraint, $\hat{B}^+(m)(\hat{B}(m))$ is the boson creation (annihilation) operator on the m site. $V(mm) = \infty$ assumed to exclude double occupation on the m site.

The QLBG Hamiltonian is equivalent to that of the anisotropic Heisenberg magnet ($s = \frac{1}{2}$) with the temperature dependent external magnetic field

$$\hat{H}_B = \mu\sum_m \hat{S}_z(m) + \sum_{m<n} [t(mn)(\hat{S}_x(m)\hat{S}_x(n) + \hat{S}_y(m)\hat{S}_y(n)) + V(mn)\hat{S}_z(m)\hat{S}_z(n)], \quad (7)$$

where the spin operators are connected with the creation (annihilation) operators

$$\hat{B}(m) = \hat{S}^+(m) = \hat{S}_x(m) + i\hat{S}_y(m),\ \hat{B}^+(m) = \hat{S}^-(m) = \hat{S}_x(m) - i\hat{S}_y(m),\ \hat{N}(m) = \tfrac{1}{2} - \hat{S}_z(m), \quad (8)$$

the parameters $t(mn)$ and $V(mn)$ are the effective exchange integrals, a boson chemical potential plays the role of an external field and is determined by "the concentration constraint"

$$\langle\hat{S}_z\rangle = \sum_m \langle\hat{S}_z(m)\rangle = N(\tfrac{1}{2} - \langle\hat{N}_B\rangle), \quad (9)$$

where N is a lattice site number, $\langle\hat{N}_B\rangle$ is an average site boson concentration.

The long-range quantum charge modes for the QLBG are determined by the relationship between the magnitudes of the transfer integral t_{BB} and the effective boson–boson interaction V_{BB} [25]: these correspond to the non-ordered metallic NO-phase, the charge ordering CO-phase (or charge density wave CDW-phase), the superconducting bose-superfluid BS- and the mixed (CO + BS)-phases with a nonzero value of the superconducting order parameter $\Psi(\mathbf{r}) = \langle\hat{S}^-\rangle$.

Similar to the real spin moment the superconducting order parameter density distribution can be linked with the electron density distribution for the local boson. An appropriate wave function for the cuprates has the $^1A_{1g}$ symmetry and within a simplified model corresponds to the b_{1g}^2 electron configuration. However, the local boson moves in the PJT lattice so its effective symmetry should correspond to one of the local symmetry types A_{1g}, B_{1g} (B_{2g}), E_u peculiar to the PJT center. Thus a local boson should in general exhibit both the usual

s- and unconventional p- or d-type symmetry both even and odd. Note that the problems with the superconducting order parameter symmetry within the conventional BCS approach and that of the local bosons are essentially different. On the one hand, we have to deal with the gap-function symmetry in $\boldsymbol{k}$-space, on the other hand the local boson symmetry is defined in a real $\boldsymbol{r}$-space. In the absence of a theory for the high-T_c superconductivity the hot discussion of the superconducting order parameter symmetry is a rather scholastic. Practically, it is necessary to discuss certain experimental data.

Both the boson transfer integral $t(mn)$ and the effective (screened) Coulomb interaction $V(mn)$ can be varied within a relatively large range providing the optimal conditions both for superconductivity ($V \leqslant t$) and for charge ordering ($V > t$). Fig. 6 presents qualitatively a phase (T, v) diagram with v-parameter determining the specific behavior of V and t (see inset in Fig. 6) and also a temperature dependence of the charge fluctuations $\langle\delta\hat{N}(m)\delta\hat{N}(n)\rangle_{\omega,T}$ and the fluctuations of the superconducting order parameter $\langle\delta S^+(m)\delta S^-(n)\rangle_{\omega,T}$ for three regimes with $V > t$, $V \approx t$ and $V \leqslant t$. Note the "pseudo-gap" behavior of the appropriate fluctuations at $T < T_{BS}$ and $T < T_{CO}$.

An effective local boson Hamiltonian becomes extremely complicated for the PJT centers phase with the triplet local bosons as in substituted manganites since we cannot separate the charge and spin systems. Even for the maximally simplified case with the full neglect of the near degeneracy and the PJT effect, when the PJT centers $[MnO_6^{8-}]_{JT}$ and $[MnO_6^{10-}]_{JT}$ are transformed to the conventional electron ($Mn^{2+}: 3d^5: {}^6A_{1g}$) and hole ($Mn^{4+}: 3d^3: {}^4A_{2g}$) polar centers, the disproportionated system as a system of the triplet local bosons moving in a lattice of the hole Mn^{4+}-centers can be described by the unconventional Hamiltonian of the generalized quantum lattice bose-gas

$$H_B(\text{triplet}) = \sum_{m>n} t(mn)(\hat{T}^+(m)\cdot\hat{T}(n)) + \sum_{m>n} J(\hat{N}(m),\hat{N}(n))(\hat{S}(m)\cdot\hat{S}(n)) + \sum_{m>n} V(mn)\hat{N}(m)\hat{N}(n) + \mu\sum_m \hat{N}(m) + \text{h.c.}, \quad (10)$$

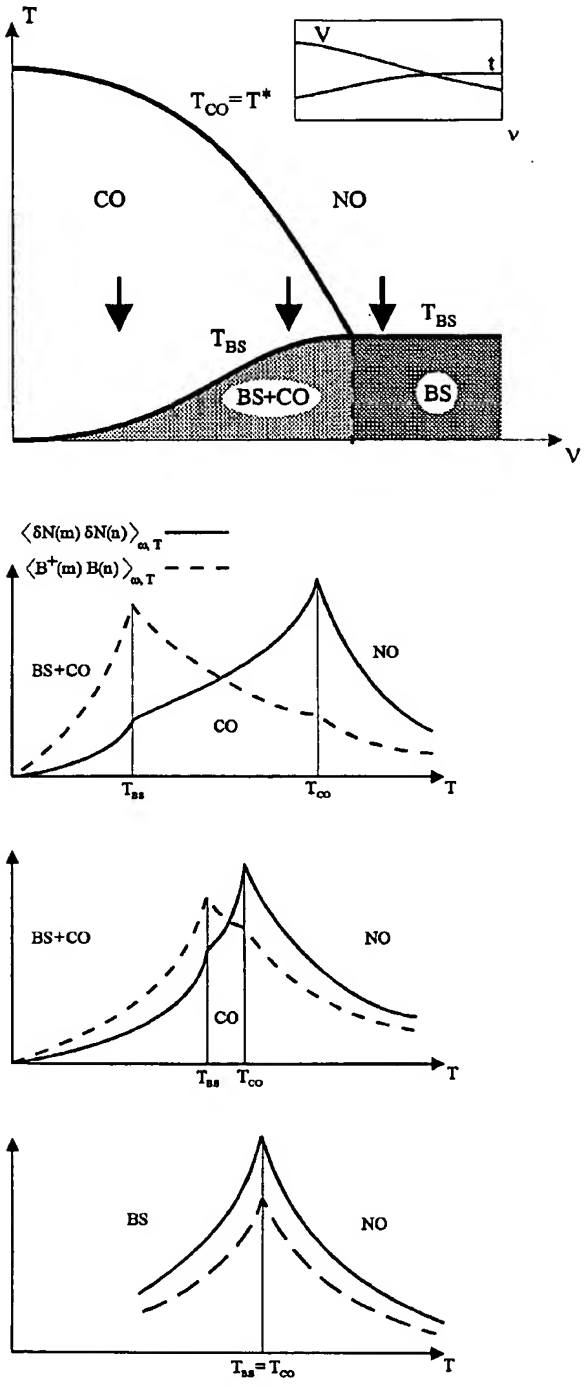

Fig. 6. Upper panel: a model (T, v) phase diagram for the quantum lattice bose-gas ($N_B \approx 0.5$) with v being a parameter (in particular, N_B or doping content!) determining a certain change of V and t (see the inset). Lower panels show a qualitative T-dependence of the charge fluctuations and the superconducting order fluctuations for three regimes marked by arrows in the upper panel for $V > t$ (weak screening), $V \geqslant t$ (optimal screening) and $V < t$ (over-screening), respectively.

where the vector operators $T^+(m)(T(m))$ create (annihilate) the triplet local bosons with different spin projection (the x, y, z- or 0, ± 1 bosons) and simultaneously change the spin multiplicity ($S = \frac{3}{2} \leftrightarrow S = \frac{5}{2}$), S is the usual spin operator, $J(mn)$ is the effective exchange integral. The T and S operators are coupled by a kinematic constraint resulting from the spin algebra and the Hund's rule. An exchange interaction Mn^{3+}–Mn^{3+}, Mn^{2+}–Mn^{2+}, Mn^{4+}–Mn^{4+} is antiferromagnetic, whereas the Mn^{2+}–Mn^{4+} exchange can be antiferromagnetic or ferromagnetic depending on the superexchange geometry. As in the well-known double exchange problem we have a competition between the antiferromagnetic nonmetallic and ferromagnetic metallic states. In general we can describe the system by the order parameters $\langle T^+ \rangle$, $\langle T \rangle$, $\langle S \rangle$, $\langle \hat{N} \rangle$ and by the appropriate fluctuations. The first two parameters describe the triplet boson condensate with "kinematically" induced ferromagnetic or canted spin ordering. The last two parameters describe the rather conventional spin (predominantly antiferromagnetic) and charge ordering. A full MFA description of the phase diagram for manganites within the simplified model Hamiltonian (10) will be presented elsewhere.

One of the peculiar features of the localisation in the rare earth manganites like $La_{1-x}Sr_xMnO_3$ as for other strongly correlated PJT oxides is a formation of the low lying hybrid spin–charge-local structure ordering modes like static magnetic-lattice polaron. An interplay between coexisting metallic and non-metallic phases within the framework of the static or dynamic phase separation is directed by the level of the nonisovalent substitution, the isotopic ($^{16}O \rightarrow {}^{18}O$) substitution, external magnetic field, external pressure or the temperature. As in [20] we conjecture this unconventional interplay is revealed in many exotic "phase transition-like" peculiarities observed in the substituted manganites [20,26], providing, in particular, the so-called percolative contribution to the isotope shift effect [27].

6. Conclusions

We have suggested a new approach to the strongly correlated oxides like cuprates ($YBa_2Cu_3O_{6+x}$, $La_{2-x}Sr_xCuO_4$, $La_2CuO_{4+\delta}$, ...), manganites ($La_{1-x}Sr_xMnO_3$, ...), nickellates ($La_2NiO_{4+\delta}$), bismuthates ((K, Ba)BiO_3) as to systems where the nonisovalent substitution promotes the local disproportionation reaction with a formation of the electron and hole PJT centers phase. The new phase can be considered as a generalized quantum lattice bose-liquid or a system of the local singlet (cuprates) or triplet (manganites) bosons moving in a lattice of the hole PJT centers.

The unconventional properties of the substituted strongly correlated oxides are connected with an active interplay of the charge, spin, orbital and local structural (PJT) modes taking account of the strong charge inhomogeneity, multi-granularity, static and dynamic phase separation and percolation phenomena.

Note added in proof

A convincing experimental argument in favor of an instability with regard to the disproportionation reaction like

$$Mn^{3+} + Mn^{3+} \rightarrow Mn^{2+} + Mn^{4+}$$

has been recently obtained by M.F. Hundley and J.J. Neumeier (Phys. Rev. B 55 (1977) 11511) as a result of a detailed examination of the temperature dependence of the thermoelectric power in $La_{1-x}Ca_xMnO_3$.

Acknowledgements

I thank K. Bärner, N.A. Loshkareva, Yu.P. Sukhorukov, A.S. Ovchinnikov and Yu.D. Panov for stimulating discussions.

References

[1] A.S. Moskvin, Sov. Phys. JETP Lett. 58 (1993) 342.
[2] I.B. Bersuker, V.Z. Polinger, Vibronic Interactions in Molecules and Crystals, Springer, Berlin, 1989.
[3] A.S. Moskvin, N.N. Loshkareva, Yu.P. Sukhorukov, M.A. Sidorov, A.A. Samokhvalov, Sov. Phys. JETP 105 (1994) 967.
[4] A.S. Moskvin, Physica C 282–287 (1997) 1807.

[5] M.V. Patrakeev, I.A. Leonidov, A.A. Lakhtin et al., Fizika Tverdogo Tela 38 (1996) 2650 (in Russian).
[6] B.B. Krichevtsov, R.V. Pisarev, A. Burau et al., J. Phys.: Condens. Matter., to be published.
[7] A.A. Makhnev, L.V. Nomerovannaya, M.M. Kirillova et al., Superconductivity 4 (1991) 609.
[8] Yu.P. Sukhorukov, N.N. Loshkareva, A.A. Samokhvalov, A.S. Moskvin, Sov. Phys. JETP 81 (1995) 998.
[9] J.E. Hirsch, S. Tang, Phys. Rev. B 40 (1989) 2179.
[10] Y. Yoshinari, P.C. Hammel, J.A. Martindale et al., Phys. Rev. Lett. 77 (1996) 2069.
[11] M. Takata, E. Nishibori, T. Takayama et al., Physica C 263 (1996) 176.
[12] M.A. Teplov, Yu.A. Sakhratov, A.V. Dooglav et al., JETP Lett. 65 (1997) 782.
[13] Gen Matsumoto, J. Phys. Soc. Japan 29 (1970) 606, 615.
[14] P. Mendels, H. Alloul, G. Collins, G.F. Marucco, Physica C 282–287 (1997) 226.
[15] B.O. Wells, R.J. Birgeneau, F.C. Chou et al., Z. Phys. B 100 (1996) 535.
[16] G. Cao, J. Bolivar, J.E. Crow et al., J. Supercond. 8 (1995) 607.
[17] V.J. Emery, S.A. Kivelson, Physica C 263 (1996) 44.
[18] T. Egami, J. Low Temp. Phys. 105 (1996) 791.
[19] J. Zaanen, A. Oles, Ann. Physik 5 (1996) 224.
[20] E.L. Nagaev, Uspekhi Fiz. Nauk 166 (1996) 833 (in Russian).
[21] A.S. Moskvin, Yu.D. Panov, JETP 84 (1997) 354.
[22] N. Loshkareva, Yu.P. Sukhorukov, B.A. Gizhevskii et al., Phys. Status Solidi A 164 (1997) 863.
[23] S.G. Kaplan, M. Quijada, H.D. Drew et al., Phys. Rev. Lett. 77 (1996) 2081.
[24] A.S. Alexandrov, JETP 68 (1989) 167.
[25] R. Micnas, J. Ranninger, S. Robaszkiewicz, Rev. Mod. Phys. 62 (1990) 113.
[26] Y. Tokura, Y. Tomioka, H. Kuwahara, Physica C 263 (1996) 544.
[27] A.S. Moskvin, Yu.D. Panov, to be published.

ELSEVIER

Materials Science and Engineering B63 (1999) 36–43

MATERIALS SCIENCE & ENGINEERING B

www.elsevier.com/locate/mseb

Superconducting cuprates and magnetoresistive manganites: similarities and contrasts

T. Venkatesan [a,*], R.P. Sharma [a], Y.G. Zhao [a,f], Z.Y. Chen [a], C.H. Lee [a], W.L. Cao [a], J.J. Li [a], H.D. Drew [a], S.B. Ogale [b], R. Ramesh [b], M. Rajeswari [b], T. Wu [a], I. Jin [a], S. Choopun [a], M. Johnson [c], W.K. Chu [d], G. Baskaran [e]

[a] *Department of Physics and Electrical Engineering, University of Maryland, College Park MD 20742, USA*
[b] *Materials and Nuclear Engineering Department, University of Maryland, College Park MD 20742, USA*
[c] *Naval Research Laboratories, USA*
[d] *Texas Center for Superconductivity, University of Houston, Houston TX, USA*
[e] *Institute for Mathematical Sciences, Taramani, Chennai, India*
[f] *Department of Physics, Tsinghua University, Beijing, China*

Abstract

We report on three different experiments on high temperature superconducting (HTS) cuprates and colossal magnetoresistive (CMR) manganites, which clearly bring out some of the important similarities and differences between the two material systems. The experiments involve the measurement of temperature dependence of the mean squared displacement of Cu and Mn ions from their equilibrium site in the case of the cuprates and the manganites, respectively, and their correlation with the transport property. In both cases the key ions in the materials (Cu for HTS and Mn for CMR) exhibit vibration amplitudes larger than that of ions in simple Debye solids and clearly show discontinuities in the vibration amplitudes as a function of temperature close to the phase transition temperatures. These point to the unequivocal participation of phonons in the transport processes and possibly in the onset of the phase transitions (i.e. superconductivity and ferromagnetism). The second set of experiments, involves femtosecond optical excitation of micro-strip resistors made of cuprates or manganites, and the subsequent measurement of the changes in the impedance on a 20 ps time scale. In the case of the manganites one measures the time scales involved in the ionization and reformation of a Jahn–Teller polaron and also the decay times of magnon excitors. In the case of the cuprates one sees a highly efficient pair breaking process with a very sharp resonance, with a width of only 100 meV, which is indicative of the role of a large intermediate excitation in the mechanism of high temperature superconductivity. In the third experiment, spin-polarized electrons injected from a manganite electrode into a superconductor are observed to break pairs at a rate far larger than unpolarized electrons. This effect seems very orientation dependent for the case of YBCO, which may shed new light on the transport of quasi-particles at YBCO interfaces.

Keywords: High temperature superconducting (HTS) cuprates; Colossal magnetoresistive (CMR) manganites; Cu and Mn ions

1. Introduction

Since the end of 1986, when high temperature superconductors came into being, the subject has captured the interest of one of the largest segment of the research community in any sub-field of Physics [1–5]. Despite the level and pace of the research, the origin of the nature of transport in the cuprates is still known piece meal and the microscopic mechanism of the pairing process still eludes us [6–9]. Even the normal state transport properties continue to challenge our understanding and truly innovative experiments are needed to get at the root of these issues [10–12]. Over the last 5 years or so the condensed matter community has been pursuing yet another family of perovskites, the colossal magnetoresistive manganites, with a degree of intensity second only to the high T_c cuprates [13,14]. This is simply because the underlying physics behind the observed phenomena, encompass some of the most exciting ideas in condensed matter Physics involving highly correlated electronic systems with strong electron–phonon coupling and magnetic interactions [15–18]. In

* Corresponding author.

0921-5107/99/$ - see front matter
PII: S0921-5107(99)00049-5

addition, familiar ideas in solid state chemistry involving electronic orbitals and bond hybridization have been readily adopted in this field [19,20]. The manganite system may be an enabler in furthering our understanding of the cuprates. In this system, the strong electron–phonon interaction results in a precisely and relatively easily measurable correlation of transport properties with lattice distortions from which lessons may be drawn regarding similar effects in the case of the cuprates. The more visible role of electron spins on the transport properties of the manganites may shed light on the role of antiferromagnetic order in the Cooper pairing mechanism in the cuprates. In this paper we present three different experiments involving both the cuprates and the manganites, which we believe are very important for furthering our understanding of these rather enigmatic materials systems.

2. Ion channeling study of ion dynamics

Let us consider some of the important similarities between the cuprates and the manganites. In the less conducting state of the materials the electrical transport can be understood as due to charge hopping between adjacent Cu or Mn sites. The hopping frequencies increase as the conductivity of the material increases and this has effects on the dynamic lattice distortions whose frequencies are comparable with phonon frequencies. Thus the lattice distortions would no longer follow the charge hopping when the system becomes very metallic and the hopping times become very fast. The role of lattice distortions and their impact on transport properties arises from an important similarity between the Cu^{2+} and Mn^{3+} ions which are both Jahn–Teller ions [21] and would strongly favor lattice

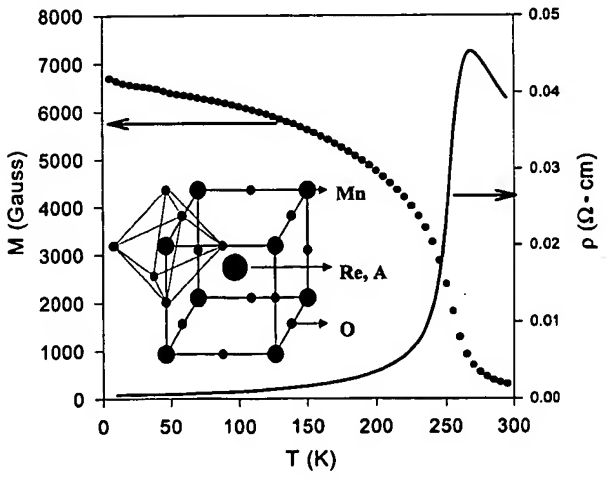

Fig. 1. Resistance vs. temperature curve for a film of $La_{0.7}Ca_{0.3}Mn_{0.3}$ film deposited by pulsed laser deposition. In the inset is shown the perovskite crystal structure of the manganite.

distortions to reduce the electronic degeneracies of the valence electrons. Let us now take the case of the manganites and the cuprates one by one.

The manganites, characterized by the formula $R_{x-1}M_xMnO_3$ (where R = a trivalent rare earth ion such as La, Nd, Pr etc. and M = a divalent ion such as Ca, Ba, Sr), for the case of $x = 1/3$, can be represented by the transport property described by Fig. 1 [22,23]. In this case of $La_{0.7}Ca_{0.3}MnO_3$, the resistivity vs. temperature curve shows a bell shaped curve with the resistance exhibiting a peak close to the Curie temperature (270 K), so that above this peak the material is a paramagnetic semiconductor [24] and below this peak it is a ferromagnetic metal as evidenced by the onset of magnetization. The unique transport properties of this compound is understood as due to the hopping of an electron from a Mn^{3+} ion to an adjacent Mn^{4+} ion, via an intermediate oxygen atom. In this process the electron from the Mn^{3+} exchanges position with an electron in the $2p$ orbital of the oxygen and the original oxygen electron jumps concurrently into the Mn^{4+} valence level. In this 'double exchange' process [25], the strong Hund's rule coupling of the valence electrons to the core electrons, imposes a condition that the transition probability of the electron is proportional to the overlap of the spins at the two Mn core levels. The unusually large magnetoresistance and the ferromagnetic transition can be understood to some extent based on this double exchange idea. However, the observation of metallic behavior in this system at large resistivity values requires other mechanisms for charge localization and the Jahn–Teller distortion of the Mn–O–Mn bond is one such mechanism [26]. The Mn^{3+}–O and the Mn^{4+}–O bonds are not symmetric and the resultant distortion localizes the charge thereby raising the resistivity values. One of the important consequences of this idea is that when the electron hops from one Mn^{3+} to the next Mn^{4+}, it will be followed by a renormalization of the Mn–O bond configuration, provided the hopping times are comparable with phonon frequencies, which is true in the paramagnetic semiconducting state. However, as one gets into the metallic state where the hopping times become faster than the phonon response times, this effect becomes progressively weaker. Another way of looking at this is to say that in the semiconducting state the transport is via a small polaron whose size becomes progressively large as the metallicity increases with the electron becoming eventually itinerant as in conventional metals. So if the atomic displacements could be measured in these materials with a precision of better than 10^{-10} cm, then one ought to see dynamic displacements of the Cu or Mn ions in excess of the thermal vibrations expected for a Debye solid. One experimental technique that measures such displacements accurately is ion channeling spectrometry [27], though in the case of the manganites the

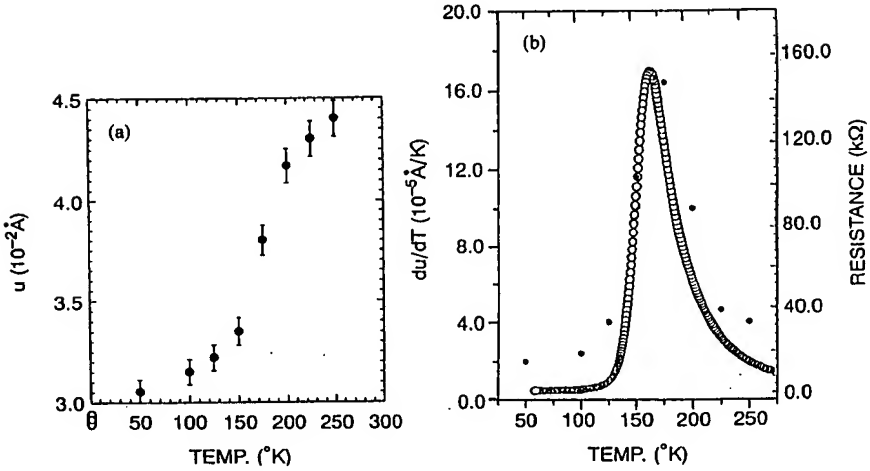

Fig. 2. (a) The displacement u of the Mn atoms from their equilibrium lattice positions as measured by ion channeling as a function of temperature in a 2000 Å thick film of $Nd_{0.7}Sr_{0.3}Mn_{0.3}$ grown on $LaAlO_3$ substrate. (b) The resistance vs. temperature curve for the manganites and the temperature derivative of the lattice displacement (u) [32].

effect is so large that even neutron scattering is able to measure such displacements unambiguously. However, in the case of the cuprates neutron scattering has not been as successful as ion channeling [28,29]. Details of the ion channeling technique can be obtained from a variety of references [30,31] and for brevity we will only deal here with the results of the measurements.

2.1. Ion channeling in the manganites

In Fig. 2 is shown the dynamic displacements measured for the compound $Nd_{0.7}Sr_{0.3}MnO_3$ by ion channeling technique in comparison with what is expected for a Debye solid [32]. Interestingly, in the paramagnetic state ($T > 170$ K) there are excess dynamic lattice distortions by as much as 50% of the thermal vibrations which vanish as one goes below the ferromagnetic transition (~ 170 K). In Fig. 3 is shown similar data for $La_{1.2}Sr_{1.8}Mn_2O_7$ a bilayer manganite system (an analog of YBCO, a Cu bilayer superconductor) and here again, the channeling data shows excess distortions in the system above the Debye values which then vanish below the Curie temperature (~ 100 K) progressively as the system becomes more metallic [33,34]. In some sense we could make a general remark that a system that has polaronic transport would at an insulator to metal transition show significantly larger vibration amplitudes than in a Debye solid and in the metallic state this excess distortion must vanish. Hence at a metal–insulator or normal metal–superconductor transition in a polaronic conductor one would expect to see dramatic changes in the excess lattice distortions.

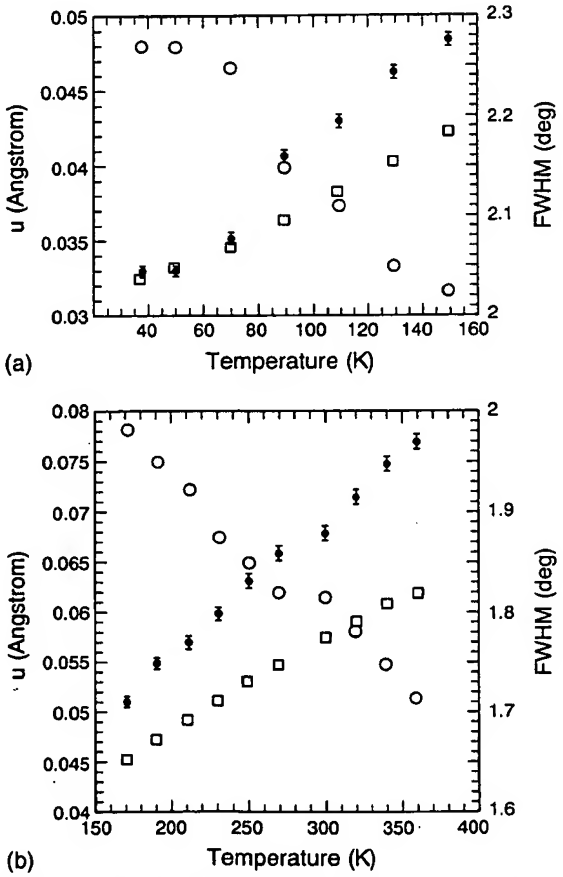

Fig. 3. (a) The displacements of the Mn atoms from their equilibrium lattice positions as measured by ion channeling as a function of temperature for a bilayer manganite, $La_{1.2}Sr_{1.8}Mn_2O_7$ in the temperature range of 36–150 K, the circles represent the FWHM of the channeling angular scans. (b) The same in the temperature range of 150–350 K [33,34].

2.2. Ion channeling in the cuprates

In Fig. 4 is shown the channeling data for single crystal YBCO with the vibration amplitudes of Cu plotted for an oxygen deficient YBCO (non-superconducting) and a fully superconducting YBCO ($T_c = 92.5$ K) [35]. Also shown are the Debye curves for both the systems (with Debye temperatures $T = 330$ and 380 K for the non-superconducting and superconducting samples). The non-superconducting YBCO shows a monotonic behavior while the superconducting sample shows a variety of unusual discontinuities with temperature. The fact that the non-superconducting sample shows a larger vibration amplitude, and that the superconducting sample shows a drop in this vibration amplitude abruptly at the transition temperature is proof that there is a dramatic difference in the role of phonons in the transport properties above and below T_c. If we took the analogy from the manganites one would say that the system has evolved from a polaronic behavior above T_c to some thing less polaronic below the T_c. While the polaron in the case of the manganite arises because of the difference in the Mn–O bond configuration depending on the valence state of the Mn, in the case of the cuprates the polaron may arise from a different origin. Since the Cu valences are believed to be predominantly 2+ in the superconducting phase, the argument arises as to where the hole responsible for transport resides. Energetics arguments preclude the hole from being localized either on the Cu or the O atom. Molecular entities such as Zhang–Rice singlets (ZRS) [36], where the hole is shared by a square of four oxygen atoms with the spin of the Cu electron and that of the hole forming a singlet seem highly plausible. If such molecular entities facilitate the hopping of charge from site to site, then the Cu–O bond configuration of the ZRS would be affected by the hole occupancy of the site. Thus by arguments similar to the case of the manganites one would expect an ion channeling signature in the less conductive state of the material as is indeed seen. Further, in the superconducting state, where the electrons become truly itinerant the excess vibrations die down completely. What is indeed remarkable is that even at 90 K, the system already reaches the zero-point vibration of the system suggesting a coherent state for the ionic sites as well! The freezing of the Cu motion has been further verified recently by EXAFS technique [37]. The unusual transitions seen at 150, 200 K and at higher temperatures show the possibility of other phonon mediated behavior in the system, not obvious in the transport measurements which would require further exploration.

In summary, ion channeling experiments with ability to measure small vibration amplitude of the atoms from their equilibrium positions may be a very valuable tool for understanding the transport properties of the perovskite based conductors where strong electron–phonon effects are seen in addition to strong electron correlation.

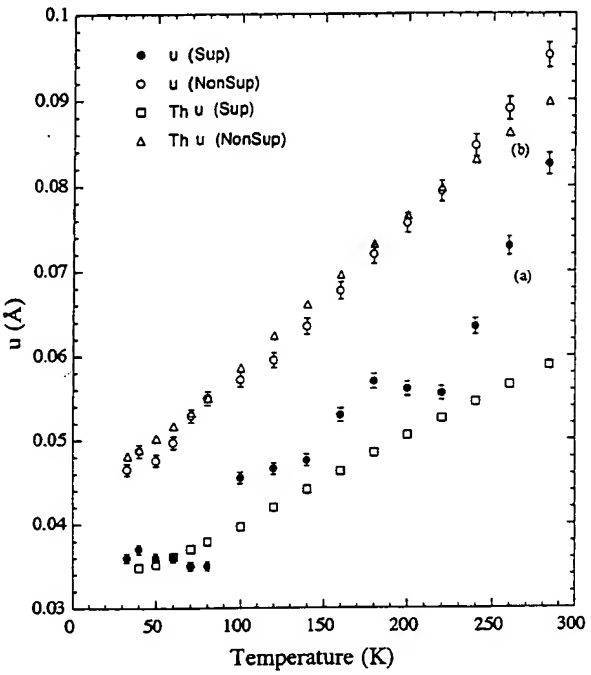

Fig. 4. Displacements of the Cu atom in the case $YBa_2Cu_3O_{7-\delta}$ superconductor as measured by ion channeling as a function of temperature for $\delta = 0.77$ (non-superconducting) and $\delta = 0.05$ (superconducting) samples. In the non-superconducting case the Debye fit (triangles) with a Debye temperature of 330 K, and in the superconducting case the Debye fit (squares) with a Debye temperature of 380 K is shown [31].

3. Optical excitation study of electron dynamics

We can learn significant information about the material systems by studying their electron dynamics. In retrospect the previous section dealt with dynamics of the ions measured by a technique which takes snap shots of the nuclei at very short time intervals ($\sim 10^{-20}$ s determined by the ion scattering times)[1]. Now we want to focus on the electron dynamics. In the following technique we use 100 fs laser pulses to excite the electrons in the system and see the rise and decay times

[1] The Ion Scattering time depends on the distance of closest approach or the impact parameter which is of the order of a few Fermi and depends on the atomic number of the incident ion and the target nucleus. Since the velocity of the incident ion is $\sim 10^9$ cm per s, these times are in the range of 10^{-19}–10^{-21} s.

at different temperatures where the property of the material changes. The experiment consists of measuring the changes in the impedence of a transmission line built out of the material of interest. While readers can get details elsewhere [38], the measurement times are essentially limited by the oscilloscope rise time, which is 20 ps, as a result of which processes faster than 20 ps will be averaged in this time scale. Once again, let us consider the case of the manganites first since the data

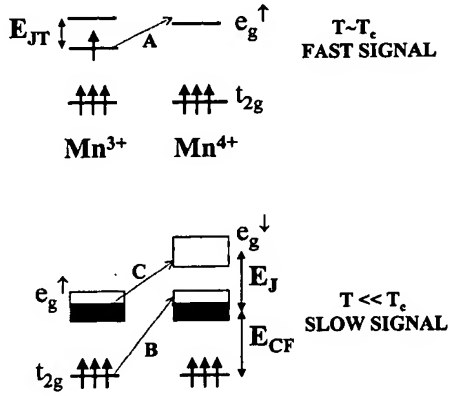

Fig. 5. The electronic energy levels and the possible optical transitions in the paramagnetic and ferromagnetic states of the manganites [41].

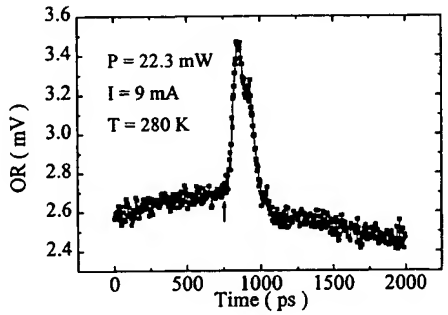

Fig. 6. Optical response consisting of a photoconductivity signal at a temperature of 280 K, close to the ferromagnetic transition temperature in the case of $La_{0.7}Ca_{0.3}MnO_3$ (LCMO) film [41].

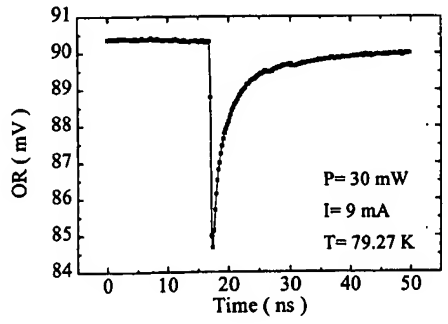

Fig. 7. Optical response consisting of a photoresistive transient at a temperature of 79.27 K, where the LCMO is in the fully ferromagnetic state [41].

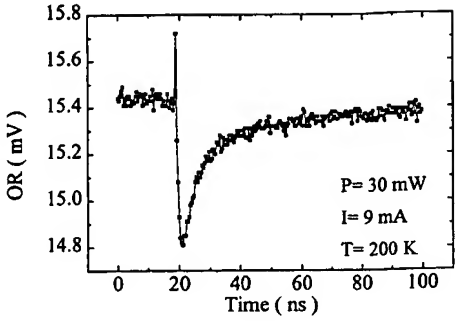

Fig. 8. Optical response at an intermediate temperature of 200 K for LCMO where both the conductive and resistive transients are seen [41].

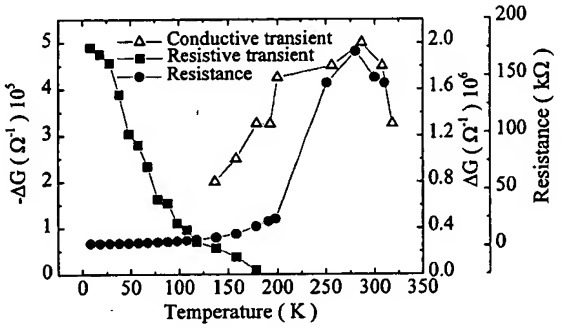

Fig. 9. The behavior of the resistive and conductive transients with respect to temperature and comparison with the resistance curve [41].

is relatively easier to interpret. At temperatures close to the Curie temperature where the system has Jahn–Teller splitting, the energy levels for the electronic transition can be considered as shown in Fig. 5 [39,40]. For the 1.5 eV photon the most likely transition is that of an electron from the lower e_g orbital of the Mn^{3+} to the e_g orbital of the Mn^{4+} ion (Transition A) [41]. This essentially ionizes the polaron, which will increase the conductivity and indeed such a signal is seen as shown in Fig. 6. The rise time of the conductivity transient signal is of the order of 40–60 ps and the fall time is of the order of 150 ps. It is not clear at this point as to what these times signify. Besides the Jahn–Teller distortion arising from the Mn^{3+} ion, the Mn^{4+} ions exhibit an oxygen-breathing mode distortion which also causes changes in the electronic energy levels promoting localization. So when the electron is promoted from the Mn^{3+} to the Mn^{4+} ion the Jahn–Teller and the breathing mode distortions must change sites effectively. Since the hopping ti2mes close to the ferromagnetic transitions are likely to be slow one ought to see polaronic effects accompanying charge transfer. The fall time represents the trapping time for the excited electron or the reformation time for the Jahn–Teller polaron. At very low temperatures where the system becomes a good ferromagnetic metal the signal has opposite behavior; it is a resistive transient and is

significantly slower (Fig. 7). Based on the slow response and resistance increase, this signal is interpreted as due to magnon formation and its recombination. This time comes out to be of the order of tens of nanoseconds and is also very temperature dependent with the time constant becoming longer with increasing temperature. Transition B in Fig. 5, the most resonant, would produce a spin flip excitation with some help from the weak spin orbit coupling in the system, and the relaxation will be via magnon decay. The magnon decay times are an order of magnitude larger than those for conventional metallic magnetic systems such as Ni [42–44], which is consistent with the order of magnitude narrower resonance line width measured in the manganites by ferromagnetic resonance experiments [45]. (What is still not resolved is the strength of the transition B which seems comparable with that of A, though the former should be weak on account of the small spin orbit coupling in the manganite system). At intermediate temperatures one observes both the conductive and resistive components

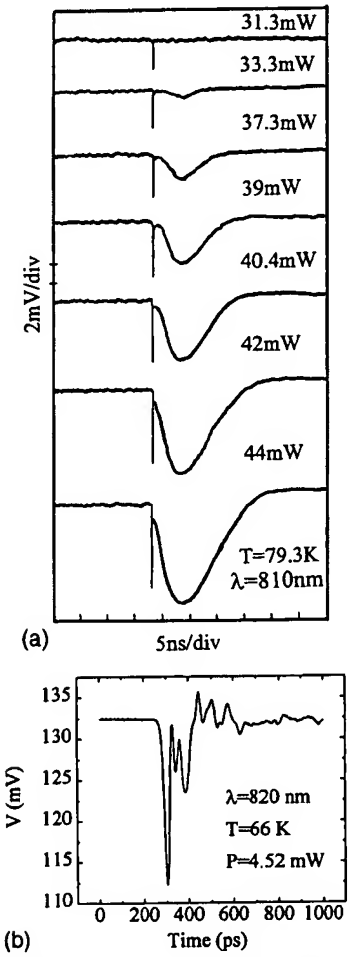

Fig. 10. (a) The fast and slow optical response observed under fs. laser excitation of the superconductor. (b) The fast response on an expanded time scale [38,50]

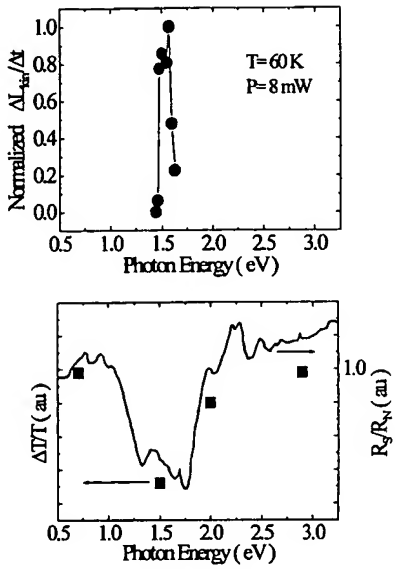

Fig. 11. The Optical response (proportional to the Cooper pair breaking rate) vs. excitation energy of the photon for YBCO (upper panel), compared with the data from Refs. [46] (solid line) and [47] (solid squares) as shown in lower panel [50].

(Fig. 8) which tells us that the evolution of the system from a paramagnetic semiconductor to a ferromagnetic metal is a gradual evolution and as shown in Fig. 9 the system crosses over at temperatures below $T_c/2$ from a predominantly paramagnetic behavior to a ferromagnetic behavior. The system evolves from an ionic bond picture to an itinerant metallic band picture!

Let us look at the case of the cuprates now. What one sees at a given photon energy is a two component excitation (Fig. 10a) where the slow component has been clearly identified as due to thermal effect while the fast initial component (Fig. 10b) is interpreted as a kinetic inductance change arising from pair breaking effects [38]. The photon dependence of this fast component (Fig. 11) is quite exciting since one sees a resonance centered at about 1.53 eV with a FWHM of only 100 meV. This is indeed an unusual result in the sense that such a narrow excitation is possible at all in such a strongly correlated electronic system in the superconducting state. Two different observations [46,47] prior to this have confirmed the existence of a resonance around 1.5 eV in the case of the cuprates, but neither of them involved direct pair breaking. Instead they were measurements of index changes and had much broader features ($\sim$ 500 meV) as seen in Fig. 11. While the intrinsic processes of excitation and decay are much faster than our measurement times of 20 ps, the optical resonance is qualitatively correct and identifies a high-energy excitation responsible for the pair breaking, in consistence with the observation of [46,47]. Taking the analogy of the manganites if one considers this as an ionization of a ZRS (whose separation from the upper

Hubbard band has been identified via photoemission experiments [48,49] to be around 1.4 eV), then the pair breaking could be consistently explained [50]. Thus the optical excitation experiment further supports the findings from the channeling results.

4. Spin-polarized quasi-particle injection into high temperature superconductors

In the last set of experiments, we have coupled the HTS and CMR together to study the effect of spin-polarized electrons on the superconductor. All the efforts in this direction to date [51–53] consist of FET structures in which the critical current of the HTS channel is modulated by spin-polarized current injected from a CMR gate electrode. This modulation is compared with the gate electrode replaced by a non-ferromagnetic electrode such as Lanthanum nickel oxide, which is structurally and thermodynamically very similar to the manganites. When the gate current is injected along the c-axis with the super current flowing in the a–b plane, the spin-polarized electrons are effective at breaking Cooper pairs at least a factor of 15–30 times larger than unpolarized electrons (Fig. 12) [52]. When such an experiment is performed for the case where the channel is replaced by an a-axis oriented YBCO film, with gate current along the a-axis and the super current along the huxis in the b–c plane, the difference between the spin-polarized and unpolarized pair breaking efficiency becomes much smaller. This result has significant impact on some of the current theoretical description of charge transport in the cuprates. Anderson [54] has postulated that in the case of the cuprates it may be easier to transport a paired electron along the c-axis as opposed to a single quasi-particle. From a ferromagnetic electrode it will be difficult to produce a singlet pair of electrons and any alternative would enable better pair breaking than the case where the electrons are injected as correlated pairs as can happen from a non-ferromagnetic gate electrode. However, there are still some unresolved issues relating to thermal effects in these experiments which need to be put to rest before the results can be fully considered. The connections with the previous two experiments is as follows. The concept of the unusual pair transport along the c-axis of cuprates applies to the system where spin-charge separation exists. ZRS will manifest spin-charge separation and thus the spin-polarized quasi-particle pair breaking data may be an indirect proof of YBCO being a system in which spin-charge separation exists [12].

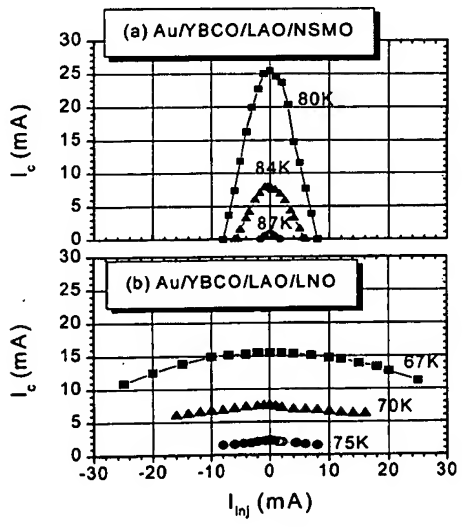

Fig. 12. Critical Current vs. gate injection current at different temperatures for: (a) ferromagnetic manganite ($Nd_{0.7}Sr_{0.3}MnO_3$) gate injector and (b) non-ferromagnetic metallic gate injector ($LaNiO_3$).

5. Summary

These three sets of experiments, which probe ion, electron and spin dynamics, need to be refined further, though even at this stage the data produced by these experiments clearly point to exciting ways for us to unravel the mystery of these materials. The rejuvenation of research in the manganite is certainly having a synergistic effect on the cuprate research.

Acknowledgements

The authors would like to acknowledge ONR Grant No. ONR-N000149611026 (Program Monitor: Deborah Van Vechten) and NSF MRSEC Grant No. DMR96-32521. T. Venkatesan would like to thank the Institute of Mathematical Sciences, Chennai (Madras), India for their hospitality, during a portion of this work.

References

[1] J.G. Bednorz, K.A. Muller, Z. Phys. B64 (1986) 189.
[2] Proceedings of the 19th International conference on low temperature physics, Physica B, 165–166 (1990).
[3] Proceedings of the International conference on Materials and Mechanisms of Superconductivity, M. Tachiki, Y. Muto, Y. Syono (Eds.), High Temperature Superconductors III, Kanazawa, Japan (1991).
[4] Proceedings of the 1996 Applied Superconductivity Conference, IEEE Trans. Appl. Supercond., Vol. 7 (1997)
[5] Proceedings of the 21st International Conference on Low Temperature Physics, Czechoslov. J. Phys. 4 Suppl. (1996).
[6] D. Pines, P. Monthoux, J. Phys. Chem. Solids 56 (1995) 1651.
[7] D.J. Scalpino, J. Phys. Chem. Solids 56 (1995) 1669.
[8] P.J. Hirschfeld, W.O. Putikka, D.J. Scalapino, Phys. Rev. B50 (1994) 10250.

[9] P.J. Hirschfeld, W.O. Putikka, D.J. Scalapino, Phys. Rev. Lett. 71 (1993) 3705.
[10] P.W. Anderson, Science 235 (1987) 1196.
[11] P.W. Anderson, G. Baskaran, Z. Zou, T. Hsu, Phys. Rev. Lett. 58 (1987) 2790.
[12] Q. Si, Phys. Rev. Lett. 78 (1997) 1767.
[13] Proceedings of Telluride Summer Research Center workshop on Magnetoresistive Oxides, Telluride, Collorado (1998).
[14] Proceedings of Mat. Res. Soc. Symp. CMR materials, Boston (1997).
[15] A.J. Millis, P.B. Littlewood, B.I. Shraiman, Phys. Rev. Lett. 74 (1995) 5144.
[16] N. Furukawa, J. Phys. Soc. Jpn. 64 (1995) 2754.
[17] N. Furukawa, J. Phys. Soc. Jpn. 64 (1995) 2734.
[18] N. Furukawa, J. Phys. Soc. Jpn. 65 (1996) 1174.
[19] J.B. Goodenough, Phys. Rev. 100 (1955) 564.
[20] J. Toepfer, J.B. Goodenough, J. Solid. State. Chem. 130 (1997) 117.
[21] C. Kittel, Introduction to Solid State Physics, John Wiley and Sons, New York, 1986.
[22] G.C. Xiong, Q. Li, H.L. Ju, S.N. Mao, L. Senapati, X.X. Xi, R.L. Greene, T. Venkatesan, J.M. Byers, M. Rubinstein, Appl. Phys. Lett. 66 (1995) 1427.
[23] G.C. Xiong, Q. Li, H.L. Ju, S.N. Mao, L. Senapati, X.X. Xi, R.L. Greene, T. Venkatesan, J.M. Byers, M. Rubinstein, Appl. Phys. Lett. 66 (1995) 13.
[24] G.C. Xiong, S.M. Bhagat, Q. Li, M. Dominguez, H.L. Ju, R.L. Greene, T. Venkatesan, J.M. Byers, M. Rubinstein, Solid State Comm. 97 (1996) 599.
[25] C. Zener, Phys. Rev. 82 (1951) 403.
[26] A.J. Millis, P.B. Littlewood, B.I. Shraiman, Phys. Rev. Lett. 77 (1996) 175.
[27] L.C. Feldman, J.W. Mayer, S.T. Picraux, Materials Analysis by Ion Channeling, Academic Press, 1982.
[28] R.P. Sharma, F.J. Rotella, J.D. Jorgensen, L.E. Rehn, Physica C174 (1991) 409.
[29] P. Schweiss, W. Reichardt, M. garden, G. Collin, G. Heger, H. Claus, A. Erb, Phys. Rev. B49 (1994) 1387.
[30] R.P. Sharma, L.E. Rehn, Studies of High Temperature Superconductors Advances in Research and Applications, in: Anant Narlikar (Ed.), Nova Science Publishers, vol. 15, 1995, pp. 1–48.
[31] R.P. Sharma, T. Venkatesan, Z.H. Zhang, J.R. Liu, R. Chu, W.K. Chu, Phys. Rev. Lett. 77 (1996) 4624.
[32] R.P. Sharma, G.C. Xiong, C. Kwon, R. Ramesh, R.L. Greene, T. Venkatesan, Phys. Rev. B54 (1996) 10014.
[33] R.P. Sharma, P. Fournier, R.L. Greene, T. Venkatesan, J.F. Mitchell, D. Miller, J. Appl. Phys. 83 (1998) 7351.
[34] R.P. Sharma. P. Fournier, M. Downes, S. Choopun, R.L. Greene, T. Venkatesan, J.F. Mitchell, D. Miller, T. Kimura, Y. Tokura, unpublished.
[35] R.P. Sharma, T. Venkatesan, Z.H. Zhang, J.R. Liu, R. Chu, W.K. Chu, B. Veal, A Paulikas, H. Zheng, unpublished.
[36] F.C. Zhang, T.M. Rice, Phys. Rev. B37 (1988) 3759.
[37] J. Röhler, P.W. Loeffen, S. Müllender, K. Conder, E. Kaldis, Proceedings of the NATO ASI on Materials Aspect of High T_c Superconductors, in: E. Kaldis, et al. (Eds.), Kluwer Academic, 1997, p. 469.
[38] Y.G. Zhao, S.B. Ogale, R. Shreekala, Z.W. Dong, S.P. Pai, M. Rajeswari, T. Venkatesan, W.L. Cao, W. Lu, C. Lee, J. Appl. Phys. 83 (1998) 1531.
[39] J.M.D. Coey, M. Virt, R.K. Ounadjela, Phys. Rev. Lett. 75 (1995) 3910.
[40] S. Kaplan, M. Quijada, H.D. Drew, D.B. Tanner, G.C. Xiong, R. Ramesh, M. Rajeswari, T. Venkatesan, Phys. Rev. Lett. 77 (1996) 2081.
[41] Y.G. Zhao, J.J. Li, R. Shreekala, H.D. Drew, C.L. Chen, W.L. Cao, C.H. Lee, M. Rajeswari, S.B. Ogale, R. Ramesh, G. Baskaran, T. Venkatesan, Phys. Rev. Lett. 81 (1998) 1310.
[42] E. Beaurepaire, J.C. Merle, A. Daunois, J.Y. Bigot, Phys. Rev. Lett. 76 (1996) 4250.
[43] A. Scholl, L. Baumgarten, R. Jacquemin, W. Eberhardt, Phys. Rev. Lett. 79 (1997) 5146.
[44] M. Aeschlimann, M. Bauer, S. Pawlik, W. Weber, R. Byrgermeister, D. Oberli, H.C. Siegmann, Phys. Rev. Lett. 79 (1997) 5158.
[45] M.C. Robson, C. Kwon, K.C. Kim, R.P. Sharma, R. Ramesh, T. Venkatesan, S.E. Lofland, M. Domingue, S.D. Tyagi, S.M. Bhagat, J. Appl. Phys. 80 (1996) 2334.
[46] M.J. Holcomb, C.L. Perry, J.P. Collman, W.A. Little, Phys. Rev. B53 (1996) 6734.
[47] C.J. Stevens, D. Smith, C. Chen, J.F. Ryan, B. Podobnik, D. Mihailovic, G.A. Wagner, J.E. Evetts, Phys. Rev. Lett. 78 (1997) 2212.
[48] M. Mertz, N. Nucker, E. Pellegrin, P. Schweiss, S. Schuppler, M. Kielwein, M. Knupfer, M.S. Golden, J. Fink, C.T. Chen, V. Chakarian, Y.U. Idzerda, A. Erb, Phys. Rev. B55 (1997) 9160.
[49] M. Mertz, N. Nucker, P. Schweiss, S. Schuppler, C.T. Chen, V. Chakarian, J. Freeland, Y.U. Idzerda, M. Klasre, G. Muller-Vogt, Th. Wolf, Phys. Rev. Lett. 80 (1998) 5192.
[50] Y.G. Zhao, W.L. Cao, J.J. Li, R. Shreekala, C.H. Lee, H.D. Drew, S.P. Pai, M. Rajeswari, S.B. Ogale, G. Baskaran, T. Venkatesan, unpublished.
[51] V.A. Vas'ko, V.A. Larkin, P.A. Kraus, K.R. Nikolaev, D.E. Grupp, C.A. Nordman, A.M. Goldman, Phys. Rev. Lett. 78 (1997) 1134.
[52] Z.W. Dong, R. Ramesh, T. Venkatesan, M. Johnson, Z.Y. Chen, S.P. Pai, V. Talyansky, R.P. Sharma, R. Shreekala, C.J. Lobb, R.L. Greene, Appl. Phys. Lett. 71 (1997) 1718.
[53] R.J. Soulen, M.S. Osofsky, D.B. Chrisey, J.S. Horwitz, D. Coller, R.M. Stroud, J. Kim, C.R. Eddy, J.M. Byers, B.F. Woodfield, G.M. Daly, T.W. Clinton, M. Johnson, R.C.Y. Auyeung, Appl. Supercond. 1–2 (158) (1997) 789.
[54] P.W. Anderson, The Theory of High Temperature Superconductivity, Princeton University Press, Princeton, USA, 1997.

Available online at www.sciencedirect.com
SCIENCE DIRECT
ELSEVIER
Journal of the European Ceramic Society 25 (2005) 1965–1969
ECERS
www.elsevier.com/locate/jeurceramsoc

Transition metal oxides: Promising functional materials

B. Raveau *

Laboratoire de cristallographie et des sciences de la matière, UMR 6508, 6 bd Maréchal Juin, 14050 CAEN Cedex, France

Available online 16 April 2005

Abstract

Transition metal oxides represent a considerable potential for the generation of new frameworks with new magnetic and transport properties with a view of applications in the field of electronics. Three examples of ceramics are reviewed herein, which are all characterized by a mixed valence of the transition element, allowing electronic delocalization to be produced: high T_c superconducting cuprates (Cu^{2+}/Cu^{3+}), thermoelectric cobaltites (Co^{3+}/Co^{4+}) and colossal magnetoresistance manganites (Mn^{3+}/Mn^{4+}).

Keywords: Functional applications; Electrical properties; Magnetic properties; Superconductivity

For a long time considered as compounds of academic interest, transition metal oxides have been studied these last 15 years for their extraordinary magnetic and transport properties susceptible of various applications. In this respect, oxides involving copper, manganese and cobalt have a great potential. Their remarkable magnetic and transport properties originate from the ability of these elements to adopt various oxidation states and electronic configurations. For these oxides, the mixed valence Cu^{2+}/Cu^{3+}, Mn^{3+}/Mn^{4+} or Co^{3+}/Co^{4+} reflects the possibility of electronic delocalization over the metal–oxygen framework, whereas the Jahn Teller effect of several of their cations, such as Cu^{2+}, Co^{2+} or Mn^{3+}, favors the formation of anisotropic structures and consequently of anisotropic transport and magnetic properties. The spin configurations of several of these cations are also very complex especially for cobalt, so that complex magnetic transitions are often generated.

The cuprate family[1–4] exemplifies the great impact of the transition metal oxides in the discovery of new concepts in solid state physics, and in the realization of new functional materials. Beside the famous cuprate $La_{2-x}Ba_xCuO_4$ synthesized for the fist time in the 80s[5] and which was found to be superconductor below $T_c = 40\,K$,[6] the cuprates $YBa_2Cu_3O_7$ (often called "123"), $Bi_2Sr_2CaCu_2O_{8+\delta}$ and $Bi_{2-x}Pb_xSr_2Ca_2Cu_3O_{10+\delta}$ (called "2212" and "2223", respectively) are now considered as materials for the future. Their critical temperature, ranging from 92 K for $YBa_2Cu_3O_7$ to 110 K for Bi-2223 allows to use liquid nitrogen, a cheap cooler, for working. Moreover they are almost ecological, since they contain few or even no heavy toxic elements such as thallium, mercury or lead. The high Curie temperature of these oxides originates from the bidimensionnal character of their structure (Fig. 1). The latter forms indeed layers built up of CuO_5 pyramids and CuO_4 square planar groups, sharing corners. High temperature superconductivity results form the delocalization of hole carriers in the CuO_2 planes, whereas in classical superconductors the delocalization is tridimensionnal. In contrast to the latter, the high T_c superconductors exhibit a low coherence length. The latter characteristic is a handicap for the propagation of holes and requires an almost perfect alignment of the CuO_2 planes in order to reach high current densities for applications. For this reason, numerous studies of the sintering of these ceramics were carried out these last years, bearing in mind the complex chemistry of these compounds. For instance in the case of $YBa_2Cu_3O_7$, the most successful methods are based on the texturation, using either the melt textured growth (MTG) or the top seeding melt growth (TPMG). These methods allow to elaborate discs of reasonable size (5–10 cm diameter) without any microcracks, which can then be assembled by soldering for various applications. In this way, current density values of 70,000 A/cm^2 can be reached in "YBCO". Thus, this material is close to the application for the realization of

* Tel.: +33 2 3145 2616; fax: +33 2 3195 1600.
E-mail address: bernard.raveau@ensicaen.fr.

0955-2219/$ – see front matter © 2005 Elsevier Ltd. All rights reserved.
doi:10.1016/j.jeurceramsoc.2005.03.220

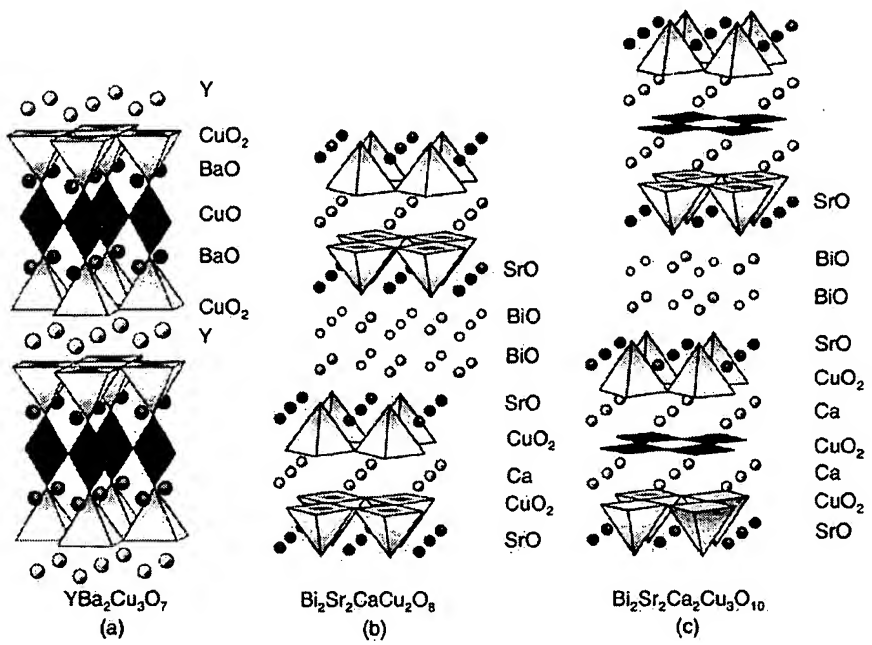

Fig. 1. Structures of the high T_c superconductors (a) $YBa_2Cu_3O_7$ $T_c = 92$ K (b) $Bi_2Sr_2Ca_2Cu_2O_{8+\delta}$, $T_c \approx 90$ K and (c) $Bi_{2-x}Pb_xSr_2Ca_2Cu_3O_{10+\delta}$, $T_c = 110$ K.

generators and magnets. Propulsion motor prototypes developing a power of 100 kW, were realized by several staffs in Moscow and Iena. In the same way, magnetic levitation of this material is actually being used for the realization of magnetic bearings. The magnetic levitation train "MAGLEV", realized by Japanese researchers, which runs over 45 kms, is another example of the potential of "YBCO". For bismuth cuprates, the shaping methods are different, using either forging or hot rolling for the realization of wires. For these materials the application is close at hand for the realization of connecting cables, transformers and generators and MHD ship propulsion systems. Several prototypes have been realized by different companies. This is exemplified by the realization of fault current limiters of 1.2 MVA, made of Bi cuprate "2212", realized by ABB and current leads of 13 kA realized by Alcatel, whereas with the Bi "2223" cuprate current transformers were realized by ABB and EDF and connecting cables at Detroit Edison. The latter show the great potential of this cuprate since current transportation can be performed in cables of 120 m length, and 110 kg of Bi-2223 replace efficiently 8 tons of copper. Superconductivity coils based on Bi-2223 cuprate, were also fabricated recently to be used in nuclear magnetic resonance for medical imaging. The applications in the field of electronics are more distant, especially for fast electronics which requires to adapt these materials to the silicon technology, main unsolved problem to date. Nevertheless, important progresses have been achieved in the field of interconnectors and hyperfrequency transmission. The realization of superconducting quantum interference devices (SQUIDs) for various detection (submarine, brain etc...) is also close to the outcome. Less than twenty years after their discovery, cuprates appear as functional materials with great potential. The recent discovery of superconductivity in the layered cobalt oxide $NaCoO_2$, yH_2O,[7] shows that the exploration of oxides in view of discovering new superconductors is so far not finished, and that efforts have to be done to understand this phenomenon in oxides whose chemistry is complex.

Lamellar cobaltites are the second example of oxides whose transport properties are much studied due to their potential application in the field of energy conversion especially at high temperature. The cobaltite $NaCo_2O_4$ whose structure (Fig. 2) consists of layers of edge-sharing CoO_6 octahedra, interleaved with Na^+ cations[8] shows very attractive transport properties.[9] This oxide exhibits at room temperature a high thermoelectric power $S = +100\ \mu V/K$, a low resistivity close to that of a metal, $\rho = 0.2\ m\Omega\ cm$, and a rather low thermal conductivity $K = 2\ W\ m^{-1}\ K^{-1}$. This leads for this material to a figure of merit, $Z = S^2/\rho K$, very acceptable at high temperature which should allow the realization of thermoelectric generators. The recent discovery of cobalt oxides with a "misfit" structure[10–16] speeds up the research activity on the thermoelectrics technology[17,18] especially in Japan. The misfit cobaltites are in fact composite structures built up of two distinct layers with different crystal lattices. This family is exemplified by $Ca_3Co_4O_9$ whose structure (Fig. 3) consists of the stacking of "CoO_2" layers with a monoclinic symmetry ($a \sim 4.8$ Å, $b_1 \sim 4.6$ Å, $c \sim 10.9$ Å, $\beta \approx 98°$) and of "$CaCoO_3$" layers with the same symmetry, a, c and β parameters being identical but b parameter being different, $b_2 \approx 2.8$ Å. These two sorts of layers have thus a very different structure, namely CdI_2 type for "CoO_2" and rock salt type for "Ca_2CoO_3". The structural misfit between these two types of layers is better evidenced by the chemical

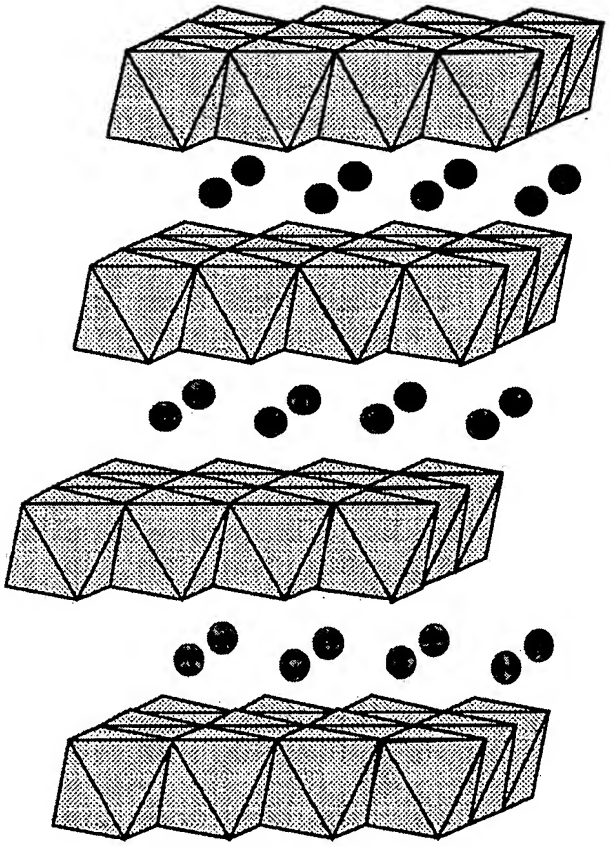

Fig. 2. Structure of the cobaltite $NaCo_2O_4$.

formula $[Ca_2CoO_3][CoO_2]_{b1/b2}$, with $b_1/b_2 = 1.625$. Thanks to its high thermoelectric power $S = +120\ \mu V/K$, independent on the temperature for $T > 200$ K, and to its low resistivity (Fig. 4), $Ca_3Co_4O_9$ has a great potential for thermoelectric application, similar to $NaCo_2O_4$. Advantageously, this oxide has a better stability than $NaCo_2O_4$ and has a greater potential for high temperature utilization. The great flexibility of the "misfit" structure has allowed a large family of compounds to be generated, where the rock salt layer can host various cations such as strontium, barium, thallium, bismuth, mercury and lead. As a result, the structural misfit characterized by the b_1/b_2 ratio can vary significantly. The thickness of the rock salt layers, or more exactly their multiplicity can also vary. This is illustrated by the recent discovery of the bismuth cobaltites $[Bi_{1.7}Sr_2O_4][CoO_2]_{1.82}$ whose structure (Fig. 5) is also built up of single "CoO_2" layers but in which double "bismuth–oxygen" are sandwiched between single strontium–oxygen layers, replacing the "$Ca_2Co_2O_3$" layers. This great variety in the composition, but also in the stoichiometry, influences significantly the carrier density and consequently the thermoelectric properties of these oxides. In this way, a thermoelectric power of 160 μV/K can be reached in lead misfits $[PbSr_{2-x}Ca_xO_3][CoO_2]_{b1/b2}$. The physics of these materials is so far not perfectly elucidated. The origin of metallic conductivity stems to the mixed valence, engendered by the Co^{3+} and Co^{4+} species, which exhibit a low spin

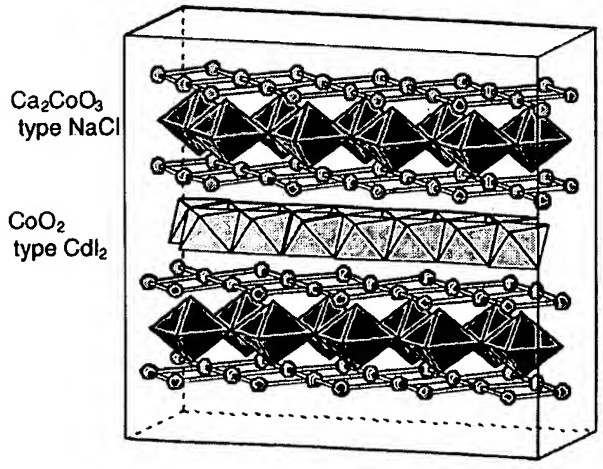

Fig. 3. Misfit structure of the cobaltite $Ca_3Co_4O_9$, $(Ca_2CoO_3)(CoO_2)_{1.62}$, built up of CdI_2 type"CoO_2" layers and rock salt type "Ca_2CoO_3" layers.

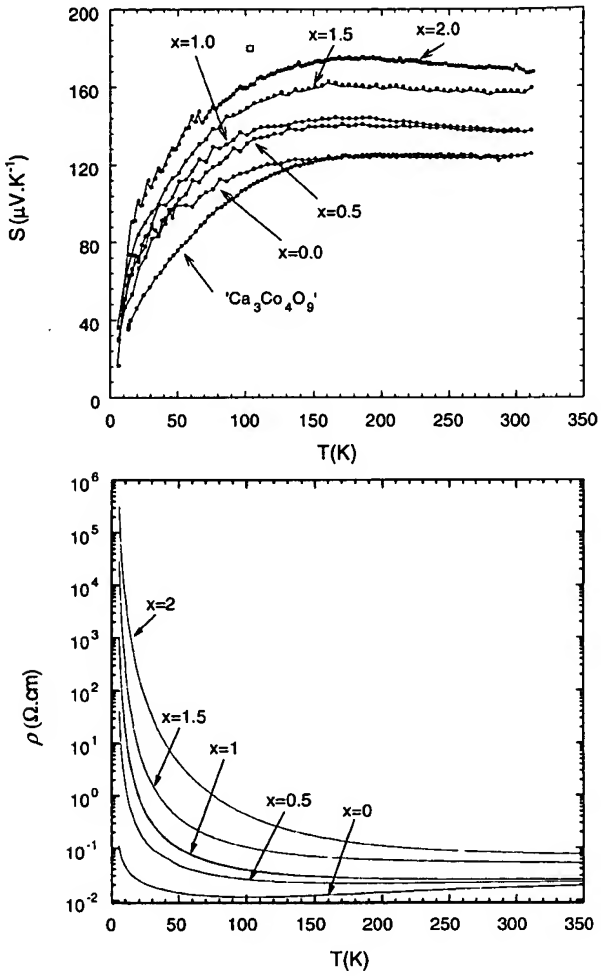

Fig. 4. Evolution of the thermoelectric power S and of the resistivity ρ of the cobaltite vs. temperature.

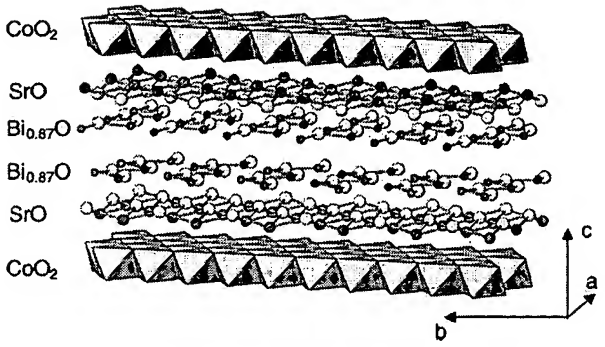

Fig. 5. Structure of the misfit cobaltite $[Bi_{1.7}Sr_2O_4][CoO_2]_{1.82}$ built up of "CoO_2", layers and rock salt type "$Bi_{1.74}Sr_2O_4$" layers.

configuration. It results in a splitting of the t_{2g} states into e'_g and a_{1g}, leading to a broad e'_g band, which is necessary for the appearance of metallicity. On the other hand the magnetic interactions are attenuated by the magnetic frustration which results from the triangular geometry of the "CoO_2" layers. Finally, the weaker thermal conductivity could be due to the disordering of cations and anions in the rock salt layers, which would then behave as phonon glass. Thus it appears that the bidimensionnal character of theses oxides and their mixed valence, play a very crucial role in their remarkable thermoelectric properties. In this respect these oxides show a great similarity with high T_c superconducting cuprates which also require a bidimensionality of the structure and the mixed valence Cu^{2+}/Cu^{3+}. The route is thus opened to the optimization of these materials by modifying the chemical composition of their rock salt layers, but also by texturing the corresponding ceramics in order to use advantageously their anisotropy. Demonstrators based on Peltier effect, using these materials in modules where p and n conductors are assembled, are actually working in different laboratories.

The third family deals with the manganites of generic formulation $Ln_{1-x}A_xMnO_3$[19–21] where Ln^{3+} is a lanthanide cation and A^{2+} is an alkaline earth. These oxides are the object of a considerable number of studies, due to the spectacular variation of their resistance, when submitted to a magnetic field. For instance, by tuning carefully the composition, i.e. the average size of the A-site cations, the resistance can be decreased by several orders of magnitude by applying a magnetic field as illustrated for the oxide $Pr_{0.7}Ca_{0.26}Sr_{0.04}MnO_3$ (Fig. 6). For this reason, these oxides are known as CMR effect (colossal magnetoresistance). The great sensitivity of the resistance of these materials to the magnetic field, offers a great potential for magnetic recording and as magnetic sensors and actuators. Differently from the two above families, these manganites have a tridimensionnal structure. They exhibit the classical perovskite structure, built up of corner-sharing MnO_6 octahedra, but whose distortions play a major role in the magnetic and transport properties, especially via Jahn Teller distortion of the Mn^{3+} species. In fact, like cuprates and cobaltites, the CMR manganites exhibit a mixed valence Mn^{3+}/Mn^{4+}. The latter is at the origin of the dou-

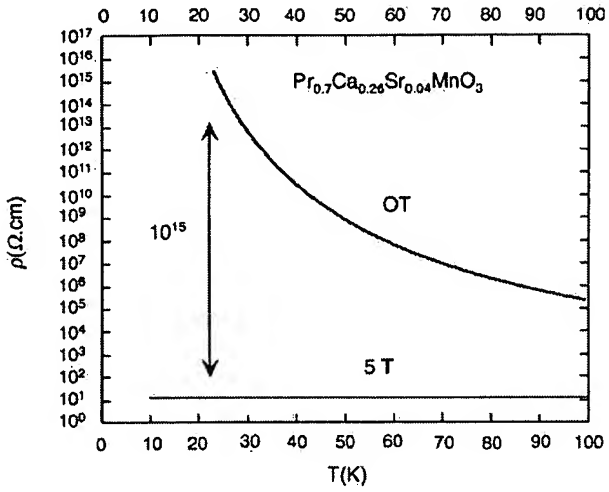

Fig. 6. Evolution of the resistivity versus magnetic field for the perovskite $Pr_{0.7}Ca_{0.26}Sr_{0.04}MnO_3$, (a) in zero magnetic field (b) under $H = 5$ T.

ble exchange (DE) mechanism between the Mn^{3+} and Mn^{4+} species[22] and is consequently responsible for the appearance of ferromagnetism and metallic conductivity often observed simultaneously at low temperature. The transition from an insulating state (paramagnetic or antiferromagnetic) to a ferromagnetic metallic state, by application of a magnetic field is thus the key of the CMR effect in these oxides. In fact, this phenomenon is often related to the existence of charge and orbital ordering between the Mn^{3+} and Mn^{4+} species. Such a behavior is exemplified by the perovskite $Pr_{0.5}Ca_{0.5}MnO_3$ which exhibits at low temperature an ordering of the Mn^{3+} and Mn^{4+} species and of the e_g orbitals in the form of stripes as schematized on Fig. 7. In this antiferromagnetic CE-type insulator the "Mn^{3+}" octahedra are strongly elongated, whereas the Mn^{4+} octahedra are much more symmetric. By applying a magnetic field larger than 25 T to this structure, a more symmetric structure is obtained, which is characterized by a charge delocalization, over the Mn–O–Mn lattice. In other words the application of a magnetic field induces a structural transition and simultaneously a magnetic transition to a magnetic metallic state. Starting from this observation, one can predict the important role of doping in the appearance of the CMR in these oxides. The substitution of a small amount of foreign elements for manganese (a few atoms per cent), such as Cr^{3+}, Co^{2+}, Ni^{2+}, Ru^{4+} destabilizes the orbital and charge ordering, making locally the structure more symmetric, even in the absence of magnetic field. In zero field, ferromagnetic islands with a symmetry higher than that of the antiferromagnetic matrix are generated coherently with the matrix around the impurities. By applying a magnetic field, these small domains tend to extend and the material becomes metallic when the domains percolate. This doping allows by structural effect, coupled with the magnetic effect of doping cations to lower considerably the critical magnetic field so that only a few teslas are necessary to obtain a magnetoresistance effect, against 25 T for the pristine phase $Pr_{0.5}Ca_{0.5}MnO_3$. Similar

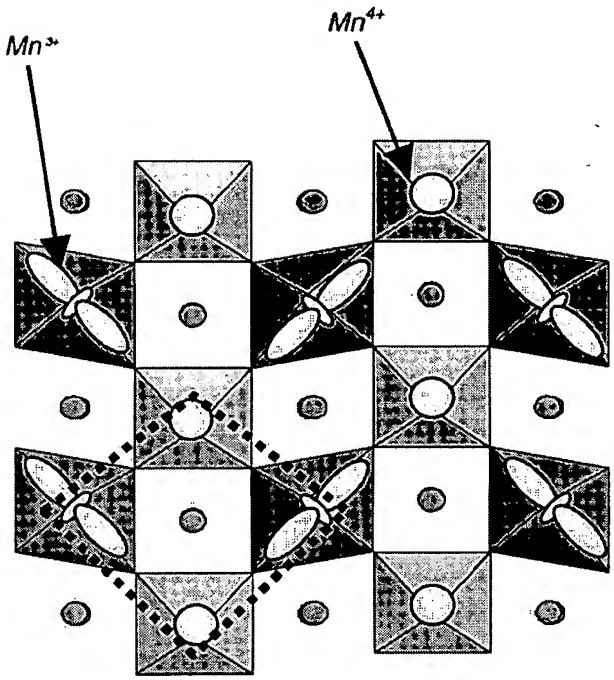

Fig. 7. Schematized structure of the antiferromagnetic insulating perovskite $Pr_{0.5}Ca_{0.5}MnO_3$, built up of octahedral "Mn^{3+}" stripes alternating with "Mn^{4+}" stripes.

effects can be obtained by doping the A sites with cations such as Ba^{2+} or Sr^{2+} which have larger size than Ca^{2+}. The latter have clearly a structural role: they generate more symmetric regions within the matrix, which become ferromagnetic. Consequently, the CMR manganites evidence a new phenomenon, called electronic phase separation which is itself generated by coherent structural phase separation. The nucleation of a more symmetric ferromagnetic phase within a less symmetric antiferromagnetic phase, and its coherent growth, is the key of the mechanism of the CMR effect. It is thus easy to understand that the possibilities of optimization of the CMR properties of these materials are still numerous and are so far not completely explored. However, all the applications in the field of magnetic recording require to work at room temperature, with magnetic fields as low as possible, i.e. smaller than 1/10 T. In these conditions, the performances that have been reached recently, corresponding to magnetoresistance values close to 10% at 300 K under 0.5 T, appear promising. The interface effects and of grain boundaries, obtained in ceramics and especially in thin films of these materials, called tunneling magnetoresistance (TMR) should allow to reach the required characteristics for applications.

In conclusion, these few examples show that the transition metal oxides are, due to the physical properties they can generate, functional materials for the future. Numerous physical properties remain to be discovered and to be explained in such strongly correlated electron systems, which have not been studied to date, because of their structural and chemical complexity. The route is opened to their exploration, which should open on applications.

References

1. Bednorz, J. G. and Millier, K. A., Earlier and recent aspects of superconductivity Springer-Verlag. *Springer Series in Solid State Sciences 90*. Springer Verlag, 1990.
2. Raveau, B., Michel, C., Hervieu, M. and Groult, D., Crystal chemistry of high Tc superconducting copper oxides. *Springer Series in Materials Sciences*. Springer Verlag, 1991.
3. Gschneider, K. A., Eyring, L. and Maple, M. B., ed., *Handbook on the Physics and Chemistry of Rare Earths, High Temperature Superconductors, Vols 30–31*. Elsevier, 2000.
4. Rao, C. N. R. and Raveau, B., *Transtion Metal Oxides*. Wiley VICH, 1998.
5. Michel, C. and Raveau, B., *Rev. Chimie Minérale*, 1984, **21**, 407.
6. Bednorz, J. G. and Müller, K. A., *Z. Phys. B*, 1986, **64**, 189.
7. Takada, K., Sakurai, H. and Takyama-Muromachi, E., *Nature*, 2003, **422**, 53.
8. Fouassier, C., Matejka, G., Réau, J. and Hagenmuller, P., *J. Solid State Chem.*, 1973, **6**, 532.
9. Terasaki, I., Sasago, Y. and Uchinokura, K., *Phys. Rev.*, 1997, **B 56**, R12685.
10. Masset, A. C., Michel, C., Maignan, A., Hervieu, M., Toulemonde, O., Studer, F. *et al.*, *Phys. Rev. B*, 2000, **62**, 166.
11. Miyazaki, Y., Onoda, M., Oku, T., Kikuchi, M., Ishii, Y. and Kajitani, T., *J. Phys. Soc. of Jpn.*, 2002, **71**, 491.
12. Boullay, Ph., Seshadri, R., Studer, F., Hervieu, M., Groult, D. and Raveau, B., *Chem. Mater*, 1998, **10**, 92.
13. Maignan, A., Wang, L. B., Hébert, S., Pelloquin, D. and Raveau, B., *Chem. Mater.*, 2002, **14**(3), 1231–1235.
14. Pelloquin, D., Maignan, A., Hébert, S., Martin, C., Hervieu, M., Michel, C. *et al.*, *Chem. Mater.*, 2002, **14**(7), 3100–3105.
15. Maignan, A., Pelloquin, D., Hébert, S., Michel, C. and Hetjmanek, J., *J. Appl. Phys.*, 2002, **92**, 1964.
16. Sano, M., Hori, S., Matsubara, I., Funahashi, R., Shikano, M., Shimuyama, J. *et al.*, *Jpn. J. Appl. Phys.*, 2003, **49**, L198.
17. Kajikawa, T., In *20th International Conference on Thermoelectrics (2001) IEEF*, 2001.
18. Riffat, S. B. and Ma, X., *Appl. Thermal Eng.*, 2003, **23**, 913.
19. Rao, C. N. R. and Raveau, B., ed., *Colossal Magnetoresistance, Charge Ordering and Related Properties of Manganese Oxides*. World Scientific, 1998.
20. R. Ibarra *et al.*, Magnetostriction in mixed valent magnetic oxides. In Gibbs, M. R. J., ed., *Modern Trends in Magnetostriction Study and Applications*. Kluwer Academic Publisher, 2000.
21. Tokura, Y., ed., *Colossal Magnetoresistive Oxides*. Gordon and Breach Science Publishers, New York, 1999.
22. Zener, C., *Phys. Rev. B*, 1951, **82**, 403.